ON THE THERMOFRACTURE BEHAVIOR OF LEAKING PIPES

by

Jefrey R. Ramsay

A Thesis
Submitted to the Faculty of Graduate Studies
in Partial Fulfillment of the Requirements
for the Degree of

MASTER OF SCIENCE

Department of Mechanical Engineering
University of Manitoba
Winnipeg, Manitoba, Canada
@ June, 1990

ISBN 0-315-71933-8

ON THE THERMOFRACTURE BEHAVIOR OF LEAKING PIPES

BY

JEFREY R. RAMSAY

A thesis submitted to the Faculty of Graduate Studies of the University of Manitoba in partial fulfillment of the requirements of the degree of

MASTER OF SCIENCE

ABSTRACT

The purpose of this thesis was to further investigate , experimentally and numerically, using the J-Integral method of analyzing the fracture behavior of thin wall pipes , the thermal effect of leaking in a thin wall pipe with a longitudinal through-wall crack, by;

1. verifying through experimentation the magnitude of the thermal effect due to leaking and the deficiency of the Leak-Before-Break theory;

2. determining how significantly the internal pressure contributes to the thermal effect; and

3. determining how significantly the initial crack length contributes to the thermal effect.

The results presented in this thesis clearly show that increases in internal pressure and crack length, coupled with the thermal effect due to leaking, magnify the thermal J-integral and thus the possibility of catastrophic failure upon leaking.

The maximum thermal J-integral/mechanical J-integral ratio (J_T/J) values reached in the later stages of leaking were found to decrease by approximately 30 percent for 50 percent increases in pressure, independent of crack length. However, in the early stages of leaking, for example at time, t=0.25 seconds, the J_T/J ratio was found to increase. At t=0.25 seconds, for pressures of 1.0, 1.5 and 2.0 MPa , the thermal J-integral increased to approximately 8, 11 and 20 times the purely mechanical J-integral , respectively, for a worst case crack length of 12 mm. At t=0.25 seconds, for crack lengths of 6, 9 and 12 mm, the thermal J-integral increased to approximately 4, 10 and 20 times the purely mechanical J-integral , respectively, for a worst case internal pressure of 2.0 MPa. Therefore, in the initial stages of leaking, as pressure and crack length increase, J_T/J increases and the thermal effect is significant.

The Leak-Before-Break theory will thus overestimate the critical crack size for catastrophic failure, since it does not take into consideration the thermal effect induced by leaking.

ACKNOWLEDGEMENTS

This study was performed with the cooperation of several individuals at the Mechanical Engineering Department, University of Manitoba. The author would like to especially thank Dr. T.R. Hsu for supervision of this thesis and for his continuous support and guidance. Mr. Z.L.Gong and Mr. N.S. Sun are gratefully acknowledged for their technical and academic assistance. Much appreciation to Wardrop Engineering Inc. for the use of their computer facilities and to Mr. James Hildebrandt for his assistance. The author also expresses his sincerest gratitude to his wife, Sherri, for her patience and understanding.

Financial support from the Natural Sciences and Engineering Research Council of Canada and the Department of Mechanical Engineering, University of Manitoba, is gratefully acknowledged.

TABLE OF CONTENTS

LIST OF TABLES

LIST OF FIGURES

Page

Page

NOMENCLATURE

a	half of the active crack length
a_c	critical crack length
a_n	ANSYS calculated temperature variable
a_1	design variable
Ao	area enclosed by contour Γ
α	coefficient of thermal expansion
α_I	mode I crack tip opening displacement parameter
b_1	design variable
B	width of crack tip opening specimen
[B]	finite element strain displacement matrix
β	Newmark β integration parameter
[D]	finite element elasticity matrix
δ_I	mode I crack tip opening displacement
δ_{IC}	mode I critical crack length
δ_{ij}	Kronecker delta
E	Young's modulus
E*	Young's modulus for plane strain
E'	plasticity modulus
ε_{ij}	strain field
ε'_{ij}	strain field including thermal effect
$\tilde{\varepsilon}_{ij}(\theta,n)$	dimensionless function of θ and n
$\{\varepsilon\}$	finite element strain matrix
$\{\Delta\varepsilon\}$	finite element incremental strain matrix
F	finite element applied force
F(g)	function of crack geometry and loading
F_{ij}	function of r and θ
{Fb}	finite element body force vector

$\{Fs\}$	finite element traction force vector
$\{Fn\}$	finite element nodal force vector
$\{\Delta F_t\}$	finite element incremental force vector
$\{\Delta F'_t\}$	finite element equivalent force matrix
G	shear modulus of elasticity
G_c	critical strain energy release rate
G_{ij}	function of r and θ
$G_{I,II,III}$	mode I, II and III strain energy release rates
γ	Newmark β integration parameter
Γ	path of integration around crack tip
$I(n)$	integration constant
J	mechanical J-Integral
J_I	mode I mechanical J-Integral
J_T	J-Integral with thermal effect
$K_{I,II,II}$	mode I, II and III stress intensity factors
K_{IC}	critical stress intensity factor
K_r	R-6 assessment curve parameter
K'_r	R-6 diagram coordinate
$[K]$	finite element stiffness matrix
λ	Lame's constant
$[M]$	finite element element consistent mass matrix
μ	shear modulus of elasticity
n	strain hardening exponent
N_i	outward unit normal vector to Γ
$[N]$	finite element displacement transformation matrix
ν	Poisson's ratio
θ	angle defining direction of r
$\{Po\}$	finite element work equivalent nodal force matrix
r	radial distance from crack tip
r_y	plastic zone size around crack tip

ρ	mass density
ds	arc length along G
S_r	R-6 plastic collapse parameter
S'_r	R-6 diagram coordinate
σ	applied stress on structure
σ_c	critical stress
σ_I	plastic collapse stress
σ_u	ultimate strength
σ_y	yield strength
σ_{ij}	stress field
σ'_{ij}	stress field with thermal effect
$\tilde{\sigma}_{ij}(\theta,n)$	dimensionless function of θ and n
σ_1,σ_2	principle stress vectors
t	finite element time variable
Δt	finite element incremental time variation
t	crack tip opening specimen thickness
T	temperature field around crack tip
ΔT	incremental temperature variation
T_i	traction vector
T_n	temperature measured at nth thermocouple
U'	finite element stored strain energy
U_i	displacement field
{ u}	finite element general displacement matrix
{Δu}	finite element incremental displacement matrix
dV	incremental volume
W	strain energy density
W'	strain energy density including thermal effect or finite element work to produce deflection
x_1, x_2	local moving cartesian coordinates at the crack tip

ymi1	error function
CST	crack surface temperature
DAU	data acquisition unit
SIGE	maximum effective stress
{ }	column matrix
[ ]	rectangular matrix
⟨ ⟩	row matrix
. superscript	derivative with respect to time

CHAPTER 1. INTRODUCTION

1.1 GENERAL

Thin wall pipes are used extensively in power and chemical process plants. In many applications, they are required to carry water at high pressure and temperature, close to saturation conditions. The failure of these pipes, especially in a nuclear power plant could be catastrophic.

Several methods have been developed to evaluate the fracture behavior of and assess the tolerance of defects in such pipelines. Some of the more prevalent safety analyses are discussed in Chapter 2.

To date the most widely used fracture behavior theory for pipelines is the Leak-Before-Break theory proposed by Irwin et al [1]. This theory suggests that a pipe will develop a leak via a through-wall crack well before the crack grows to critical size. Leak detection devices would then indicate when system shut down and pipe inspection were required.

However, Irwin's theory failed to consider the local cooling effect on the crack surfaces due to the throttling process during leaking. Hsu et al [2] used Rice's J-Integral [3], modified to incorporate this cooling effect and found that the induced temperature gradients near the crack during the initial leaking process have a significant effect on the stability of the crack.

These results would indicate that the Leak-Before-Break theory does not preclude the chance of catastrophic failure, with no possibility of detecting an impending fracture. However, research into this phenomenon is still in its early stages, and the Leak-Before-Break theory is still in acceptance.

1.2 OBJECTIVES

The purpose of this research thesis was to further investigate, experimentally and numerically, using the J-Integral method of analyzing the fracture behavior of thin walled pipes, the thermal effect of leaking in a thin wall pipe with a longitudinal through-wall crack, by;

1. verifying through further experimentation the magnitude of the thermal effect and the deficiency of the Leak-Before-Break theory;

2. determining how significantly the internal pressure contributes to the thermal effect; and

3. determining how significantly the initial crack length contributes to the thermal effect.

1.3 SCOPE

Chapters Two to Four provide the background theory required to understand the terminology and theory used in the experimental and numerical analyses and discussions presented in this thesis. Chapter Two outlines the Linear-Elastic and Elastic-Plastic Fracture Mechanics Theories and their applications. Irwin's Leak-Before-Break theory is also discussed. Chapter Three presents a derivation of Rice's J-Integral, and its extension to include the thermal effect. Basic finite-element theory, the hybrid experimental-numerical technique and the inverse heat conduction technique used to solve the numerical model in this thesis are discussed in Chapter Four.

The experimental program developed for this thesis is described in Chapter Five. Chapter Six discusses the numerical model used to simulate the physical experiment. Chapter Seven presents the experimental results and a discussion of these results. Conclusions drawn from the current work and recommendations for future development are discussed in Chapter Eight.

1.4 LITERATURE REVIEW OF SIMILAR WORK

The basic background and fundamentals of fracture mechanics parameters in the linear elastic and elastic-plastic fields are outlined in Chapter Two. From these theories, several researchers have attempted to characterize the fracture behavior of leaking thin wall pipes.

Irwin et al [1] first proposed the Leak-Before-Break theory in 1967. To date this is the most widely used criteria for the design of pressure vessel and piping components. Because of its importance to the discussion presented in this thesis, the Leak-Before-Break theory is described in greater detail in Section 2.

Hahn, Sarrate and Rosenfield [4] published a paper in 1969 on the "Criteria for Crack Extension in Cylindrical Pressure Vessels", which examined axial through-cracks in thick and thin- wall pressure vessels. Folias' [5] theoretical treatment of pressure vessels was coupled with conventional linear elastic theory, including a plasticity correction, to arrive at a crack extension parameter. Non-linear elastic, elastic-plastic and thermal considerations were not included.

Rice's J-Integral parameter [3] was utilized by Blackburn, Hellen and Jackson [6] to characterize the stress state at the crack tip in a non-elastic material. This formulation was confined to center-cracked plates in uniaxial tension, considering thermal and mechanical loading as separate cases.

The J-Integral was modified by Wilson and Yu [7], Kishimoto et al [8], Ainsworth et al [9], and Chell [10] for combined mechanical and thermal loading. These analyses were again confined to center-cracked plates under

uniaxial loading. Liebowitz et al [11] extended these theories to a biaxial loading case, and presented a numerical solution which was further improved by Hsu et al [12].

Numerous fracture behavior investigations of pressure vessels and thin wall pipes have recently been carried out. Some of the more relevalent investigations are listed here.

1982

Hellen, Cesari and Maitan [13] on the application of fracture mechanics to thermally stressed structures. Discussed axial and circumferential cracks in cylinders under pressure and thermal loading.

1983

J.M. Bloom [14] on the assessment of the structural integrity of pressure vessels. Developed the R-6 approach of fracture analysis outlined in Section 2.2.

1986

Güter and Zeibig on Leak-Before-Break (LBB) considerations for Liquid Metal Fast Breeder Reactors (LMFBR) structures [15]. Supported the LBB theory by non-destructive testing methods.

1986

Hutin and Billon on flaw analysis in steam generator tubes [16]. Stresses and critical crack sizes were estimated for specific operating conditions by the R-6 failure assessment approach. Large scale plasticity was not accounted for.

1987

B. Mukherjee on the LBB test program for the Darlington Nuclear Generating Station [17]. Used J-Integral to determine the initiation toughness of piping material at specific operating conditions.

1988

Wang and Zhang on the analysis of a low carbon seamless tube with a longitudinal crack [18]. Used J-Integral to characterize fracture under internal pressure loading only.

The obvious failings of these investigations are that the throttling effect of leakage was not considered and that not enough, if any, experimentation was done to back up the numerical results.

Hsu et al [2] first realized the importance of the throttling effect of leakage and attempted to model this situation. A temperature field induced by the leakage was assumed and the J-Integral used to characterize the fracture behavior. The J-Integral was found to be significantly higher than in the conventional analysis excluding the throttling effect.

Hsu et al further developed a hybrid experimental-numerical technique [19] to verify the preliminary results indicating the magnitude of the thermal effect. These results were proven, but a detailed investigation into the thermal effect of leakage is necessary. The author was thus prompted to more fully investigate the throttling effect of leakage in thin wall pipes, both numerically and especially experimentally.

CHAPTER 2 . REVIEW OF FRACTURE MECHANICS THEORY FOR STATIONARY CRACKS

2.1 GENERAL

Several methods of analyzing elastic-plastic fracture in pipes can be viewed as extensions of linear-elastic theory. Therefore, a review of Linear Elastic Fracture mechanics (LEFM) is provided. Elastic-Plastic Fracture Mechanics (EPFM) is then discussed with an outline of the various analysis methods currently in use. The major assumptions of the popular Leak-Before-Break theory are then presented.

2.2 LINEAR ELASTIC FRACTURE MECHANICS(LEFM)

Linear Elastic Fracture Mechanics theory (LEFM) assumes that a sudden total break will occur in a fractured pipe, causing pipe whip and a large loss of liquid. This model is only applicable to large diameter components whose large wall thickness prevents any significant distortion in the thickness direction, and confines the strain to directions perpendicular to the crack front (plane strain constraint). This model does not accurately describe the fracture mechanism for a thin wall pipe, but is presented here as Elastic-Plastic Fracture Mechanics extends from the LEFM foundation.

Fracture mechanics theory for members containing cracks was pioneered by A.A. Griffith in 1920 [20]. This theory is well documented in many text books and publications [21,22] and is therefore not described in detail in this thesis. Griffith's theory successfully predicted the strength of glass, but was unreliable for even the most brittle materials. Further theories needed

to be developed. Some of the more popular theories are outlined here.

1. Strain Energy Release Rate, G_c

This approach was used to introduce the parameter, G_c, which represents the total energy associated with a unit length crack. Griffith's stress equation could then be written as,

$$\sigma_c = \left[\frac{G_c E}{\pi a}\right]^{1/2} \qquad (2.2.1)$$

where G_c, the critical strain energy release rate, is a material property,

σ_c is the critical stress,

E is the elastic modulus, and

a is half of the active crack length.

2. Stress Intensity Factor, K_I

The three basic modes of crack surface displacements were then established, as shown in Figure 2.2.1. Each of these modes has a particular stress field in the vicinity of the crack tip. Referring to Figure 2.2.2, for a mode I opening crack, the two-dimensional elastic crack tip stress-displacement field can be expressed by [23],

$$\sigma_{ij} = \frac{K_I F_{ij}(\theta)}{\sqrt{2\pi r}} + \ldots \qquad (2.2.2a)$$

$$U_i = K_I \sqrt{r}\, G_i(\theta) + \ldots \qquad (2.2.2b)$$

where σ_{ij} and U_i are the stress and displacement fields, respectively,

r is the radial distance from the crack tip,

F_{ij} and G_i are functions of the angle θ defining r, and
K_I is the stress intensity factor given by,

$$K_I = F(g) \quad \sigma \quad \sqrt{\pi a} \tag{2.2.3}$$

where F(g) is a function of the crack geometry and loading and σ is the applied stress on the structure.

The remaining terms depend on the specimen geometry and are dominated by the $1/\sqrt{r}$ singularity in the first term. K_I is a measure of the magnitude of the stress field around the crack tip. Fracture is considered to occur when K_I reaches a critical value, K_{IC}, which can be regarded as a material parameter. Thus, equation (2.2.3) can be written as,

$$\sigma_c = \frac{K_{Ic}}{F(g) \sqrt{\pi a}} \tag{2.2.4}$$

Critical values for mode II and III cracks, K_{II} and K_{III}, also exist, but are much harder to define.

Mode I, II and III critical strain energy release rates, G_{IC}, G_{IIC}, and G_{IIIC}, have also been developed. In the elastic region for a mode I opening crack, the strain energy release rate, G_{IC}, and the stress intensity factor, K_{IC}, are related by,

$$G_I = \frac{K_{Ic}^2}{E^*} \tag{2.2.5}$$

where E* is the elastic modulus, E, for the plane strain case, with,

$$E^* = \frac{E}{(1 - \nu^2)} \quad , \text{ for plane strain} \tag{2.2.6}$$

3. Crack Tip Opening Displacement (CTOD)

In 1961, Wells [24] discovered that a load applied to a solid containing a crack will cause a displacement of the crack surfaces, termed the Crack Tip Opening Displacement (CTOD). The crack opening displacement measured from the lines of load application is referred to as simply the Crack Opening Displacement (COD). These two measurements are illustrated in Figure 2.2.3.

It has been shown that for small scale yielding,

$$\delta_I \cong \frac{G_I}{\alpha_I \sigma_y} \qquad (2.2.7)$$

where δ_I is the CTOD in mode I, with parameter,

$\alpha_I = \pi/4$ [24],

$\alpha_I = 1$ [25], and

σ_y is the yield strength.

Crack growth will occur when δ_I reaches a critical value, δ_{IC}. The CTOD fracture criterion has also been extended to be used in elastic-plastic fracture mechanics. It will be discussed further in Section 2.3.

4. CRACK TIP DEFORMATION

The elastic stress-field equations (2.2.2a) produce large stresses in the vicinity of the crack tip when $r \rightarrow a$. However, this is not the case, as a small amount of plastic deformation occurs around the crack tip. To account for

this plasticity, the plastic zone size , r_y , was estimated by,

$$r_y = \frac{1}{2\pi}\left[\frac{K_{Ic}}{\sigma a}\right]^2 \qquad \text{for plane stress, and} \qquad (2.2.8a)$$

$$r_y = \frac{1}{6\pi}\left[\frac{K_{Ic}}{\sigma a}\right]^2 \qquad \text{for plane strain.} \qquad (2.2.8b)$$

This plastic zone was considered part of the crack length. Equation (2.2.3) then becomes,

$$K_I = F(g)\ \sigma \sqrt{\pi (a + r_y)} \qquad (2.2.9)$$

The plastic zone size will differ through the thickness of a specimen (Figure 2.2.4). The plastic zone will be smaller at the interior, which is in plane strain, than at the surface which is in plane stress. Therefore, the plastic zone correction is only valid for small plastic zone sizes, which are dependent on the specimen geometry.

From the testing procedures outlined in ASTM:E399-83, plane strain conditions are assured, or LEFM may be used when,

$$t > \left[\frac{K_{Ic}}{\sigma_y}\right]^2 \quad \text{and} \quad a > \left[\frac{K_{Ic}}{\sigma_y}\right]^2 \qquad (2.2.10)$$

where t is the specimen thickness, and a is half the effective crack length. Or alternatively when,

$$B \text{ or } 2a > 15\ r_y \qquad (2.2.11)$$

where B is the width of the specimen and r_y is the plastic zone size defined by equations (2.2.8).

2.3 ELASTIC-PLASTIC FRACTURE MECHANICS (EPFM)

Elastic-Plastic Fracture Mechanics (EPFM) attempts to describe the complex mixture of elastic and plastic deformation processes occurring in the fracture of a thin wall pipe. The application of the Crack Tip Opening Displacement and the R-6 EPFM methods of predicting failure in structures under small and large scale plasticity are discussed in this section. The popular J-Integral method of EPFM analysis, used extensively in this thesis, is discussed in Chapter 3.

1. Crack Tip Opening Displacement (CTOD)/Crack Tip Opening Angle (CTOA)

The definition of CTOD and the basic concepts behind it were outlined in Section 2.2, Linear Elastic Fracture Mechanics. Because CTOD measurements can be taken even when significant plasticity exists ahead of the crack tip, CTOD is a prime candidate for EPFM analysis.

Several researchers have related the CTOD to the crack surface displacement at different distances from the crack tip [26,27]. The relationship is normally logarithmic for elastic and perfectly plastic materials. A critical value of CTOD at the crack tip under certain conditions can be obtained, which can be considered a material parameter. However, CTOD has only been found reliable for small amounts of crack growth. For large scale plastic deformation the Crack Tip Opening Angle (CTOA) was developed. The CTOA is defined as the angle between the slopes of the crack faces close to the crack tip (Figure 2.3.1).

The CTOA, both theoretically and experimentally, has been found to rise to a constant value, after an initial period of variation, as a crack lengthens under extensive plastic deformation [28,29]. The crack is purported to grow

when CTOA reaches or exceeds some critical value. Numerous reports have cited success [30,31] in using the CTOA approach for plasticity cases.

2. R-6 Method

This method was proposed by Dowling and Townley [32] of the Central Electricity Generating Board (CEGB) of the United Kingdom. Harrison et al [33] modified this approach into a failure assessment diagram as shown in Figure 2.3.2 . The assessment curve is calculated from,

$$K_r = K_I/K_{IC} \qquad (2.3.1a)$$

$$S_r = \sigma/\sigma_I \equiv \text{plastic collapse parameter} \qquad (2.3.1b)$$

where K_I is the stress intensity factor,
K_{IC} is the fracture toughness of the material,

σ is the applied stress on the structure, and
σ_I is the plastic collapse stress defined by,

$$\sigma_I = (\sigma_y + \sigma_u) / 2 \qquad (2.3.2)$$

where σ_y and σ_u are the yield and ultimate stresses, respectively.

For a particular flaw size, structure, and material, the coordinates (S_r',K_r') are calculated and plotted. If this point is found to lie within the assessment curve, the structure will not fail.

This model, similar to the CTOD approach, considers the material to be elastic-perfectly plastic. Bloom [14,34] developed multiple assessment

curves using a deformation plasticity approach to handle elastic-plastic deformation. However, available curves are limited to low alloy steels under plane strain conditions with flaws remote from any discontinuities.

It should be noted that the EPFM parameters discussed in this section will produce different results depending on whether the flow theory or the deformation theory of plasticity is used. These two fracture theories and the differing parameters based on each are illustrated in Figure 2.3.3. Generally, and for this thesis, only the deformation theory is considered.

The effectiveness of the EPFM parameters discussed in this section as compared to the J-Integral will be discussed in Chapter 3.

2.4 LEAK-BEFORE-BREAK THEORY

Sections 2.2 and 2.3 of this thesis outlined the general methods currently in use to categorize a material's behavior. A specific level of performance for a particular structure or specimen then needs to be identified to assure quality or safety control. The Leak-Before-Break criterion was developed by Irwin et al [1] to estimate the necessary toughness of pressure-vessel and piping steels to ensure that a surface crack would grow through the wall and "leak" before catastrophic failure.

The first mode of failure for pressure-vessel or piping components is leaking, while the second is catastrophic failure. The purpose of a quality control parameter should, of course, be to design a component so that no failure should occur. However, due to economic and technical factors, this is not always possible. Therefore, in most cases a component is designed to withstand the first mode of failure, i.e. Leak-Before-Break.

Figure 2.4.1 illustrates how a surface crack in elliptical shape might propagate through a pipe wall into a through-thickness crack of length $2t$, where t is the pipe wall thickness. The Leak-Before-Break theory predicts a critical crack size, $2a$, from the K_{IC} value for the material. If plastic yielding is localized and the curvature is relatively small,

$$a_c = (K_{IC} / \sigma_y)^2 / \pi \qquad (2.4.1)$$

where a_c is the critical crack length = $2a$,

K_{IC} is the critical stress intensity factor, and

σ_y is the yield stress.

For larger curvatures, alternate expressions are available to calculate a_c [5]. Further details of the Leak-Before-Break theory are outlined in the ASME Boiler and Pressure Vessel Code, Section XI [44].

If it can be assumed a leaking situation will occur, allowing the leak to be detected and used as an early warning signal for effective remedial actions, the Leak-Before-Break design technique is acceptable [21]. However, no thermal effects are considered in the Leak-Before-Break theory, which could discount the desirability for the leaking assumption.

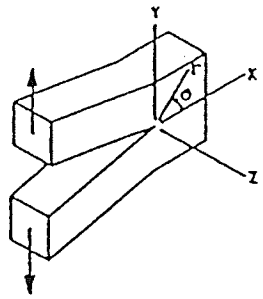

MODE I

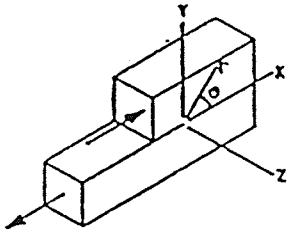

MODE II

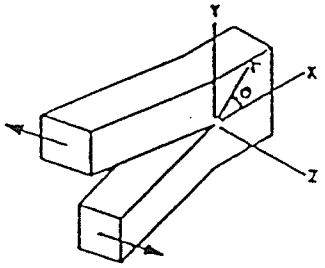

MODE III

FIGURE 2.2.1 : The Three Modes of Fracture, Mode I : Opening, Mode II : Sliding, and Mode III : Tearing.

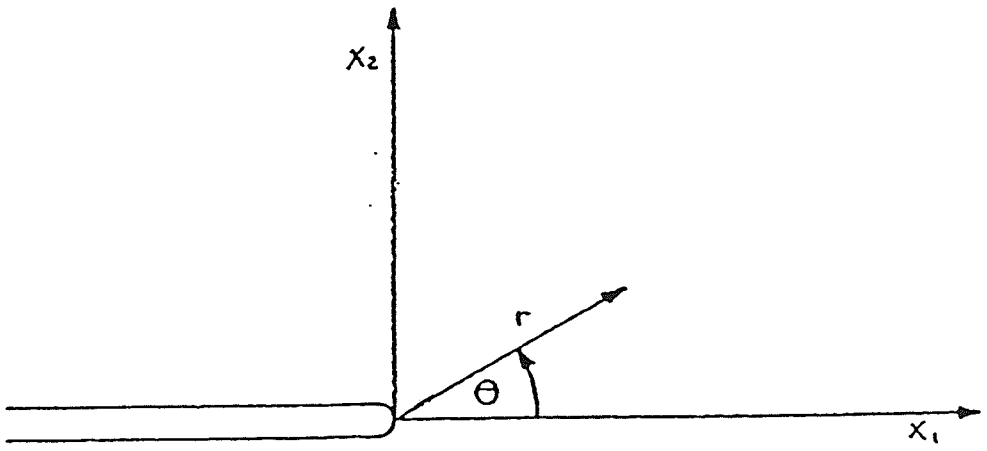

FIGURE 2.2.2 : Crack Tip Coordinates

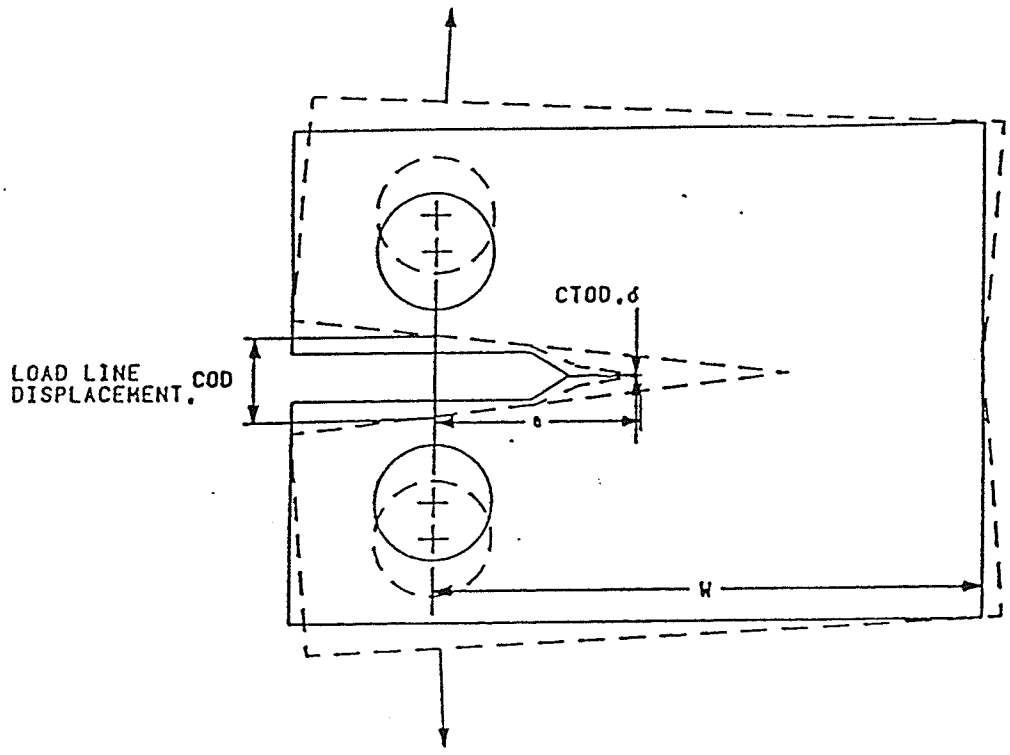

FIGURE 2.2.3 : Definition of COD and CTOD

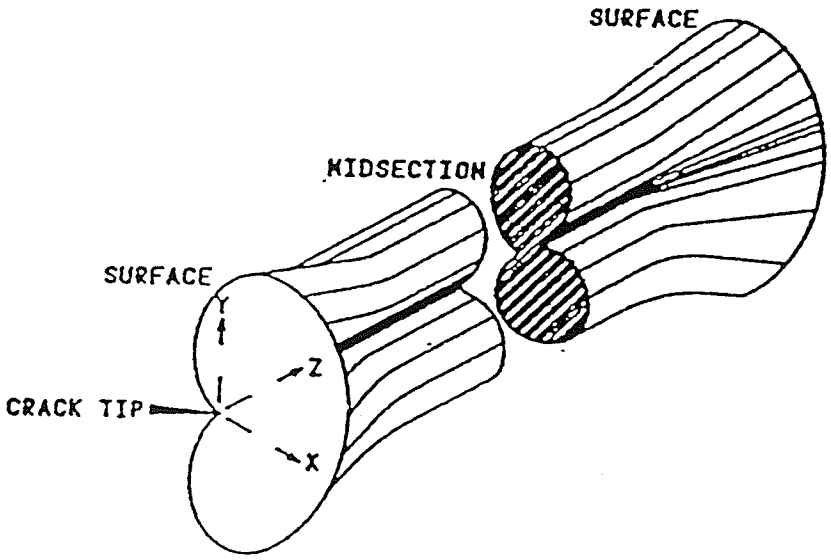

FIGURE 2.2.4 : Plastic Zone Variation Through Wall Thickness

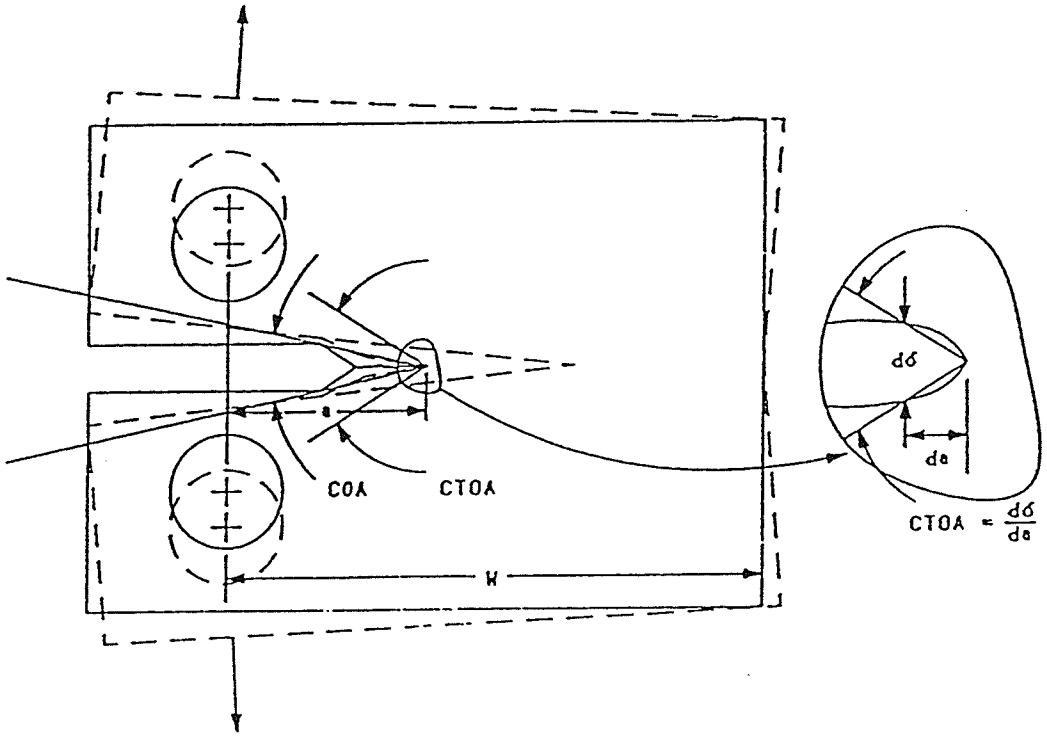

FIGURE 2.3.1 : Definition of COA and CTOA

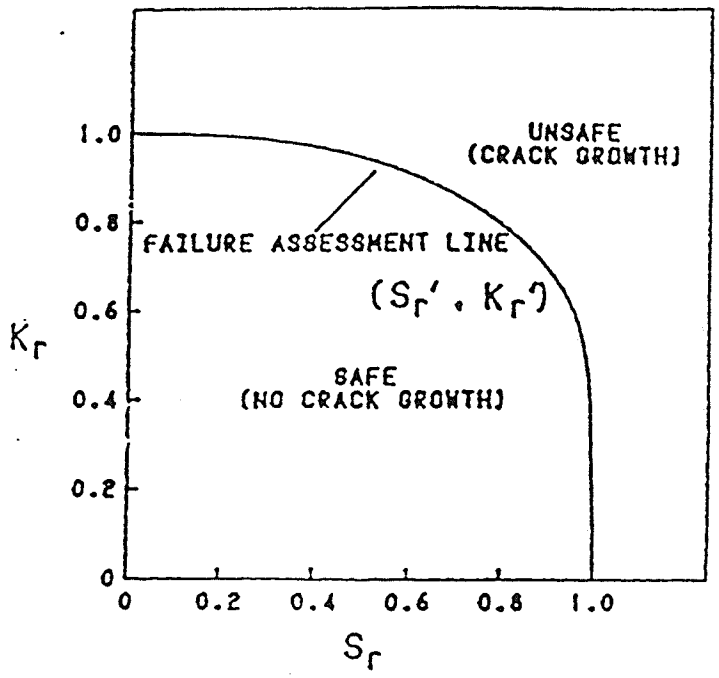

FIGURE 2.3.2 : R-6 Failure Assessment Diagram [34]

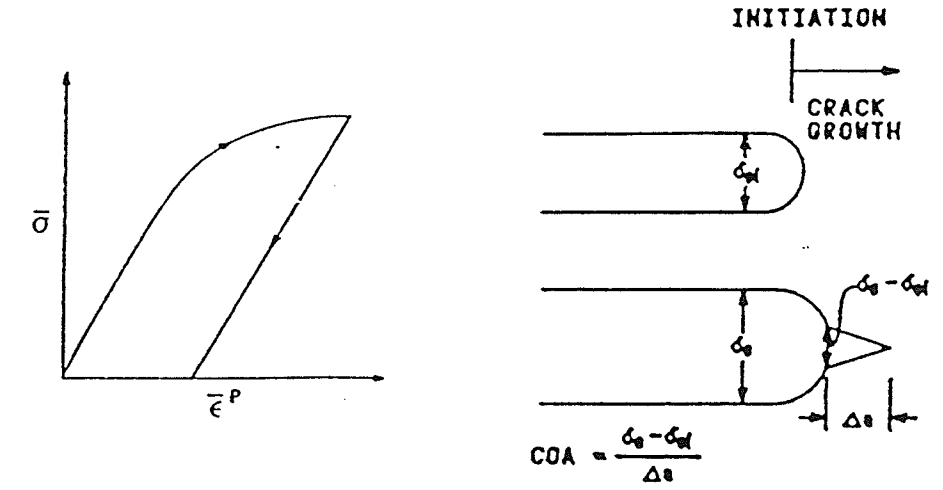

FLOW THEORY

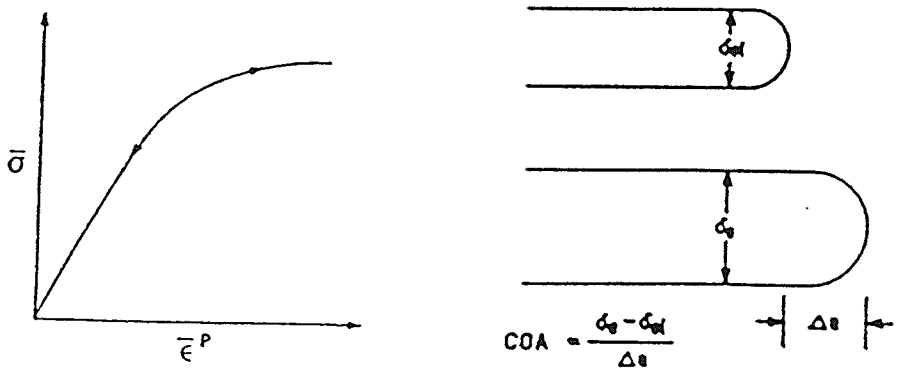

DEFORMATION THEORY

FIGURE 2.3.3 : Idealized Constitutive Behavior of Equivalent Stress, $\bar{\sigma}$, as a Function of Equivalent Strain, $\bar{\epsilon}^p$, and Crack Opening Angles Associated with Flow and Deformation Theories [45]

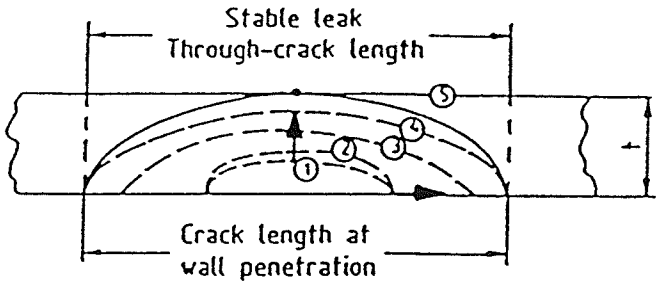

① Surface crack at start of plant

② Surface crack after plant life

③ max. surface crack leading to a stable leak after plant life

④ Surface crack at ligament-instability

⑤ Stable leak

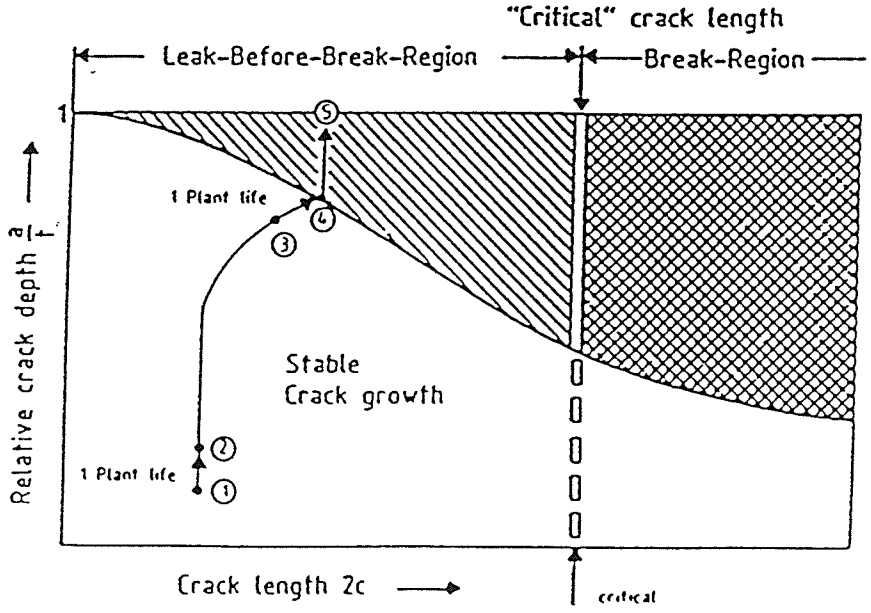

FIGURE 2.4.1 : Principles of Crack and Failure Behavior in a Structure for Leak-Before-Break Fracture Analysis

CHAPTER 3. MATHEMATICAL FORMULATION OF J-INTEGRAL WITH THERMAL EFFECT

3.1 GENERAL

The J-Integral technique is a relatively new approach to EPFM analysis. Rice [3] proposed this path independent integral as a method of characterizing the stress-strain field at the crack tip. Because of the path independency feature of the J-Integral, an integration path can be taken far from the crack tip which encompasses the plastic region near the crack tip, but uses a smoother distribution of stresses and strains away from the crack tip region. The J-integral can thus achieve much better results than other more straightforward techniques for stress anaylsis of the crack region.

The J-Integral with thermal effect is also discussed in this chapter. This integral is an extension of the J-Integral to include combined thermal and mechanical loadings, rather than simply the mechanical loading.

The following sections will also discuss the assumptions inherent in the formulation, the ease of determination and the limitations of the J-Integral and the J-Integral with thermal effect.

3.2 J-INTEGRAL

An elastic-plastic crack tip solution for power hardening solids under symmetric opening loads was first proposed by Hutchinson [35] and Rice and Rosengren [36]. This solution is referred to as the HRR solution. Referring to Figure 3.2.1, the HRR field equations for stationary cracks are,

$$\sigma_{ij} = \sigma_y \tilde{\sigma}_{ij}(\theta,n) \left[\frac{E J}{\sigma_y^2 I(n) r}\right]^{1/(n+1)} \qquad (3.2.1a)$$

$$\varepsilon_{ij} = \sigma_y \tilde{\varepsilon}_{ij}(\theta,n) \left[\frac{E J}{\sigma_y^2 I(n) r}\right]^{1/(n+1)} \qquad (3.2.1b)$$

where n is the strain hardening exponent, a material property,

σ_y is the yield stress,

r is the radial distance from the crack tip,

θ describes the angular position of r from the plane of crack surfaces,

I(n) is an integration constant which is a function of n,

$\tilde{\sigma}_{ij}$ and $\tilde{\varepsilon}_{ij}$ are dimensionless functions of θ and n.

Note that these equations approach a 1/r singularity as r approaches zero.

The J-Integral is generally considered to be the potential difference between two different crack lengths in a loaded body. Referring to Figure 3.2.2 , the J-Integral, J, is expressed by [6],

$$J = \int_\Gamma \left[W\, dx_2 - T_i \frac{\delta U_i}{\delta x_1}\right] ds \qquad (3.2.2)$$

where Γ is the path of integration around the crack tip,

W is the strain energy density function represented by,

$$W = \int_0^{\varepsilon_{mn}} \sigma_{ij} \, d\varepsilon_{ij} \qquad (m,n = 1,2) \qquad (3.2.3)$$

T_i is the traction vector, $T_i = \sigma_{ij} N_i$,

where N_i is the outward unit normal vector perpendicular to the path of integration, Γ,

ε_{ij} are the components of the elastic strain,

U_i is the displacement vector, and

ds is the arc length along Γ, and x_1 and x_2 are the axes which define the coordinate system centered at the crack tip.

This expression for J has been proven independent of paths used for the integration and is valid for applications where,

1. body forces can be neglected,
2. inertia effects can be neglected,
3. only a two-dimensional application is needed,
4. the material is homogeneous,
5. the crack is assumed to grow in a direction parallel to the crack surfaces,
6. the material is assumed to be linear elastic or nonlinear elastic with small scale plastic yielding.

Formulations of J-Integral encompassing these restrictions are available [6,8,10]. However, they are not discussed here as the relation described is sufficient for the application used in this thesis.

The HRR field equations under the above assumptions reduce to [36],

$$\sigma_{ij} = \lambda \varepsilon_{kk} \delta_{ij} + 2 \mu \varepsilon_{ij} \qquad (3.2.4a)$$

$$\varepsilon_{ij} = \frac{1+\nu}{E} \sigma_{ij} - \frac{\nu}{E} \sigma_{kk} \delta_{ij} \qquad (3.2.4b)$$

where $\lambda = \dfrac{E\nu}{(1+\nu)(1-2\nu)}$, Lame's constant,

$\mu = G$, the shear modulus of elasticity,

δ_{ij} is the Kronecker delta (=0 for $i \neq j$, =1 for i=j)

and

$$W = \frac{1}{2} \sigma_{ij} \varepsilon_{ij} \qquad (3.2.5)$$

where W is the elastic strain energy density.

If the integration path is within a region of small scale yielding, J is simply equal to G for a mode I (opening) crack,

$$J_I = G_I = \frac{K_I^2}{E^*} \qquad (3.2.6)$$

where J_I is the mode I J-Integral,

G_I is the mode I strain energy release rate,

K_I is the mode I stress intensity factor, and

E^* is defined by equation (2.2.6).

Crack propagation is expected to occur when J exceeds an experimentally determined critical value, J_{IC}. It should be noted that as a fracture parameter J is confined to crack initiation rather than propagation, since J looses its significance under irreversible deformation.

The applicability of J is compared to the CTOD and CTOA methods of analyzing elastic-plastic fracture in Table 3.2.1. From this Table it is obvious that J should be used where direct local stress measurements are not necessary and a relatively simple approach is needed. J is ideal for the application required in this thesis.

3.3 THE JOULES-THOMPSON EXPANSION EFFECT

When an actuating medium flows from a high pressure to a low pressure region, through an orifice or slit, a temperature drop will occur in the medium [37]. This temperature drop is referred to as the throttling process or the Joules-Thompson expansion effect. It is an irreversible, isenthalpic process.

Consider a thin-wall pipe with a through wall crack. If the pipe contains saturated water, the water will leak through the crack, experiencing a pressure drop. This decrease in pressure will produce a sudden drop in the boiling point and evaporation will occur in the region of the open crack. The latent heat required for vaporization will be drawn from the saturated water causing local cooling near the crack [2].

The magnitude of the cooling is large, as illustrated by Hsu et al [2] by estimating the temperature drop of saturated water going from 13.8 MPa to 0.7 MPa. The enthalpy-entropy diagram was used to find that the water cools from a temperature of 335.4 °C (635.8°F) to 165.6°C (330° F) across this pressure difference. This is a temperature differential of 169.8 ° C (305.8° F), which is significant.

3.4 THE J-INTEGRAL WITH THERMAL EFFECT (J_T)

The path independency of the J-Integral is no longer valid when a temperature field is present around the crack tip. Because the throttling effect of leakage produces such a temperature field it is necessary to modify the J-Integral presented in Section 3.2 to incorporate thermal loading and still retain path independency.

If a temperature field, $T(x_1,x_2)$, exists, then the stress and strain energy density equations must be modified to include the induced thermal stresses. Therefore,

$$W' = W(\varepsilon'_{ij},T) = \frac{1}{2}\sigma'_{ij}\,\varepsilon'_{ij} = \frac{1}{2}\sigma'_{ij}\,(\varepsilon_{ij}-\alpha\Delta T\,\delta_{ij}) \qquad (3.4.1)$$

where α is the coefficient of linear thermal expansion, a material property,

ΔT represents an incremental temperature variation,

ε_{ij} is represented by equation (3.2.4b),

and σ'_{ij} is σ_{ij} including a thermal component, or,

$$\sigma'_{ij} = \lambda\,\varepsilon_{kk}\delta_{ij} + 2\,\mu\,\varepsilon_{ij} - \frac{E}{(1-2\nu)}\,\alpha\Delta T\,\delta_{ij} \qquad (3.4.2)$$

where the variables λ, δ_{ij}, and μ are defined as in equation (3.2.4).

Using these expressions, an expression can be derived which retains path independency for J_T.

Referring to Figure 3.4.1 the J-Integral, modified to incorporate a tempera-

ture field, J_T, is expressed by [2,7,10],

$$J_T = \int_\Gamma \left[W'\delta x_2 - T_i \frac{\delta U_i}{\delta x_1} ds \right] + \int_{Ao} \alpha \sigma'_{ii} \frac{\delta T}{\delta x_1} dA \qquad (3.4.3)$$

where J_T is the thermal J-Integral

W' and σ'_{ii} are as in equations (3.4.1) and (3.4.2), respectively,

T represents the temperature field $T(x_1,x_2)$,

Ao is the area enclosed by the contour Γ,

U_i, ds, x_1, x_2 , and Γ are as in equation (3.2.2).

The thermal J-Integral, J_T, is subject to the same restrictions as the J-Integral in Section 3.2.

	J* J-INTEGRAL	COD* CRACK-OPENING DISPLACEMENT	CTOA LOCAL CRACK-OPENING ANGLE
Measure of Near-Tip Field	Yes	Yes	Yes
Constant During Crack Extension	No	No	Yes
Independence of Specimen Geometry	Mildly Dependent	Mildly Dependent	Mildly Dependent
Applicability to Instability Analyses	+Yes	+ Yes	+ Yes
Generalizable to Mixed Mode Fracture	Probable	Uncertain	Uncertain
Ease of Computation	Simple	Moderately Simple	Moderately Difficult
Sensitivity to Mesh, Process Zone and Increment Size	No	Mildly	Mildly
Direct Local Measurement	No	Possible	Difficult
Direct Global Measurements	Yes	Possible	No

* J and COD are employed as resistance parameters.

\+ For limited crack extension.

TABLE 3.2.1 : Comparison of J-Integral, COD, and CTOA Fracture Parameters [45]

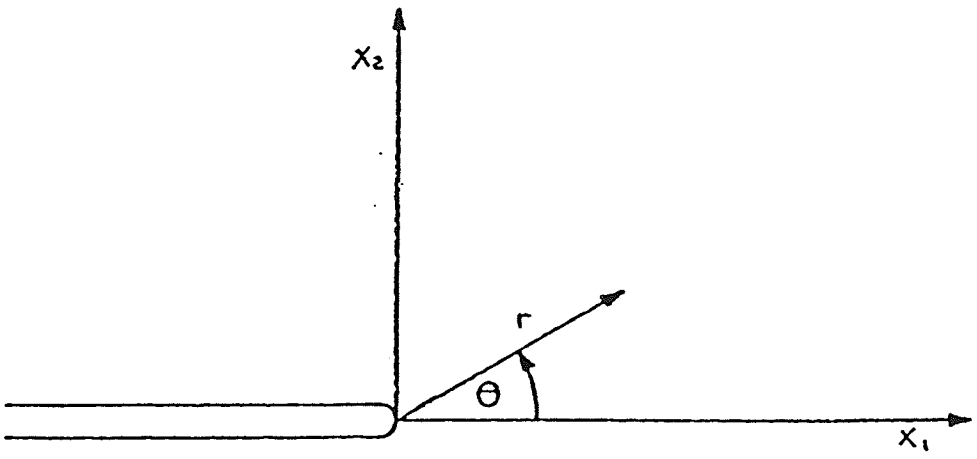

FIGURE 3.2.1 : Crack Tip Coordinates

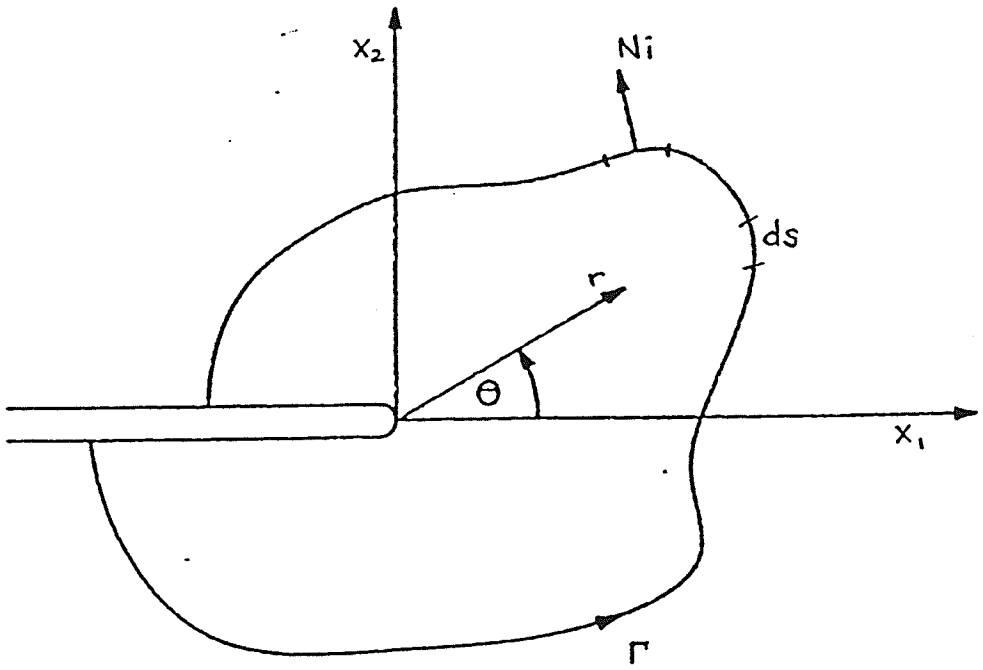

FIGURE 3.2.2 : Definition of J-integral Variables

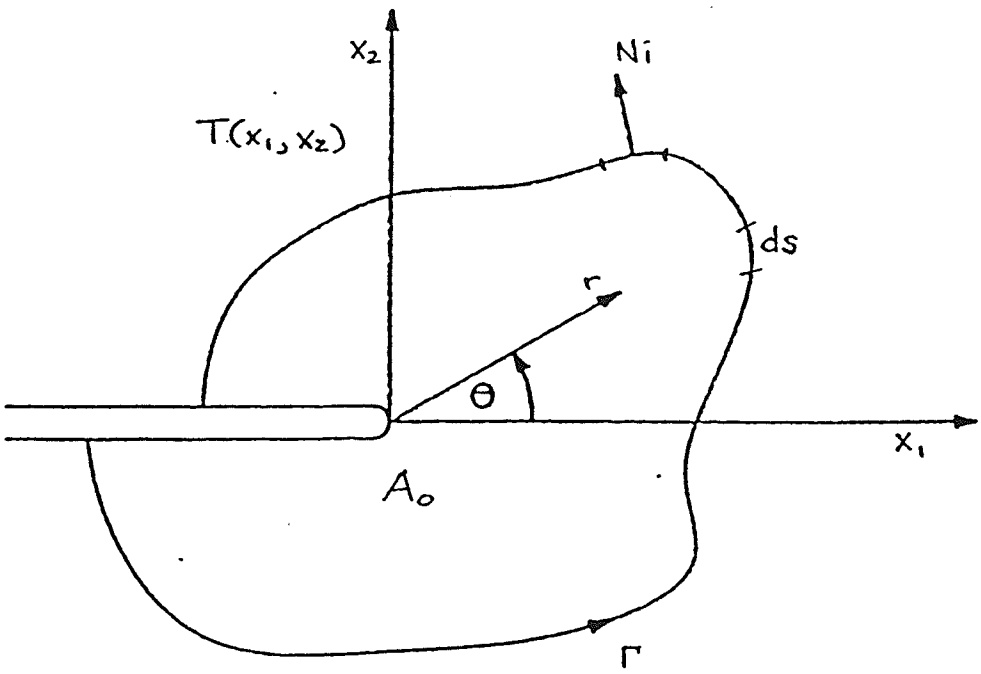

FIGURE 3.4.1 : Definition of Thermal J-integral Variables

CHAPTER 4. FORMULATION OF FINITE ELEMENT ANALYSIS

4.1 GENERAL

The finite element method (FEM) is a critical factor in the design and operation of equipment and structures. Because of complications in empirical techniques, numerical techniques, such as FEM, using the power of computers, are required. ANSYS finite element code [38] was used for all of the FE work done in this thesis.

Only the basics of FE analysis will be presented in this chapter. The numerical method of calculating the thermal J-Integral will be discussed. The details of the numerical solution of static and thermal problems, relevant to this thesis, are discussed in Appendix I.

The hybrid experimental-numerical method used in this thesis will also be discussed, including the inverse heat conduction method required to determine a temperature field from temperatures measured at isolated points.

4.2 DISCRETIZATION AND FINITE ELEMENT ANALYSIS (FEM)

In Figure 4.2.1a, a body is shown under specified actions, which produce various reactions. Because of the complexity involved to solve a problem with a large number of degrees of freedom by close form solutions, FEM is used. The continuum is subdivided into a finite number of elements connected by nodes. This is termed discretization of the body. The advantage to this is that the analysis only has to be applied to the individual elements of simple geometries, rather than the entire structure.

Once the body is discretized, the resulting nodes are entered into a FE program by their locations with respect to a specified global or local coordinate system. Elements are then defined by listing the nodes composing the element. Other information required by most FE programs are;

1. Material properties (either linear or non-linear)
2. Boundary conditions (fixed points or displacements)
3. Loading conditions (forces, pressures, temperatures, etc.)

For J-integral analysis, the path of integration must be defined.

From this model, the FE program then uses methods similar to those described in Appendix I and in [39,40], to solve for the reaction forces, displacements and stresses in the structure. Therefore, an accurate and appropriate model is essential to accurate FE analysis. Figure 4.2.1b illustrates a possible discretized model for the structure shown in Figure 4.2.1a under the given loading conditions [39].

4.3 CALCULATION OF THE J-INTEGRAL WITH THERMAL EFFECT

Consider a center-cracked plate subject to a distributed bi-axial mechanical loading, and under a temperature field inducing thermal strains. A finite element model for such a loading situation is shown in Figure 4.3.1 . The contour required to determine the thermal J-Integral is also shown.

The J-Integral with thermal effect, refering to Figure 3.4.1, was defined in Chapter 3 as;

$$J_T = \int_\Gamma \left[W' dx_2 - T_i \frac{\delta U_i}{\delta x_1} \right] ds + \int_{Ao} \alpha \sigma'_{ii} \frac{\delta T}{\delta x_2} \, dA \qquad (4.3.1)$$

where x_1,x_2, Γ and Ao are illustrated in Figure 3.4.1.

T_i is the surface traction normal to the contour, Γ,

U_i is the displacement vector of elements on the contour,

σ'_{ii} the normal stress components of elements on and within the contour,

α is the thermal expansion coefficient,

T is the temperature field on the plate,

W' is the strain energy density calculated from,

$$W' = \int_0^{\varepsilon'_{mn}} \sigma'_{ij} \, d\varepsilon'_{ij} \qquad (m,n=1,2) \qquad (4.3.2)$$

where the thermomechanical strain is found from,

$$\varepsilon'_{ij} = \varepsilon_{ij} - \alpha \Delta T \, \delta_{ij} \qquad (4.3.3)$$

ε_{ij} are the strain components due to mechanical loading,

δ_{ij} is the Kronecker delta as defined in equation 3.2.4, and

ΔT is the temperature differential.

The discretized form of equation(4.3.1), for FE analysis, can be written as [39];

$$J_T = \sum_{m=1}^{M} \left[W_m \Delta y_m - \left[(t_x)_m \left[\frac{\Delta u}{\Delta x} \right]_m + (t_y)_m \left[\frac{\Delta v}{\Delta x} \right]_m \right] \Delta S_m \right]$$

$$+ \quad \alpha \sum_{n=1}^{N} \left[\sigma_{xx,n} + \sigma_{yy,n} + \sigma_{zz,n} \right] \left[\frac{\Delta T}{\Delta x} \right]_n A_n \qquad (4.3.4)$$

where M is the total number of elements along the contour Γ,

m is a subscript denoting the mth element along Γ,

N is the total number of elements on and enclosed by Γ,

n is a subscript denoting the nth element in the region bound by Γ,

W_m is the strain energy in the mth element,

ΔS_m is the path length across element m,

Δy_m is the y- component of ΔS_m,

$(t_x)_m$ and $(t_y)_m$ are the surface tractions acting on ΔS_m in the x- and y-directions respectively,

Δu_m and Δv_m are the respective element displacement components in the x- and y-directions,

$\sigma_{xx,n}$ is the stress component in element n in the x-direction

$\sigma_{yy,n}$ is the stress component in element n in the y-direction,

$\sigma_{zz,n}$ is the stress component in element n in the z-direction,

ΔT_n is the temperature differential in element n,

A_n is the area of element n.

4.4 HYBRID EXPERIMENTAL-NUMERICAL METHOD

The temperature field used to calculate the thermal J-Integral can either be assumed [2], or found through experimentation. The former method is generally used because of the difficulty in determining a temperature field from temperature measurements at specific points. However, an experimentally determined temperature field is preferred since it exactly represents the physical model.

Most heat conduction problems involve the determination of the temperature at specific interior points when a temperature distribution or initial and boundary conditions are known. For a two-dimensional situation, Busby and Trujillo [41], devised a scheme to reverse this process, known as the inverse heat conduction solution.

This inverse heat conduction scheme was used by Hsu et al [19], to determine the temperature distribution around a longitudinal crack in a leaking thin wall pipe containing saturated water under pressure. Thermocouples were affixed to the specimen around the crack tip and a temperature field determined from these data points. ANSYS finite element software [38] "design optimization" was used in this thesis, rather than the inverse heat conduction algorithm, to determine the crack surface temperature from the experimentally measured temperature data. The ANSYS solution procedure is described in Section 6.3.

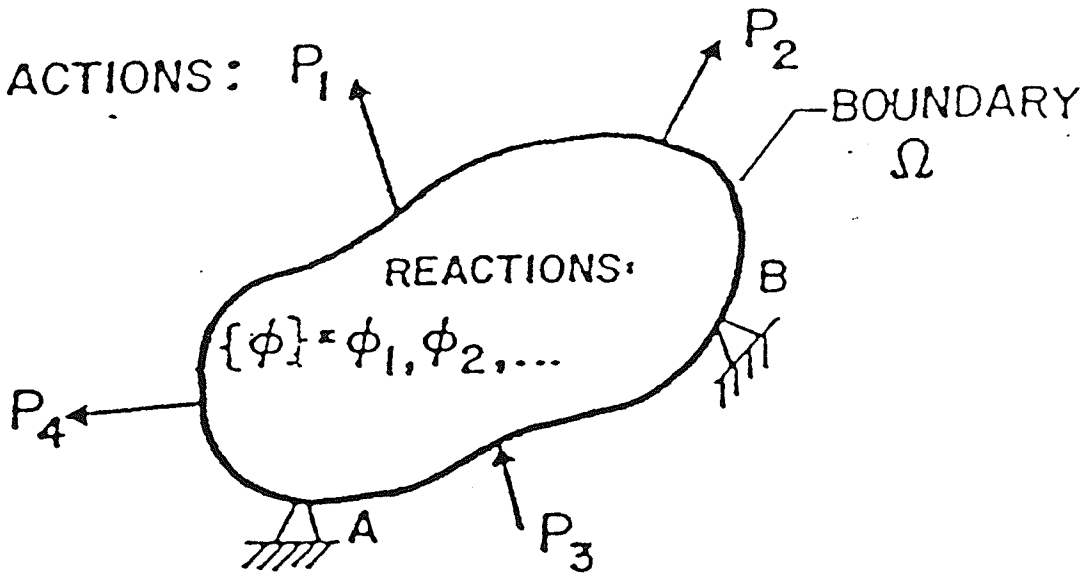

(a) Original Body

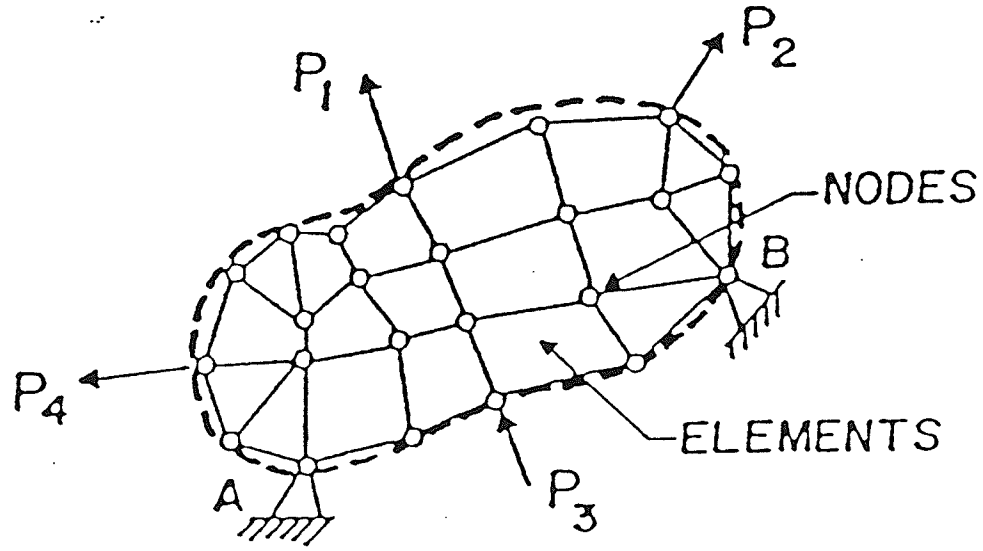

(b) Discretized Body

FIGURE 4.2.1 : (a) Body Under Applied Loads and Boundary Conditions
(b) Discretized Model of Body in (a)

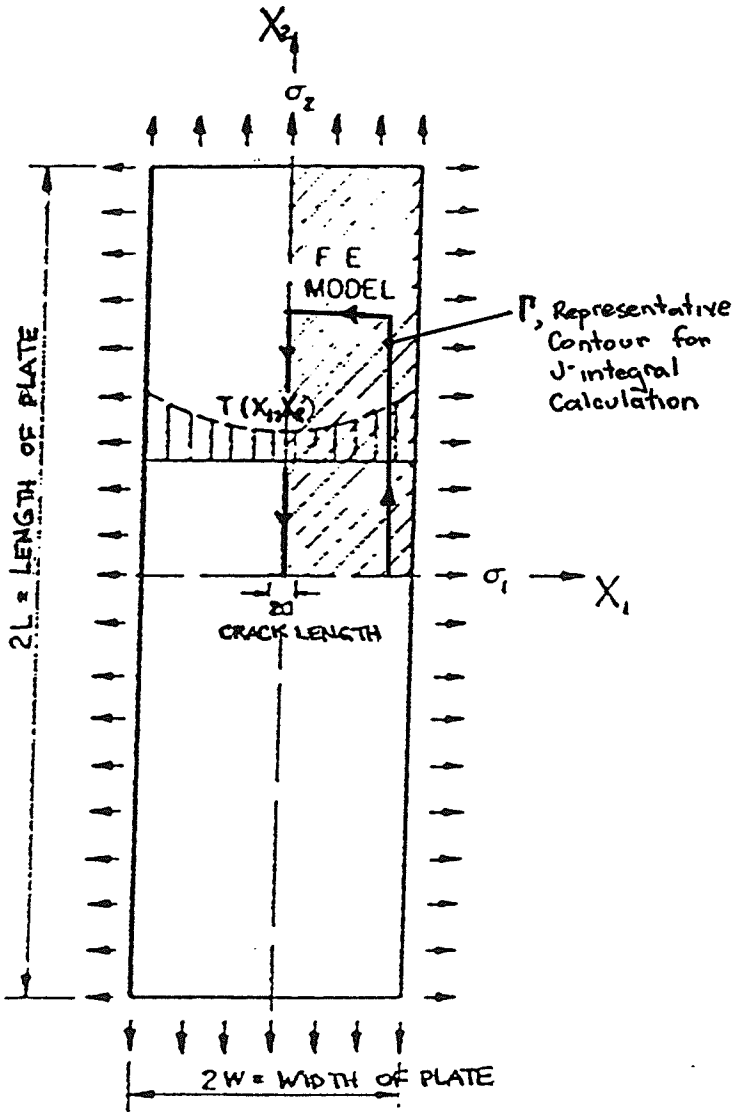

FIGURE 4.3.1 : Finite Element Model of a Plate Under Bi-axial Load with a Temperature Field

CHAPTER 5. EXPERIMENTAL PROGRAM

5.1 GENERAL

An experimental program to assess the effects of internal pressure and crack length on the thermal effect was required. Three specimens of varying longitudinal crack lengths, but with otherwise similar geometries were prepared. These specimens were tested under three different internal pressures.

This experimental approach should yield correlations between crack length, pressure, the J-integral and the thermal J-integral.

The experimental set-up, the specimen geometry and material parameters, the data acquisition and measurement procedure and apparatus, and the experimental procedure are outlined in this chapter. The results and the discussion of results are presented in Chapter Seven.

5.2 EXPERIMENTAL SET-UP

A schematic representation of the apparatus is shown in Figure 5.2.1 , with a photograph of the apparatus shown in Figure 5.2.2. A high pressure water tank, heated by immersion heaters, supplies stagnant, saturated water to the test specimen. The immersion heaters are plugged in and begin to heat the water. As the water expands under heating it comes under pressure. As heating continues the water becomes saturated (definition). Further heating is required to bring the water to a predetermined testing condition. An additional immersion heater is required in the pipe section below the test specimen to maintain a constant temperature in the bulk saturated water.

Both the pressure and the temperature of the tank are monitored to insure that the correct test conditions are attained. Supplementary pressure, required to maintain the internal pressure during leakage is supplied by the nitrogen tank.

For the leakage tests, a copper shim is soldered into the longitudinal crack, preventing the water from escaping the closed system. The shim is then pulled out by a manual car jack, when testing conditions are reached, allowing the saturated water to escape. The pressure tank is secured to the table by brackets to prevent movement of the tank and the specimen when the shim is removed.

Thermocouples mounted to the test specimen are monitored by an IBM-PC computer modified to act as a Data Acquisition Unit (DAU). The data acquisition sequence is started before leakage begins to ensure no data is missed.

A complete list of the specifications of the equipment used in this experiment is given in Appendix II.

5.3 SPECIMEN GEOMETRY AND MATERIAL PROPERTIES

As mentioned previously, three specimens are required, with geometries as illustrated in Figure 5.3.1. The specimens differ in crack length only. The crack orientations are the same, longitudinal, and the pipe wall thickness is 2 mm for all specimens. The three specimens have crack lengths of 6, 9 and 12 mm, respectively, all 0.1 mm in width. The calculations required to prove the pipe to be thin-wall and conform to safety standards are shown in Appendix III.

The cracks were all cut with an immersion arc welder, using a special copper cutting tool.

The pipe material is Electric Resistance Welded (ERW) ASME A513-73, 1026 plain carbon steel tubing. The properties and specifications are as follows [42];

Tensile Strength, σ_u	552 MPa (80 ksi)
Yield Strength, σ_y	483 MPa (70 ksi)

0.22 - 0.28 % Carbon, 0.60 - 0.90 % Manganese,
0.04 % Phosphorous - Maximum, 0.05 % Sulphur - Maximum

Specific Gravity	7.86
Density, ρ	7860 kg/m^3 (0.283 lbs/in^3)
Solidus - Liquidus	1470 - 1500 °C
Thermal Conductivity, k	41.9 W/m °C (10 calories/ms°C)
Thermal Expansion Coefficient ,α	11×10^{-6} /°C
Elastic Modulus, E	0.2×10^6 MPa
Plastic Modulus, E'	1.82×10^4 MPa

The Plastic Modulus was calculated as shown in Appendix IV.

5.4 DATA MEASUREMENT AND ACQUISITION

Thermocouples, of K type 0.5 mm constantan wire, were spot-welded to the specimens at the locations shown in Figure 5.4.1. Because of the sensitivity of the thermocouple wire to noise and external influences, the free ends of the thermocouple wires were sheathed and run to a connection box, about six inches from the specimen. From the connection box, shielded, insulated wire was run to the Data Acquisition Unit (DAU).

An IBM-PC with a Tecmar Data Acquisition Board [43] was used to collect the temperature data. A fortran program was used to modify the sampling time and frequency of the measurements. A correction to the thermocouple resistance measured was also implemented so that the DAU produced readings in degrees Celsius.

5.5 EXPERIMENTAL PROCEDURE

The experiment was conducted at three different pressures, 1.0 MPa (145 psi), 1.5 MPa (217.5 psi), and 2.0 MPa (290.0 psi), for each specimen described in Section 5.3. Table 5.5.1 summarizes the experimental schedule. Referring to Figure 5.2.1, the following steps were carried out, for each of the nine tests;

(a) Before attaching thermocouples, inserting the copper shim, or attaching the specimen to the water tank, the specimen was cleaned with sandpaper and degreaser.

(b) Thermocouples were spot-welded at the appropriate locations, as shown in Figure 5.4.1.

(c) The copper shim was soldered into place, using 50-50 lead-tin solder, with a melting point of 250°C, and a propane torch. One of the thermocouples attached to the specimen was used to monitor the surface temperature of the specimen to ensure good adhesion of the solder.

(d) The specimen was bolted to the water tank at one end, and the lower immersion heater, H2, at the other end. High pressure washers were inserted in between each connection to prevent leakage.

(e) Thermocouple lead wires were attached to the shielded wires from the DAU at the connection box.

(f) The cable from the car jack was fastened to the copper shim. A double check was made to be sure the car jack was lowered, before attaching the cable.

(g) Insulation was wrapped as closely around the specimen as possible, to prevent excessive heat loss.

(h) The lower immersion heater, specimen, and water tank were filled with tap water. The upper thermocouple was removed to allow air to escape as the tank filled, and then replaced.

(i) Immersion heaters H1 and H2 were plugged in.

(j) The water tank temperature was monitored by the water tank thermocouple, TWT. The surface temperature of the specimen was monitored by one of the thermocouples on the specimen.

(k) The correct operation of the thermocouples on the specimen was checked by periodically running the DAU for short, five second intervals.

(l) Approximately thirty to sixty minutes was required for the water temperature and pressure to equalize to the correct values. Equalization was accomplished by unplugging and replugging in the immersion heaters until a uniform temperature was sustained at all thermocouples for several minutes.

(m) Once the test conditions, outlined in Table 5.5.1 were sustained, the car jack was raised until the cable exerted some force on the copper shim, but not enough to dislodge it. This was done to reduce the time required to remove the copper shim once data acquisition was started.

(n) The pressure on the nitrogen tank was set to the same pressure inside the water tank, depending on the test conditions. The valve on the top of the water tank was then opened, allowing nitrogen into the top of the tank. This ensured a constant water pressure inside the tank when the copper shim

was removed.

(o) Data acquisition was started. Readings were taken from all thermocouples every 0.02 seconds.

(p) The car jack was raised, pulling the copper shim from the crack.

(q) After approximately one minute from the time the copper shim was removed, the nitrogen tank was shut off, and the DAU stopped.

(r) Before all of the water leaked from the tank, both immersion heaters were unplugged to prevent them from burning out.

(s) The apparatus was allowed to cool for three to four hours before the next test.

(t) The specimen was unbolted from the apparatus, the thermocouple lead wires to the connection box disconnected, and the specimen removed.

For each of the nine tests, steps (c) through (t) were repeated. For step (c), if the specimen had already been tested at one pressure, and subsequently already had the copper shim soldered in place once, excess solder was removed and the area cleaned before reinserting and resoldering the copper shim.

Steps (a) and (b) were only repeated if a thermocouple became detached from the specimen during testing, in which case, only the loose thermocouple would be rewelded. This happened on several occasion when the action of

the copper shim being pulled out and the high pressure water leaking from the crack dislodged a thermocouple.

The steam escaping from the open crack dispersed throughout the room in which the testing was done. Great care was taken so that no electrical equipment got wet. Safety precautions such as eye goggles, a protection screen, an electrical shutdown switch and pressure release valve were used for all tests.

SERIES	CRACK LENGTH (mm)	INTERNAL PRESSURE (MPa)
1	6	1.0
2	6	1.5
3	6	2.0
4	9	1.0
5	9	1.5
6	9	2.0
7	12	1.0
8	12	1.5
9	12	2.0

TABLE 5.5.1 : Experimental Schedule

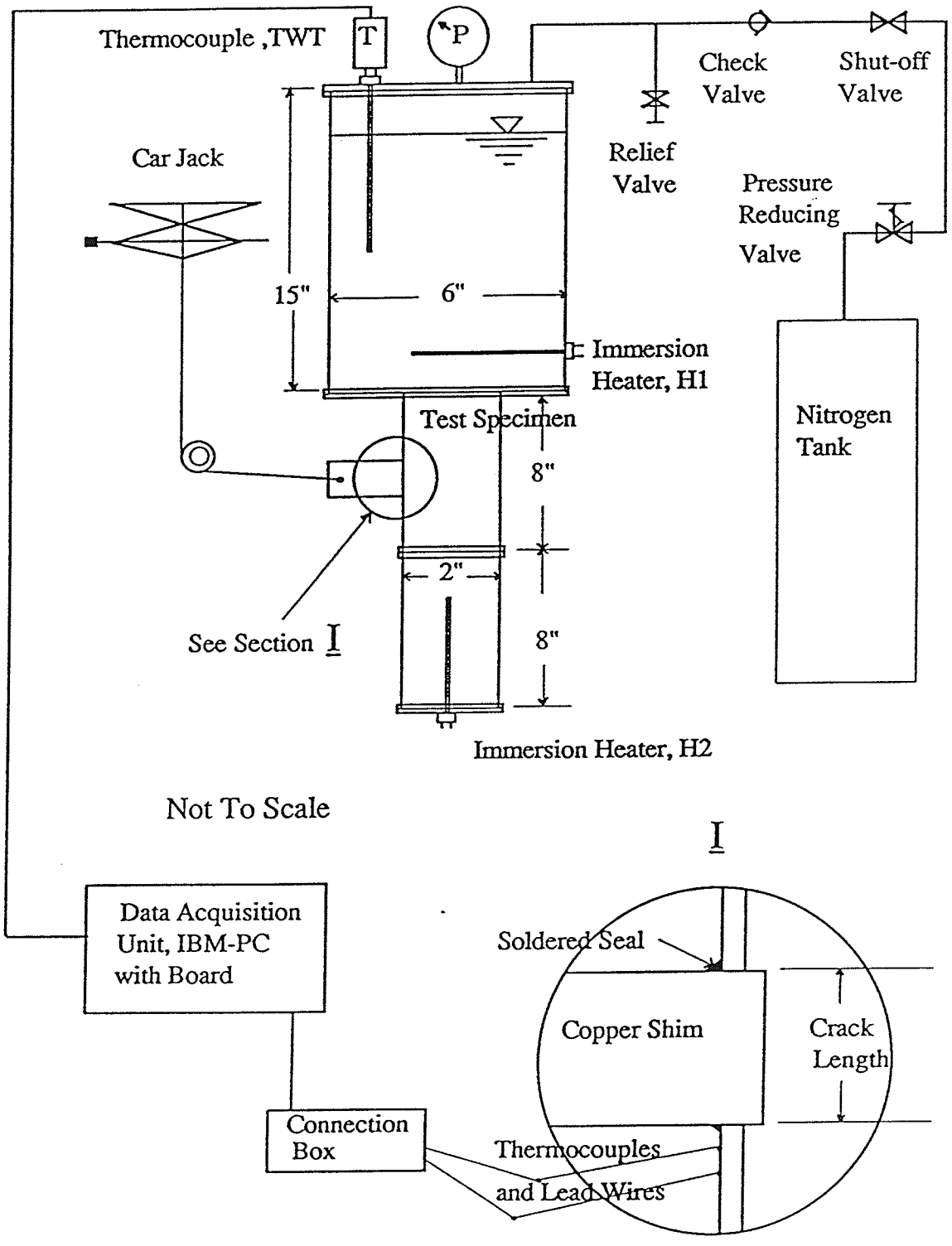

FIGURE 5.2.1 : Experimental Setup

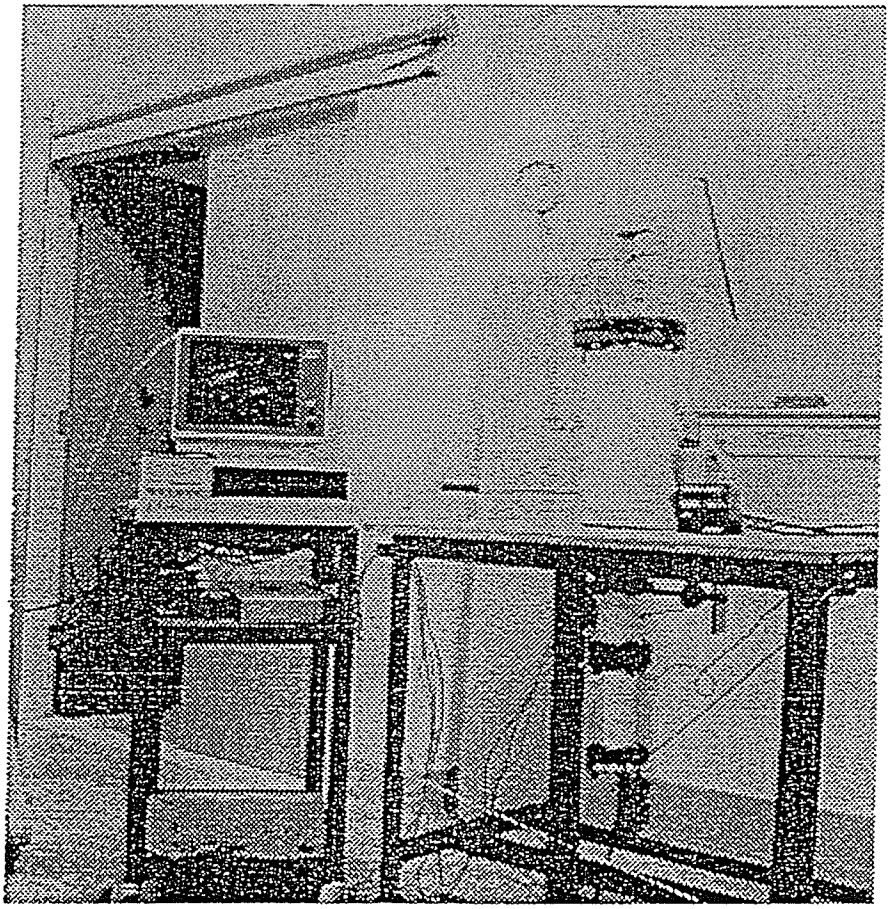

FIGURE 5.2.2 : Photograph of Apparatus

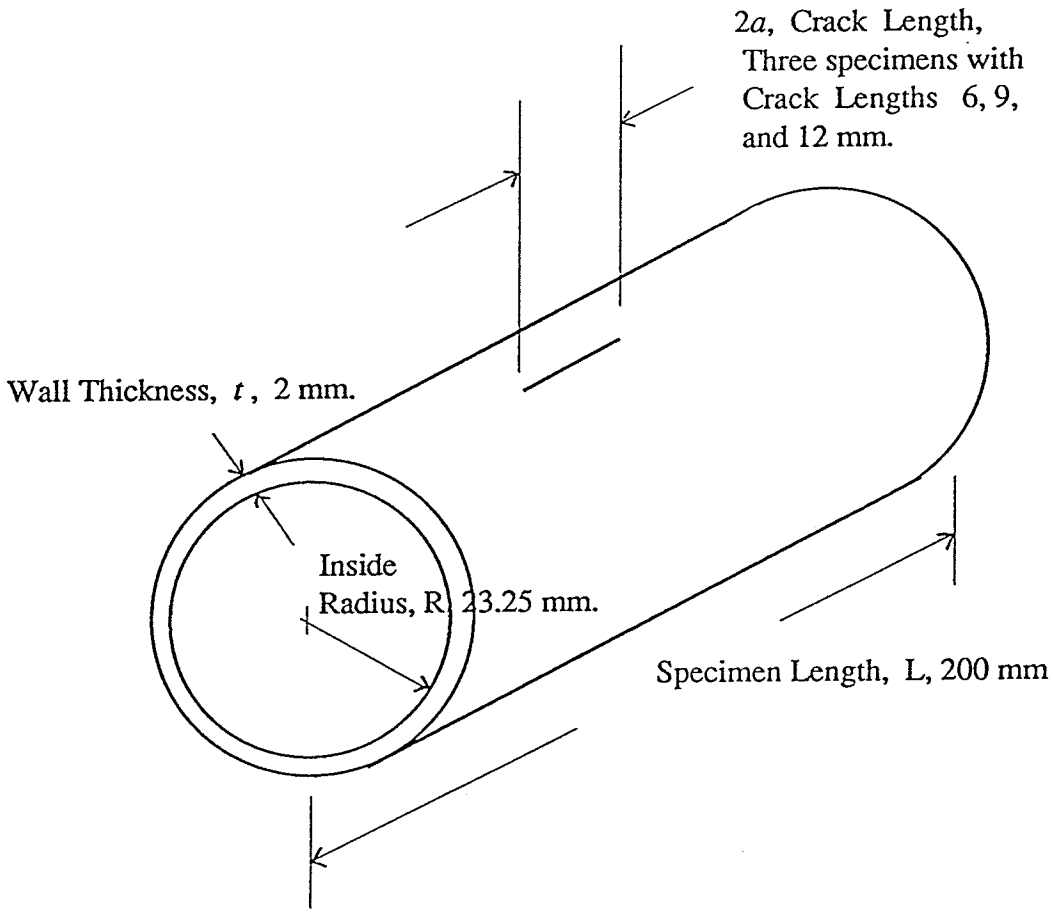

All specimens have welded, hubbed, raised face,
11/2 150 B16 A105-85N 98A KOF flanges on either end.

Pipe material is ASTM A-106 Grade B Seamless, Killed.

FIGURE 5.3.1 : Specimen Geometry

6 mm Crack Length
(#1 fell off and was not replaced)

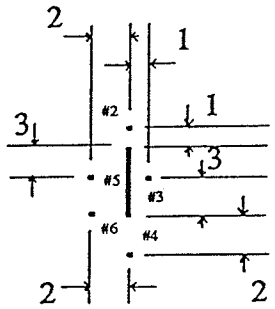

9 mm Crack Length
(#1 fell off and was not replaced)

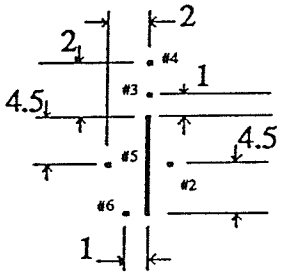

12 mm Crack Length

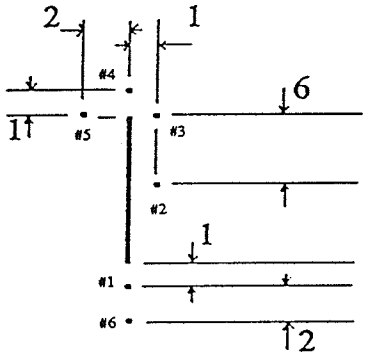

All Dimensions in Millimeters.
Not to Scale.

FIGURE 5.4.1 : Thermocouple Locations on Specimens

CHAPTER 6. NUMERICAL ANALYSIS

6.1 GENERAL

ANSYS finite element software [38] was used for the numerical analysis. Numerical analysis was used extensively to,

(a) determine the Crack Surface Temperature (CST) from the experimental data;

(b) calculate the temperature distribution from the CST;

(c) calculate the stress produced from the temperature distribution and internal pressure; and

(d) calculate the J-integral,

for all time steps of all load cases.

This chapter outlines the formulation of the base model used for all analyses, assumptions, boundary conditions, and loading for all numerical analyses.

6.2 FORMULATION OF THE BASE MODEL

The base finite element model used for all analyses is shown in Figures 6.2.1 through 6.2.5. The original curved surface of the thin-shell tube could be considered as a flat plate, as illustrated in Appendix V. A quarter model was used due to the symmetry of the geometry. The element types, boundary and loading conditions could then be adapted, depending on the analysis.

6.3 DETERMINATION OF CRACK SURFACE TEMPERATURE (CST) VERSUS TIME CURVES FROM EXPERIMENTAL DATA

ANSYS "Design Optimization" was used to determine the Crack Surface Temperature (CST) from the experimentally measured temperature data points. This procedure will be described for a general case, where temperature data has been measured by several thermocouples close to the crack surface, corresponding to nodes in the base model (Section 6.1), at an arbitrary constant test pressure. Data is taken over an arbitrary time span, divided into time steps. Referring to Figure 6.2.1, the surfaces at x=24 mm and y=24 mm are adiabatic, while the surfaces at x=0 mm and y=0 mm have symmetry boundary conditions applied.

An initial CST was specified for the first time step. ANSYS was programmed to run a thermal analysis with this initial CST, for only the first time step. ANSYS calculates the temperature distribution produced from the inital CST and compares the values it calculated for the thermocouple nodal locations to the measured values, which are input as parameters. The calculated and measured nodal temperatures are used to evaluate the minimization error function, ymil, where,

$$\text{ymil} = \sum_{n=1}^{N} |T_n - a_n| \qquad (6.3.1)$$

where N is the number of thermocouple locations,

T_n is the temperature measured at the nth thermocouple for the current time step,

a_n is the temperature ANSYS calculated for the node corresponding to the nth thermocouple location.

ANSYS then automatically varies the initially input CST, reruns the analysis with this value and recalculates ymil. ANSYS continues this process, attempting to minimize the error function. The value found for the CST

when the error function is minimized is the actual CST.

Once the CST for the first time step is found, it is input as the actual value for the first time step. The second time step is then added to the analysis file and an arbitrary value input for the CST for the second time step. The minimization procedure is repeated to find the actual CST for the second time step. This procedure is repeated until the actual CST for all time steps is known. A CST versus time curve can then be drawn.

The ANSYS "optimization" file used to minimize the error function and calculate the CST is shown in Appendix VI.

6.4 TRANSIENT THERMAL ANALYSIS

A transient thermal analysis was run for all nine tests. The crack surface time-temperature history calculated in Section 6.3 was applied to the nodes on the crack surface for all tests. Symmetric boundary conditions were applied to nodes not on the crack surface (Figure 6.2.1), at x=0 mm and the nodes at y=0 mm. Adiabatic boundary conditions were applied to the surfaces at x=24 mm and y=24 mm.

The temperature distribution around the crack was found for fifteen time instances; 0.0, 0.25, 0.5, 0.75, 1.0, 1.5, 2.0, 3.0, 4.0, 5.0, 6.0, 7.0, 8.0, 9.0, and 14.0 seconds from the time the copper shim was pulled from the crack. Five iterations were performed for each time interval to ensure convergence of the solution. The ANSYS input file for the transient thermal analysis is listed in Appendix VII.

6.5 STRESS ANALYSIS

Stresses induced by the temperature distributions from the transient thermal analyses and the internal pressure were found from the stress analysis. Symmetric boundary conditions were applied to nodes not on the crack surface (Figure 6.2.1), at x=0 mm and the nodes at y=0 mm.

The internal pressure load, Pi, was applied as a uniform pressure on the surfaces at x=24 mm and y=24 mm, where, referring to Figure 5.3.1 and Figure 6.5.1,

$$\sigma_1 = \frac{PiR}{t} \qquad \text{and} \qquad \sigma_2 = \frac{PiR}{2t} \tag{6.5.1}$$

These principle stresses are far from the crack tip and can therefore be calculated by these basic formulae. For pressures of 1.0, 1.5, and 2.0 MPa, σ_2 was calculated to be 6.6025, 9.09375, and 12.125 MPa, respectively. σ_2 was two times σ_1 in all cases. These principle stresses were used as the boundary conditions imposed on the edges of the finite element idealization of the pipe wall containing a crack as depicted in Figure 6.2.1.

The temperature distributions for all time intervals were read directly from the thermal analysis results file. Again five iterations were performed per time interval to ensure convergence of the solution. The ANSYS input file for the stress analysis is listed in Appendix VIII.

6.6 CALCULATION OF J-INTEGRAL

The J-integral is calculated using equation (4.3.4). An integration path is defined, along which the values required for equation (4.3.4) are extracted from the stress analysis results file. Referring to Figure 6.2.3, the integration paths specified for the three crack sizes were as follows,

Half Crack Length (Node at Crack Tip)	Nodes Defining J-Integral Path
3 mm (5)	7-27-23-3
4.5 mm (11)	13-33-29-9
6 mm (17)	19-39-35-15

The J-integral is calculated for each time step. The J-integral value at time, t= 0.0 seconds, represents the J-integral for the pressure loading only,J. The J-Integrals at all other time instants are the J-Integral including the thermal effect, J_T. The contribution of the thermal effect to J_T is assessed by calculating J_T/J for all time intervals. At time= 0.0 seconds, J_T/J is 1.0. A J/J_T versus time curve is found for all nine tests. From these curves, the effects of changes in crack length and internal pressure should be evident.

The ANSYS file to calculate the J-Integral are listed in Appendix IX.

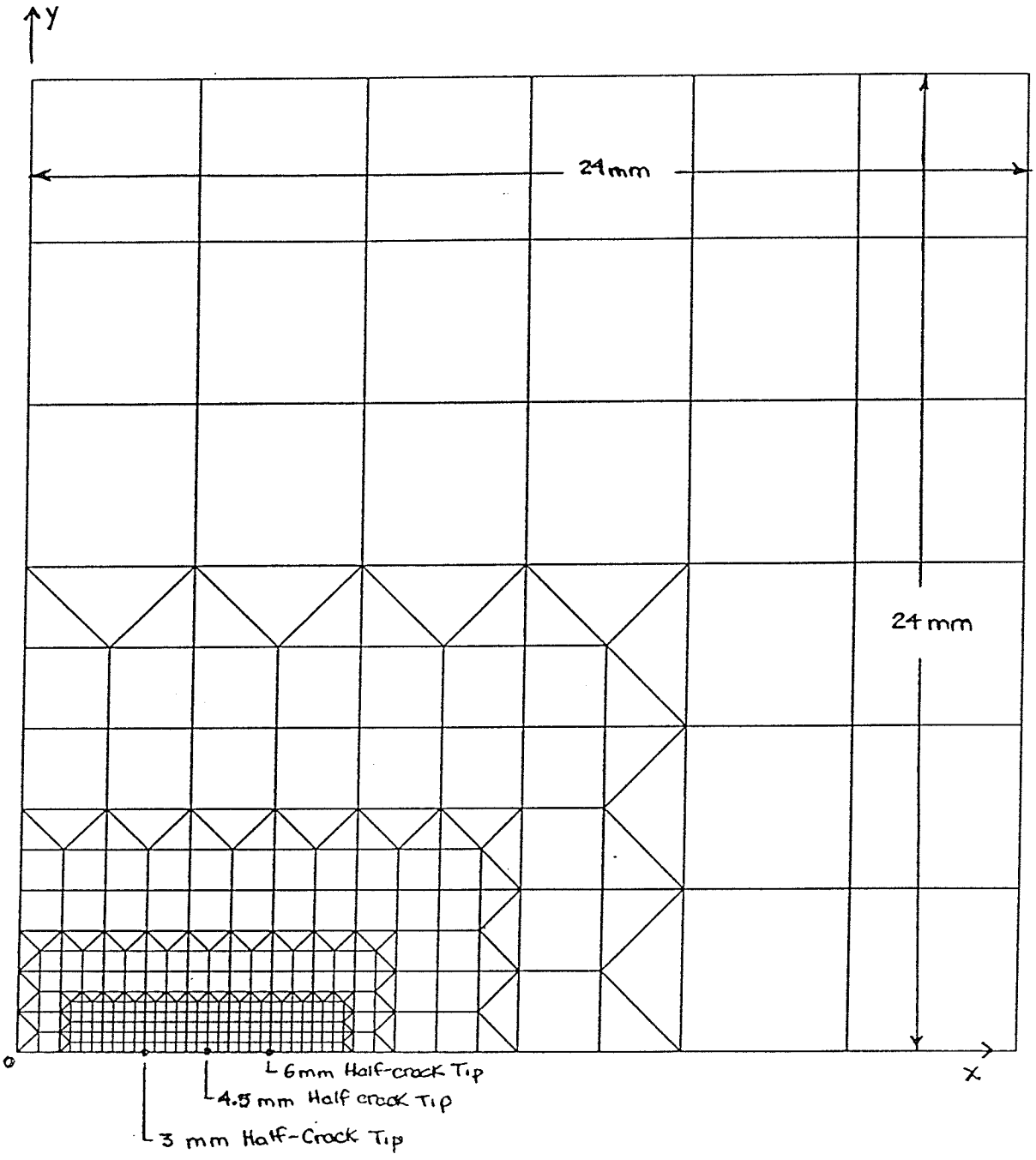

FIGURE 6.2.1 : Dimensions of Finite Element Model

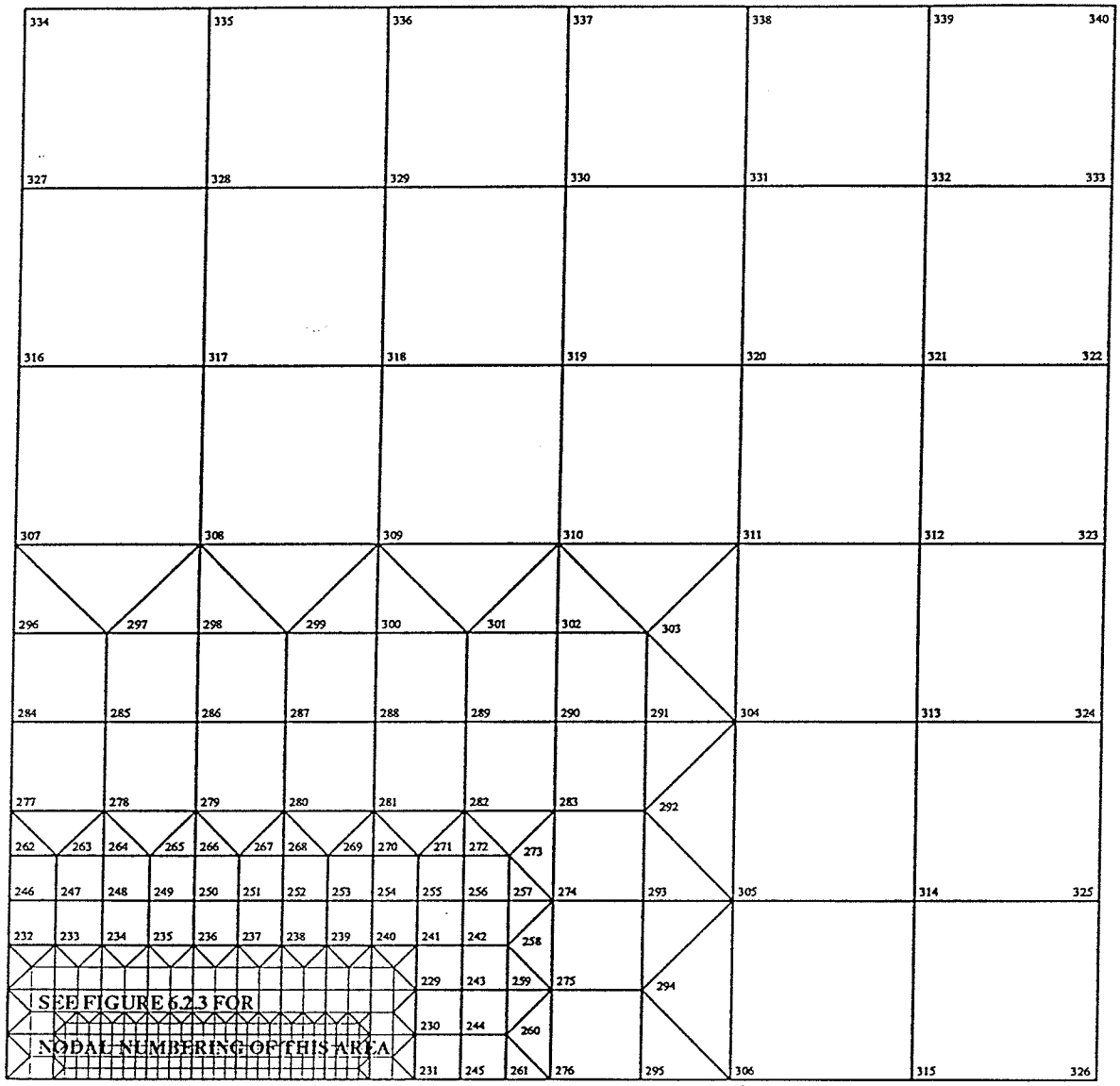

FIGURE 6.2.2 : Nodal Numbering of Finite Element Model

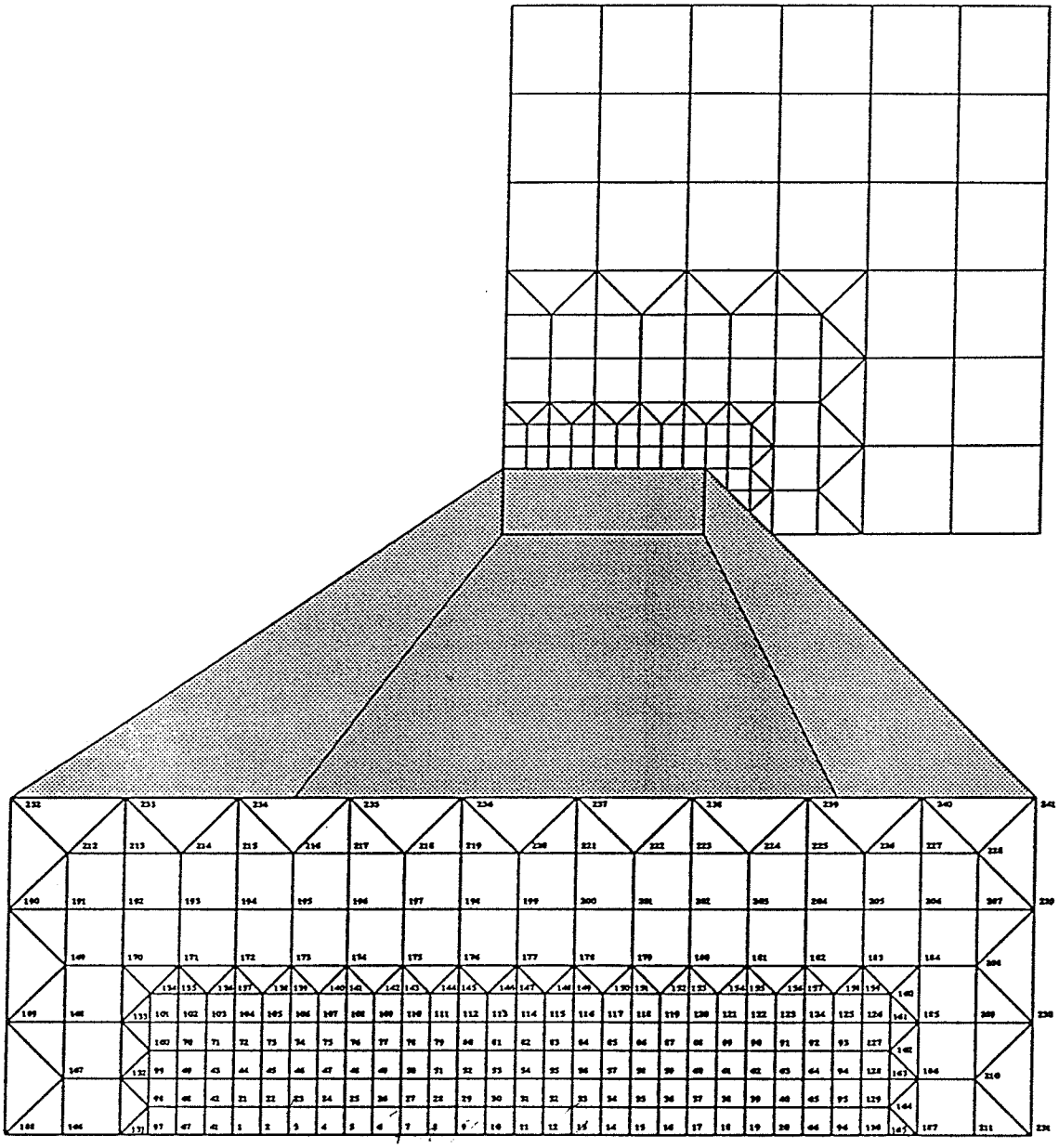

FIGURE 6.2.3 : Nodal Numbering of Section Specified in Figure 6.2.2

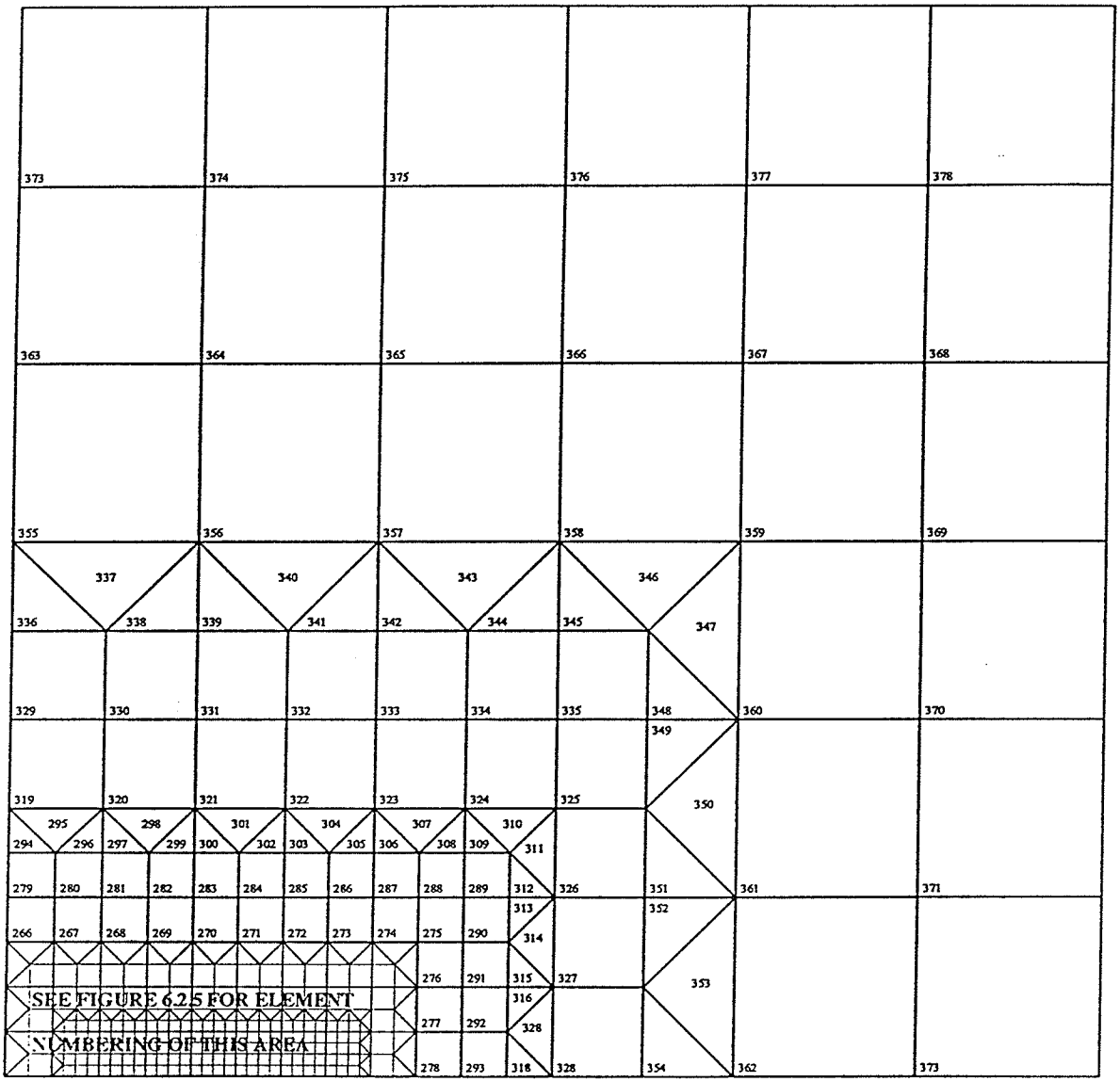

FIGURE 6.2.4 : Element Numbering of Finite Element Model

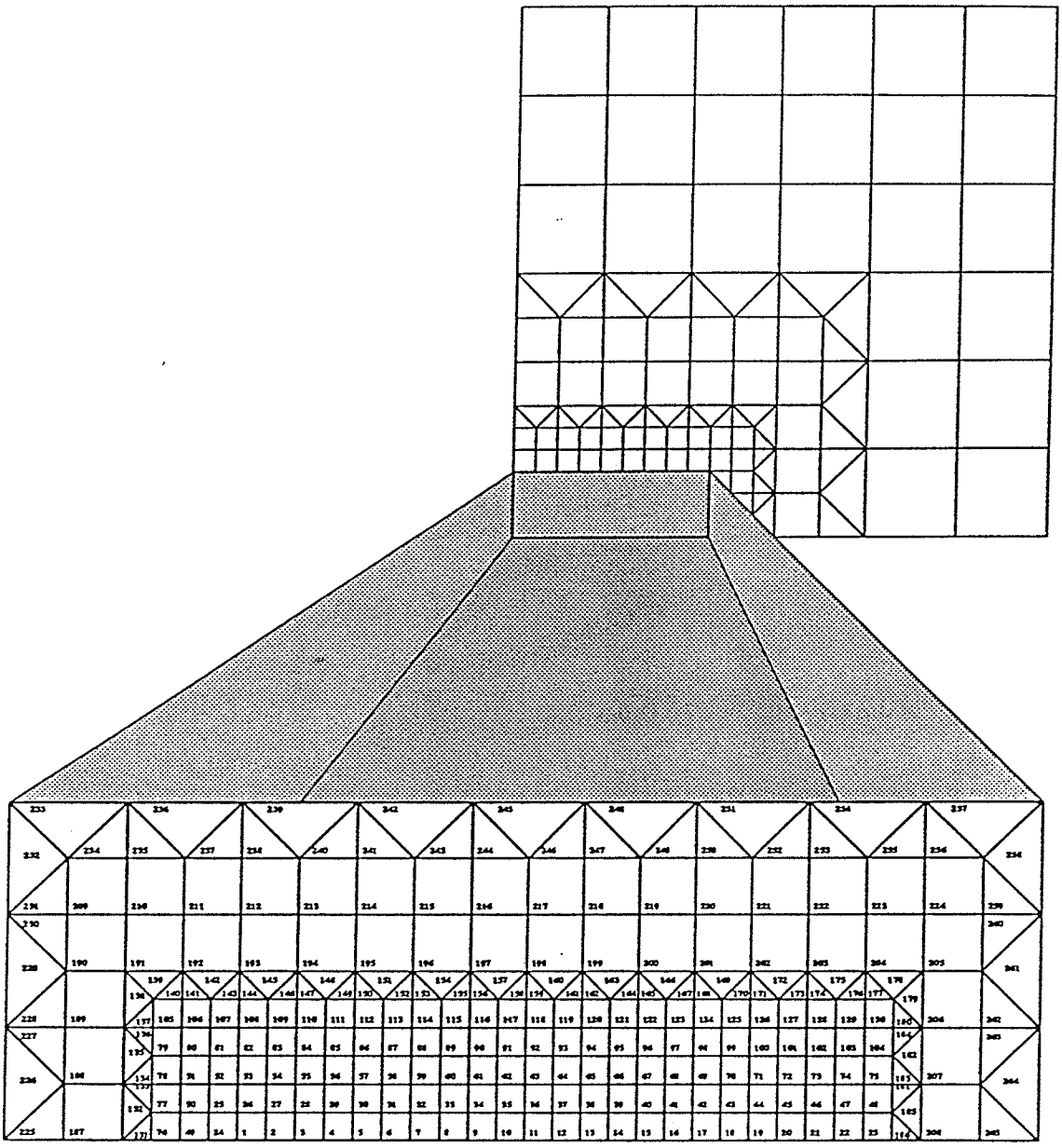

FIGURE 6.2.5 : Element Numbering of Section Specified in Figure 6.2.4

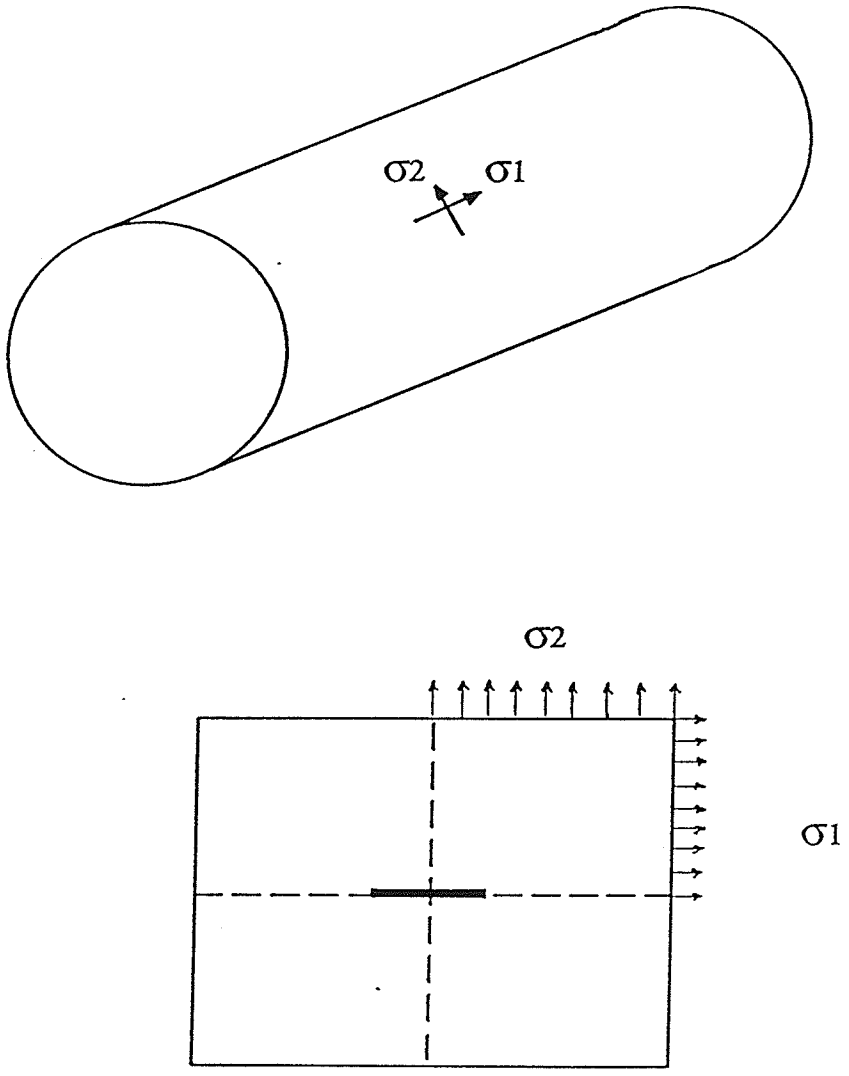

FIGURE 6.5.1 : Definition of σ1 and σ2

CHAPTER 7. RESULTS AND DISCUSSION

7.1 GENERAL

The Crack Surface Temperature (CST) versus time curves calculated by ANSYS (Section 6.3) from the experimentally measured temperature data, are shown in Figures 7.1.1a- f. Figures 7.1.1a, 7.1.1b and 7.1.1c show the CST versus time curves for series 1-3, 4-6, and 7-9, respectively. Figures 7.1.1d , 7.1.1e and 7.1.1f show the CST versus time curves for series 1,3 and 6; 2,4 and 7; and 3,5 and 9, respectively. The curve for the 12 mm crack at 2.0 MPa in Figure 7.1.1c correlated with the results obtained by Hsu et al [19], also shown in this figure. The ANSYS calculated temperature versus time curves for the thermocouple nodal locations were within 2 percent of the measured values.

The maximum effective stress, SIGE, occuring at the crack tip versus time is illustrated for all experimental series. Figures 7.1.2a through 7.1.2c show SIGE versus time curves for series 1-3, 4-6, and 7-9, respectively. Figures 7.1.2d through 7.1.2f show SIGE versus time curves for series 1,3 and 6; 2,4 and 7; and 3,5 and 9, respectively. These figures indicate that SIGE rises rapidly in the first few seconds of leaking, but begins to level off with a plateau at a constant value by time = 14.0 seconds. The effective stress distributions for series 1 through 9 (see Table 7.1.1 for series descriptions), at time = 14.0 seconds, are shown in Figures 7.1.3a through 7.1.3i, respectively. The temperature distributions producing these stress distributions are shown for series 1 through 9 in Figures 7.1.4a through 7.1.4i, respectively.

The distributions of temperature and effective stress were calculated using the CST versus time curves (Sections 6.4 and 6.5, respectively) at times ; 0, 0.25, 0.5, 0.75, 1.0, 1.5, 2.0, 3.0, 4.0, 5.0, 6.0, 7.0, 8.0, 9.0, and 14.0 seconds. Only the distributions at time = 14.0 seconds are presented as the distribution plots at the other time instances are not crucial to this discussion.

The temperature and stress distributions indicate that the cooling effect and the maximum stress are located in the vicinity of the crack tip. Very high effective stress at the crack tip is apparent in all cases. It should be noted, also, that the temperature gradients in all series decreased with an increase in time, eventually peaking and sustaining a maximum value.

J versus time curves for all series are shown in Figures 7.1.5a through 7.1.5f. In all cases the J value increased rapidly in the early stages of leaking, similarly to SIGE, and began to level off after two or three seconds. An approximately stable value was finally reached, dramatically higher than the initial value at time = 0.0 seconds, when no cooling effect was considered. J_T/J versus time curves for all series are shown in Figures 7.1.6a through 7.1.6f. These Figures show that the J value considering the thermal effect rose to a value 30 to 50 times larger than the purely mechanical J.

The results discussed in this section verify previous findings indicating that local cooling near a leaking crack in a pipeline could substantially increase the value of J, and subsequently reduce the critical crack size. Therefore, the Leak-Before-Break concept may be desirable for maintenance and safe operation pipeline design, but may be seriously offset by the thermal effect should leaking occur.

Sections 7.2 and 7.3 will more closely examine the effects of internal pressure and crack length, respectively.

7.2 EFFECT OF INTERNAL PRESSURE AND THE THERMAL EFFECT

An increase in internal pressure was found to increase the maximum effective stress, SIGE (Figures 7.1.2a-c), for a constant crack length. As leaking proceeded, the differential between SIGE values at each time interval also increased. This indicates that the thermal effect magnifies the effective stress as pressure increases.

Figures 7.1.5a-c show that the variation of the J-integral without thermal effect is approximately linearly proportional to the applied internal pressure. For example, a 50 percent increase in pressure was found to produce an approximately 50 percent increase in the mechanical J value. The peak values of the J-integral including thermal effect, reached after a few seconds of leaking, are approximately 50, 40 and 30 times larger than the purely mechanical J-integral for pressures of 1.0, 1.5, and 2.0 MPa, respectively, regardless of crack length (Figures 7.1.6a-c).

Figures 7.1.6a-c indicate a decrease in the peak J_T/J ratio reached during leaking for an increase in pressure. Although the peak J_T/J ratio decreases with pressure, the J_T/J ratio in the early stages of leaking increases with pressure. Figures 7.2.1a-c show the trend in the J_T/J ratio with pressure during leaking for all experimental series. At time=0.25 seconds the J-integral with thermal effect reaches values , for a 12 mm crack, approximately 8, 11 and 20 times larger than the purely mechanical J-Integral for pressures of 1.0, 1.5 and 2.0 MPa, respectively. Similar behavior is exhibited by the 6 and 9 mm cracks. Therefore, in the initial stages of leaking the J_T/J ratio increases significantly with increases in pressure.

Considering the high pressures used for some pipeline applications, the thermal effect is definitely an important factor for design. Depending on the pipe geometry, catastrophic failure upon leaking is more than likely.

7.3 EFFECT OF CRACK LENGTH AND THE THERMAL EFFECT

An increase in crack length was found to increase the maximum effective stress, SIGE (Figures 7.1.2d-f), for a constant internal pressure. As leaking proceeded, the differential between SIGE values at each time interval remained large. This indicates that the thermal effect magnifies the effective stress as crack length increases.

Figures 7.1.5d-f show that the variation of the J-integral without thermal effect is approximately linearly proportional to the applied internal pressure. For example, a 50 percent increase in pressure was found to produce an approximately 30 percent increase in the mechanical J value. The peak values of the J-integral including thermal effect, reached after a few seconds of leaking, are approximately 50, 40 and 30 times larger than the purely mechanical J-integral for pressures of 1.0, 1.5, and 2.0 MPa, respectively, regardless of crack length (Figures 7.1.6d-f) . This indicates that a longer crack length will increase the mechanical J-integral, but that the peak value with the thermal effect will remain constant.

Although the peak J_T/J ratio remains constant with crack length, the J_T/J ratio rises more rapidly for longer crack lengths. Figures 7.3.1a-c show the trend in the J_T/J ratio with changes in crack length during leaking for all series. At time=0.25 seconds the J-integral with thermal effect reaches values , for an internal pressure of 2.0 MPa, approximately 4, 10 and 20 times larger than the purely mechanical J-Integral for crack lengths of 6, 9 and 12 mm, respectively. Similar behavior is exhibited by the 1.0 and 1.5 MPa internal pressures. Therefore, in the initial stages of leaking the J_T/J ratio increases significantly with increases in crack length and catastophic failure is more likely to occur in the case of longer inital crack lengths when leaking occurs.

SERIES	CRACK LENGTH (mm)	INTERNAL PRESSURE (MPa)
1	6	1.0
2	6	1.5
3	6	2.0
4	9	1.0
5	9	1.5
6	9	2.0
7	12	1.0
8	12	1.5
9	12	2.0

TABLE 7.1.1 : Experimental Schedule

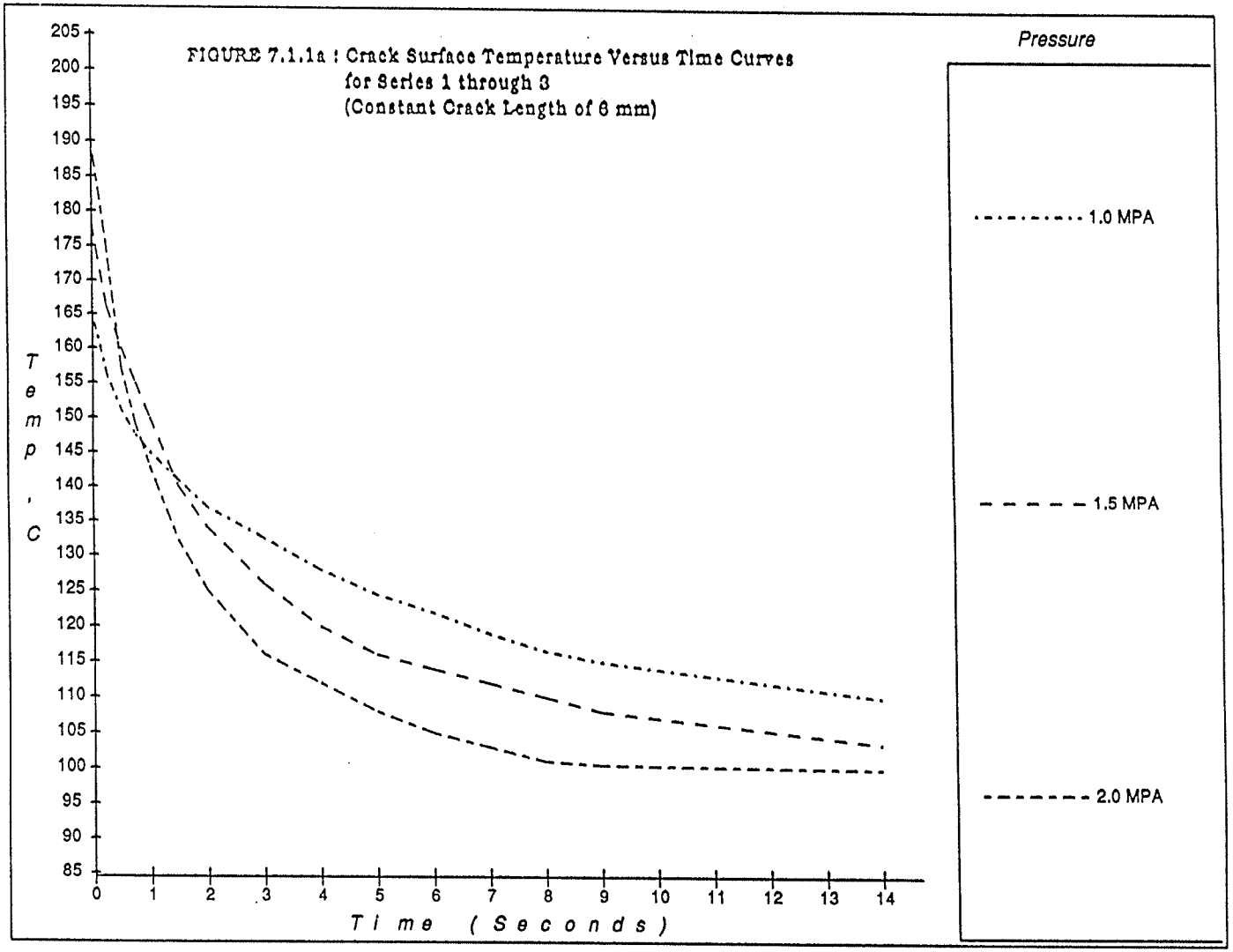

FIGURE 7.1.1a : Crack Surface Temperature Versus Time Curves for Series 1 through 3 (Constant Crack Length of 6 mm)

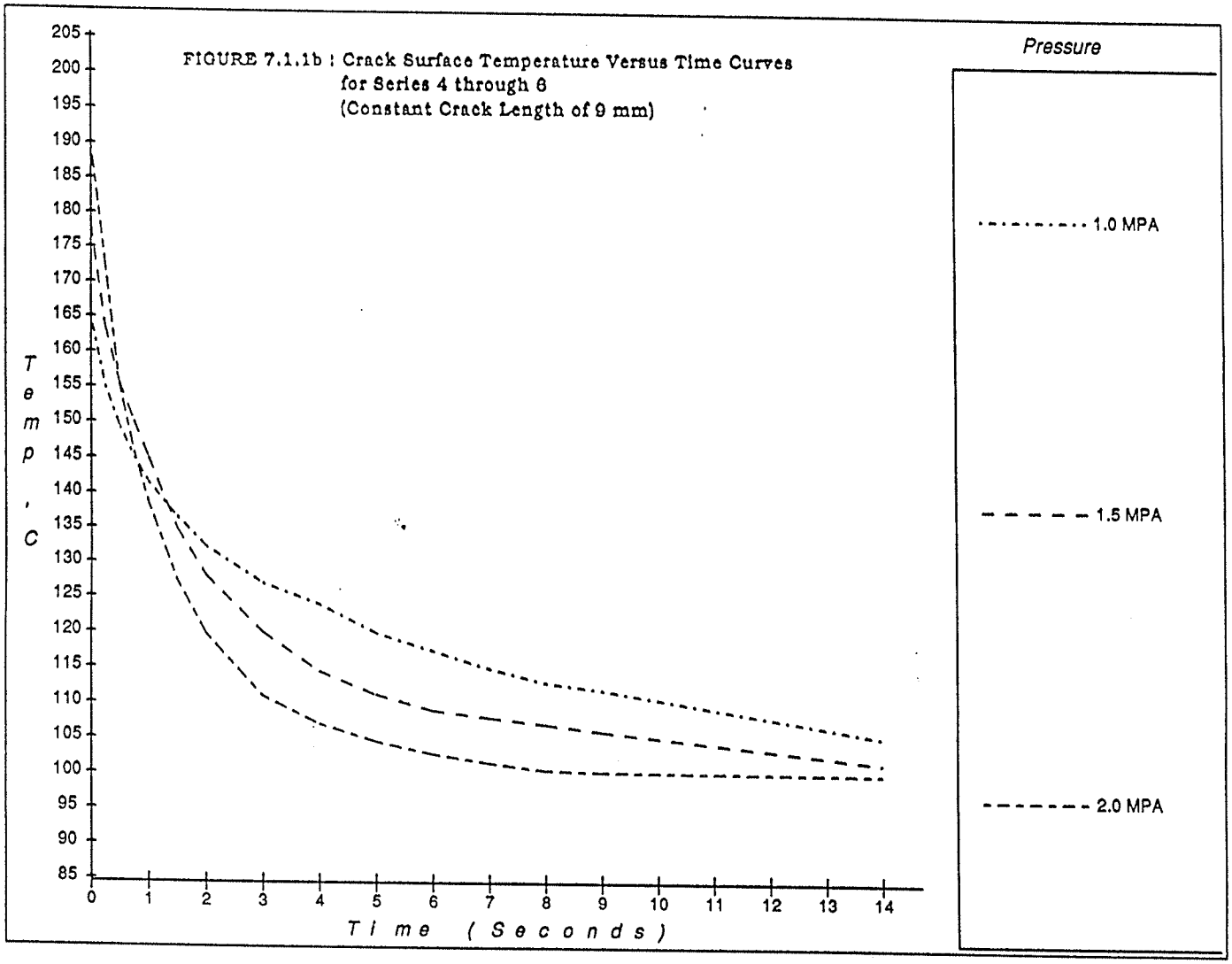
FIGURE 7.1.1b : Crack Surface Temperature Versus Time Curves
for Series 4 through 6
(Constant Crack Length of 9 mm)
Temp, C
205
200
195
190
185
180
175
170
165
160
155
150
145
140
135
130
125
120
115
110
105
100
95
90
85
0
1
2
3
4
5
6
7
8
9
10
11
12
13
14
Time (Seconds)
Pressure
1.0 MPA
1.5 MPA
2.0 MPA

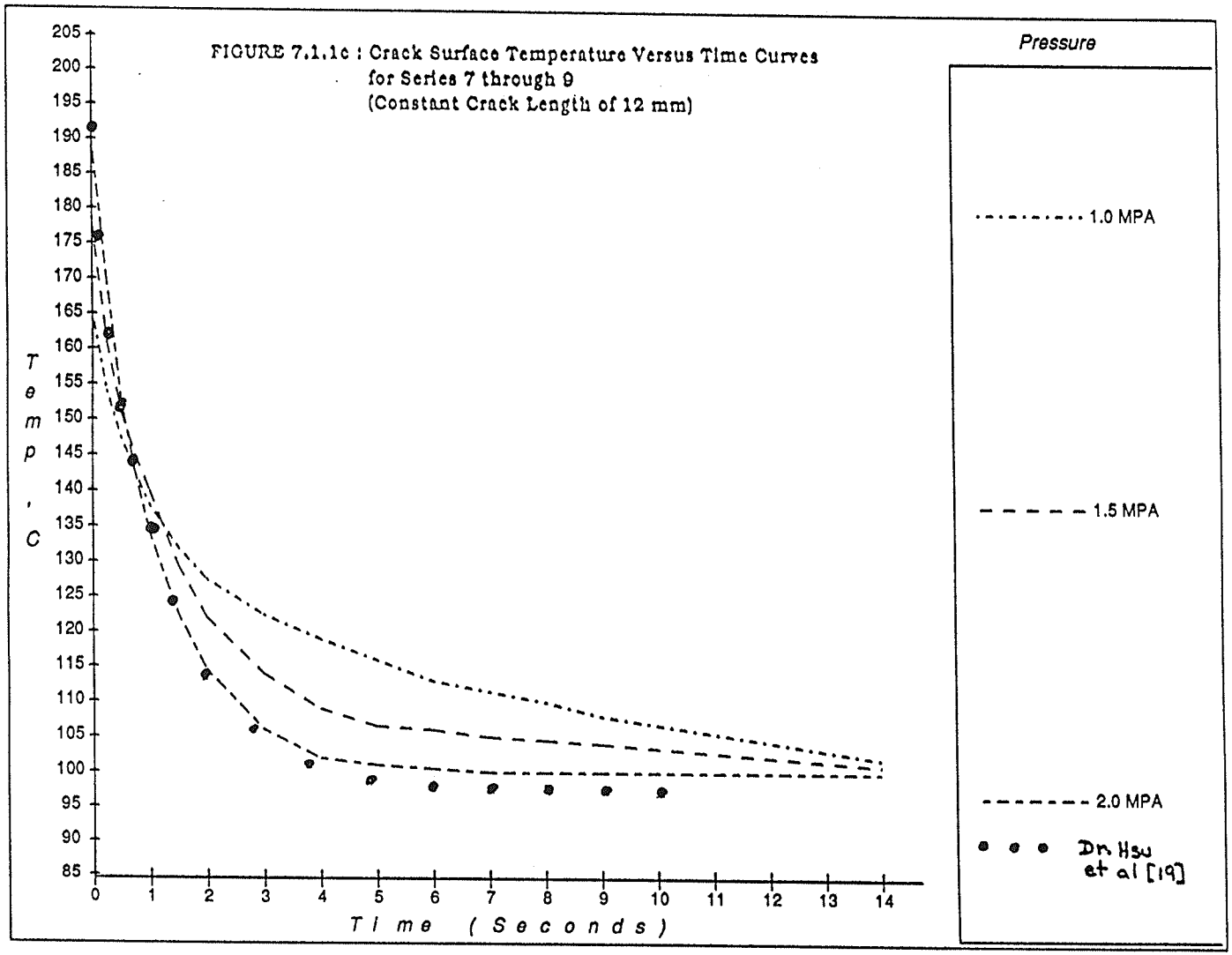
FIGURE 7.1.1c : Crack Surface Temperature Versus Time Curves
for Series 7 through 9
(Constant Crack Length of 12 mm)
Temp. C
205
200
195
190
185
180
175
170
165
160
155
150
145
140
135
130
125
120
115
110
105
100
95
90
85
0
1
2
3
4
5
6
7
8
9
10
11
12
13
14
Time (Seconds)
Pressure
1.0 MPA
1.5 MPA
2.0 MPA
Dr. Hsu et al [19]

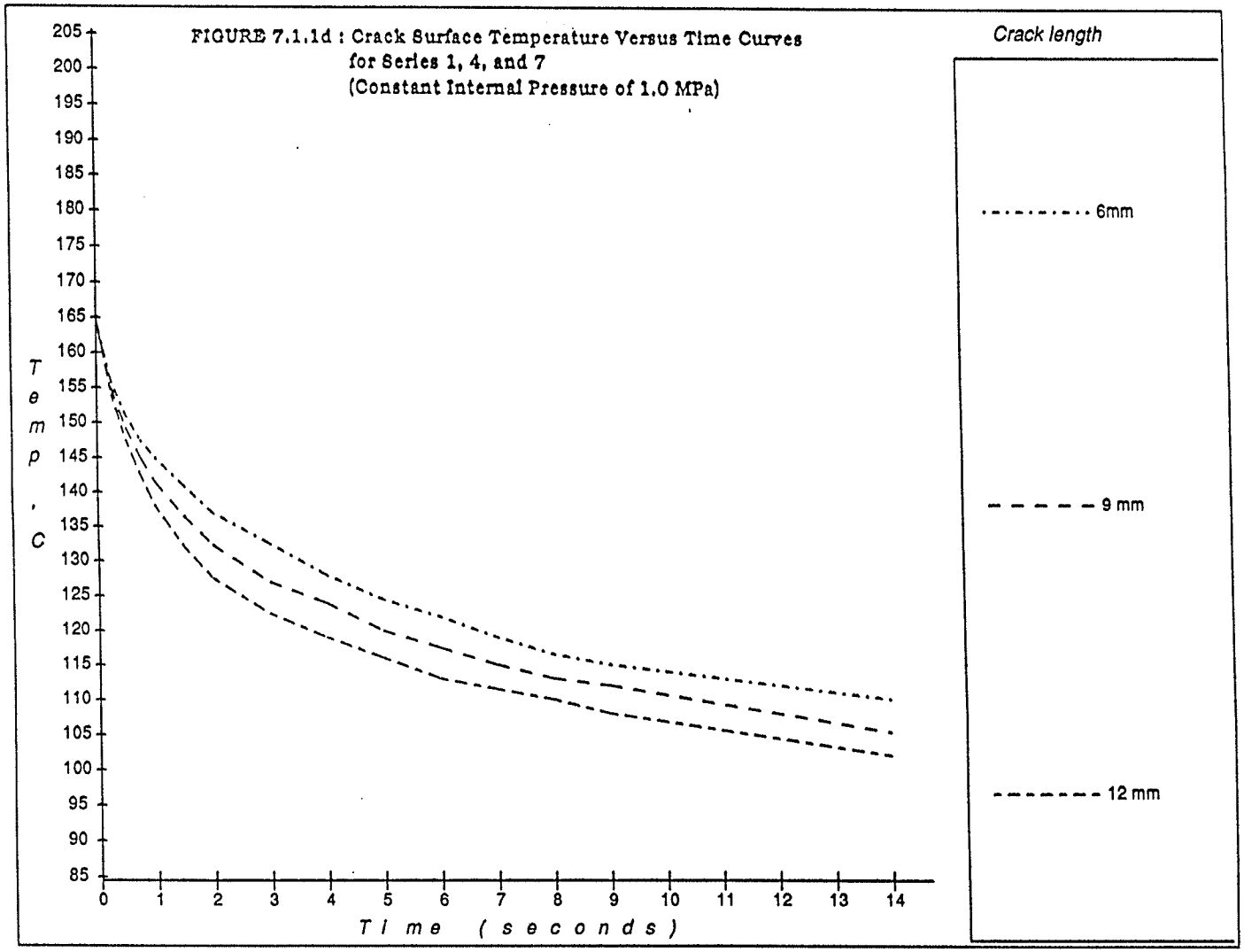

FIGURE 7.1.1d : Crack Surface Temperature Versus Time Curves for Series 1, 4, and 7 (Constant Internal Pressure of 1.0 MPa)

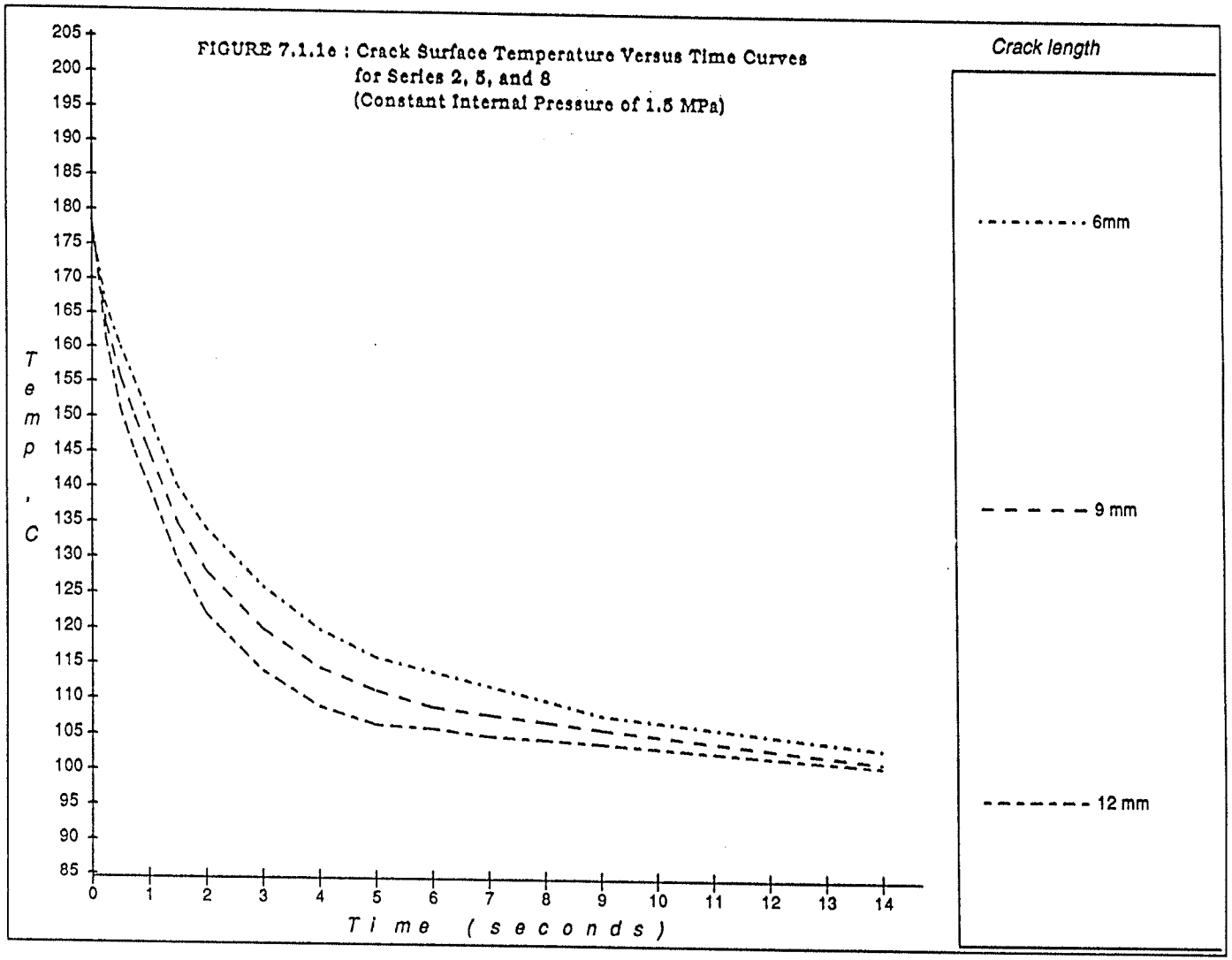

FIGURE 7.1.1e : Crack Surface Temperature Versus Time Curves for Series 2, 5, and 8 (Constant Internal Pressure of 1.5 MPa)

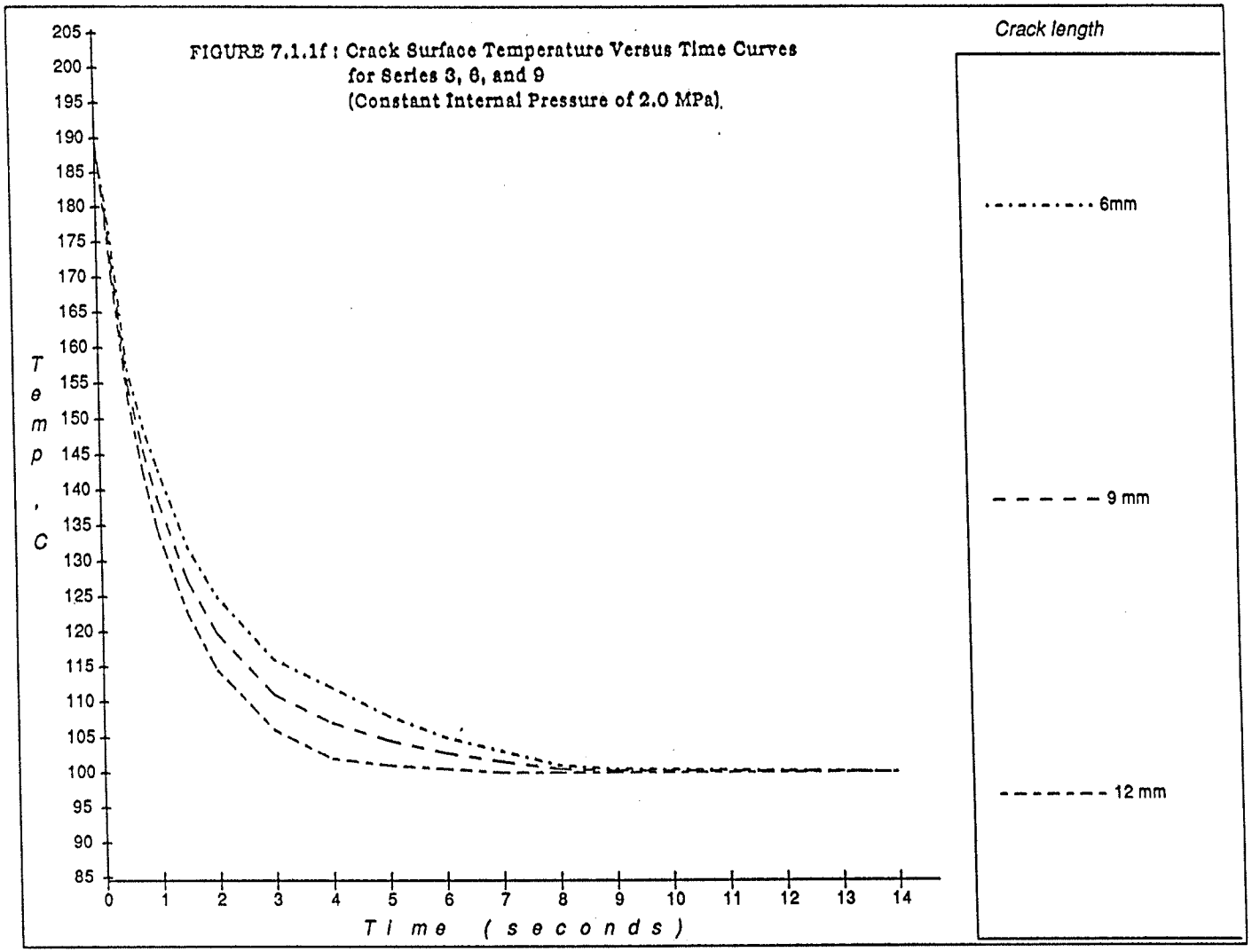
FIGURE 7.1.1f : Crack Surface Temperature Versus Time Curves
for Series 3, 6, and 9
(Constant Internal Pressure of 2.0 MPa).
Crack length
6mm
9 mm
12 mm
Temp. C
205
200
195
190
185
180
175
170
165
160
155
150
145
140
135
130
125
120
115
110
105
100
95
90
85
0
1
2
3
4
5
6
7
8
9
10
11
12
13
14
Time (seconds)

FIGURE 7.1.2a : Maximum Effective Stress, SIGE, Versus Time Curves
for Series 1 through 3
(Constant Crack Length of 6 mm)

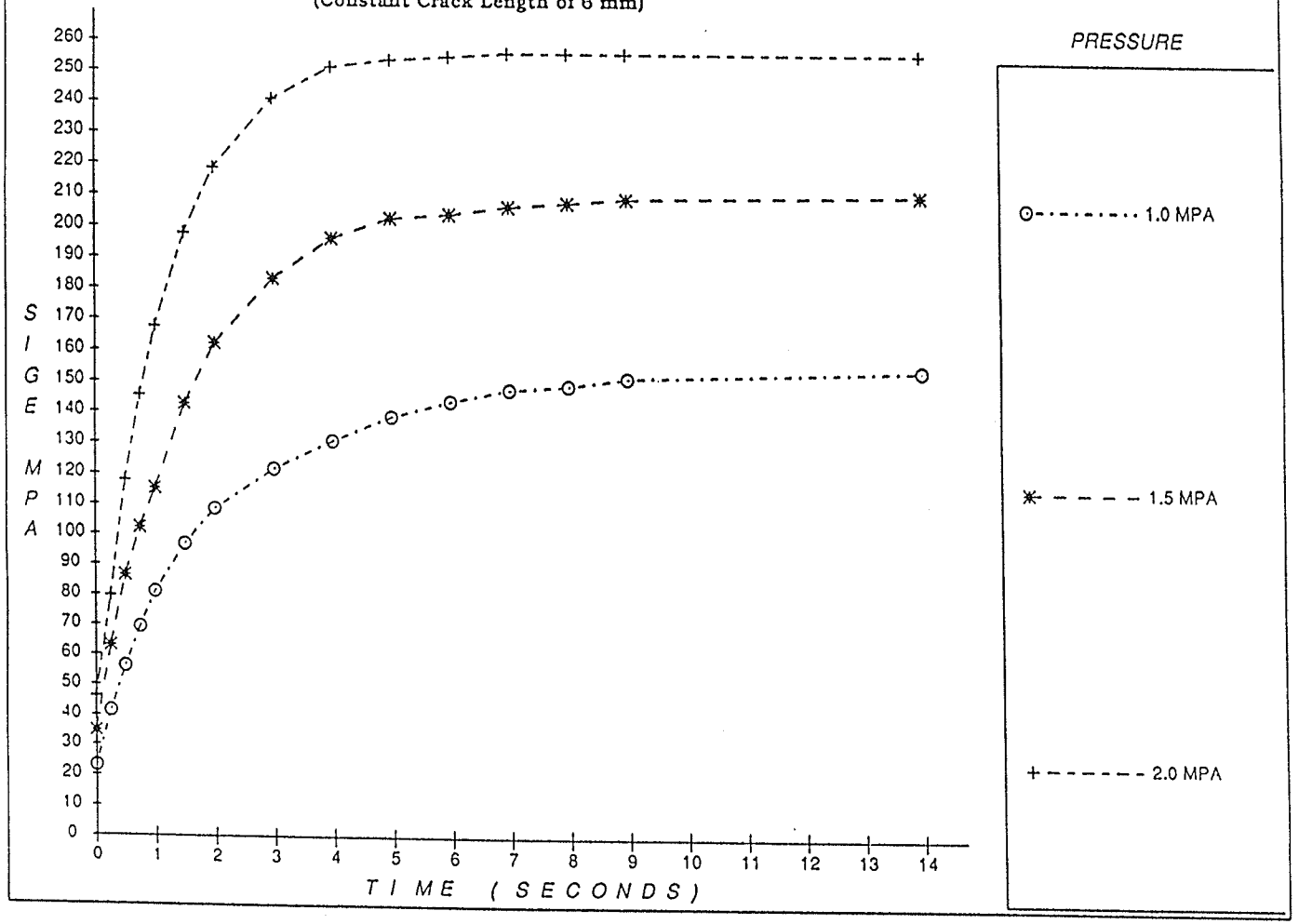

FIGURE 7.1.2b : Maximum Effective Stress, SIGE, Versus Time Curves
for Series 4 through 6
(Constant Crack Length of 9 mm)

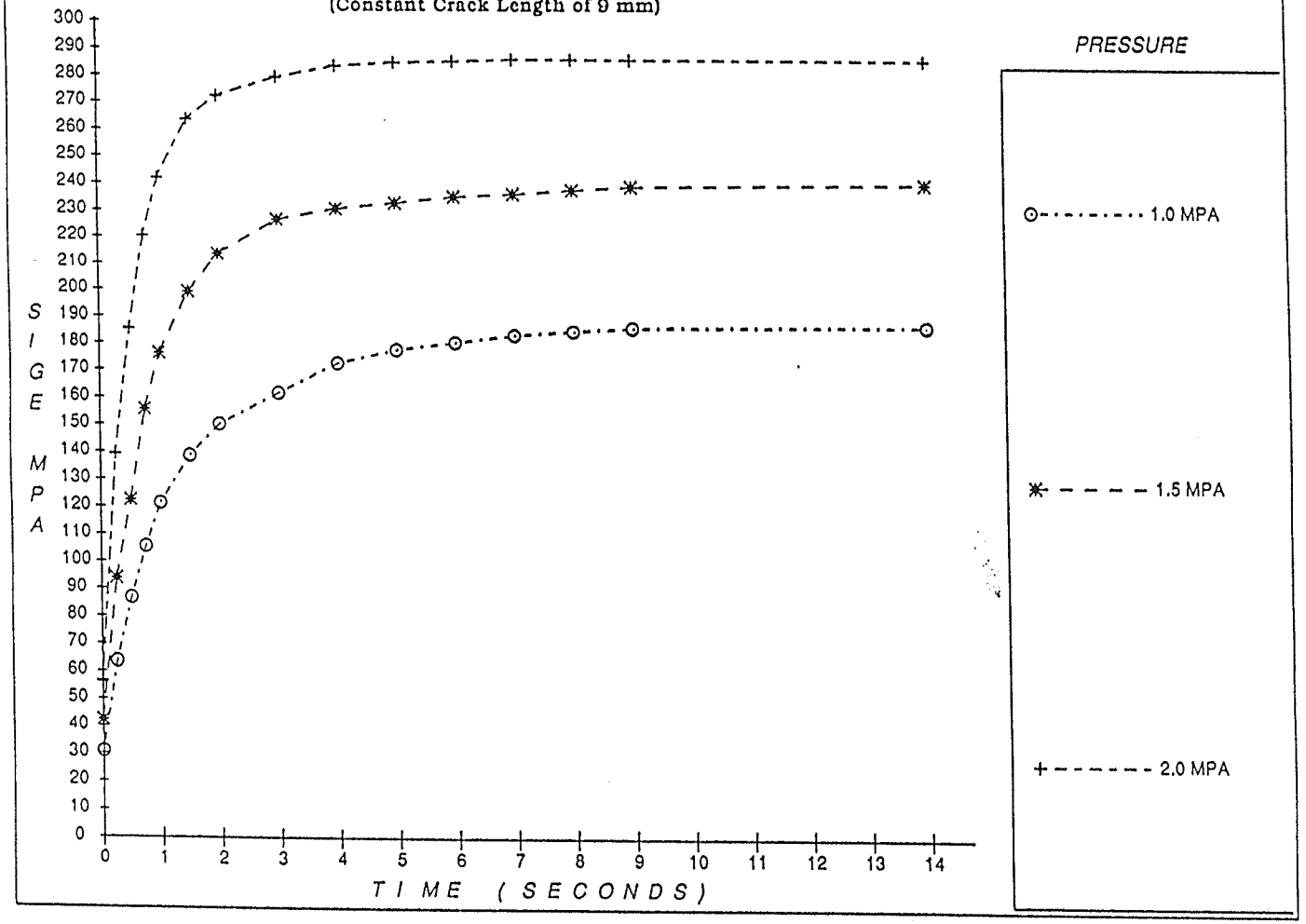

FIGURE 7.1.2c : Maximum Effective Stress, SIGE, Versus Time Curves
for Series 7 through 9
(Constant Crack Length of 12 mm)

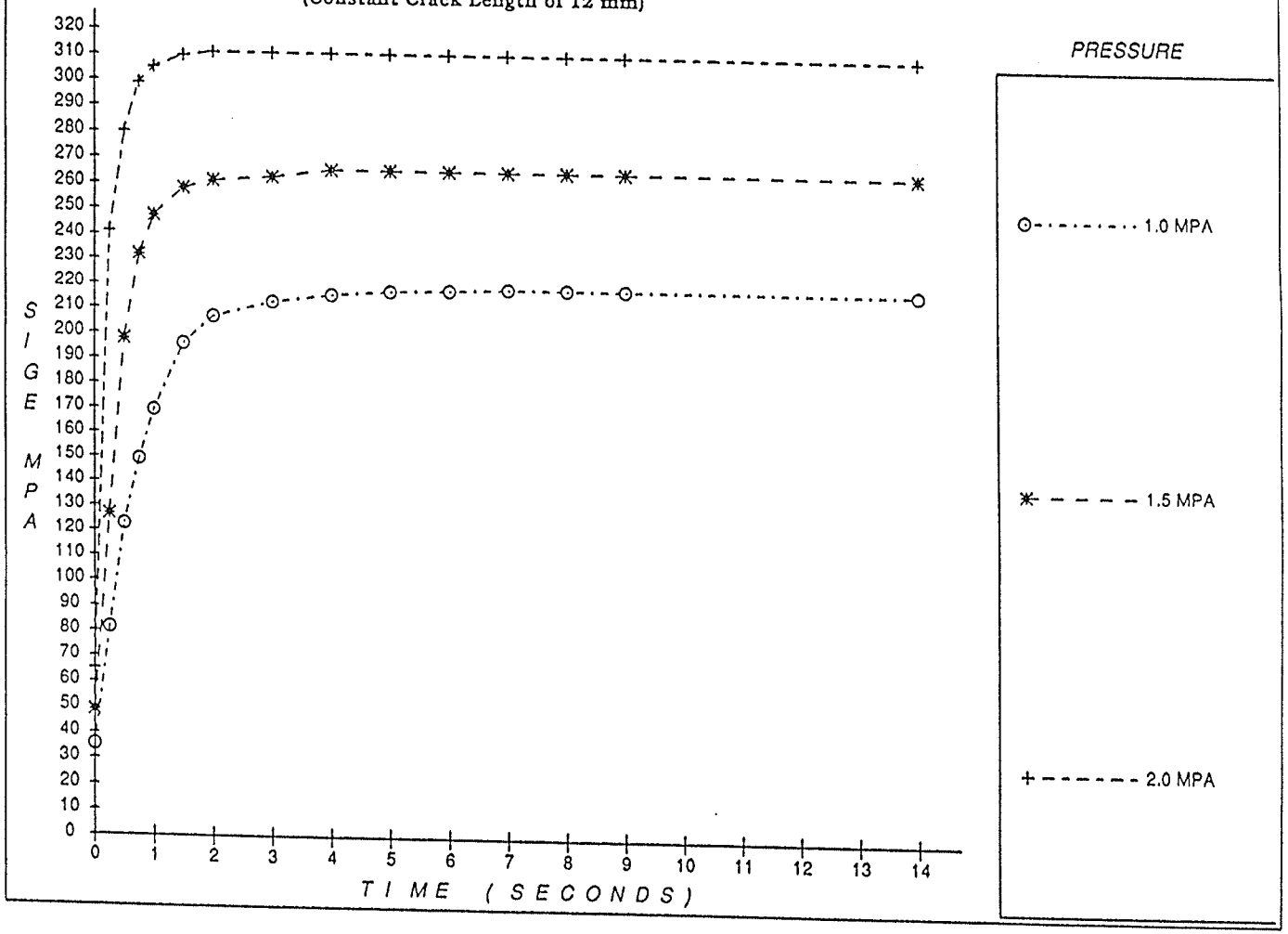

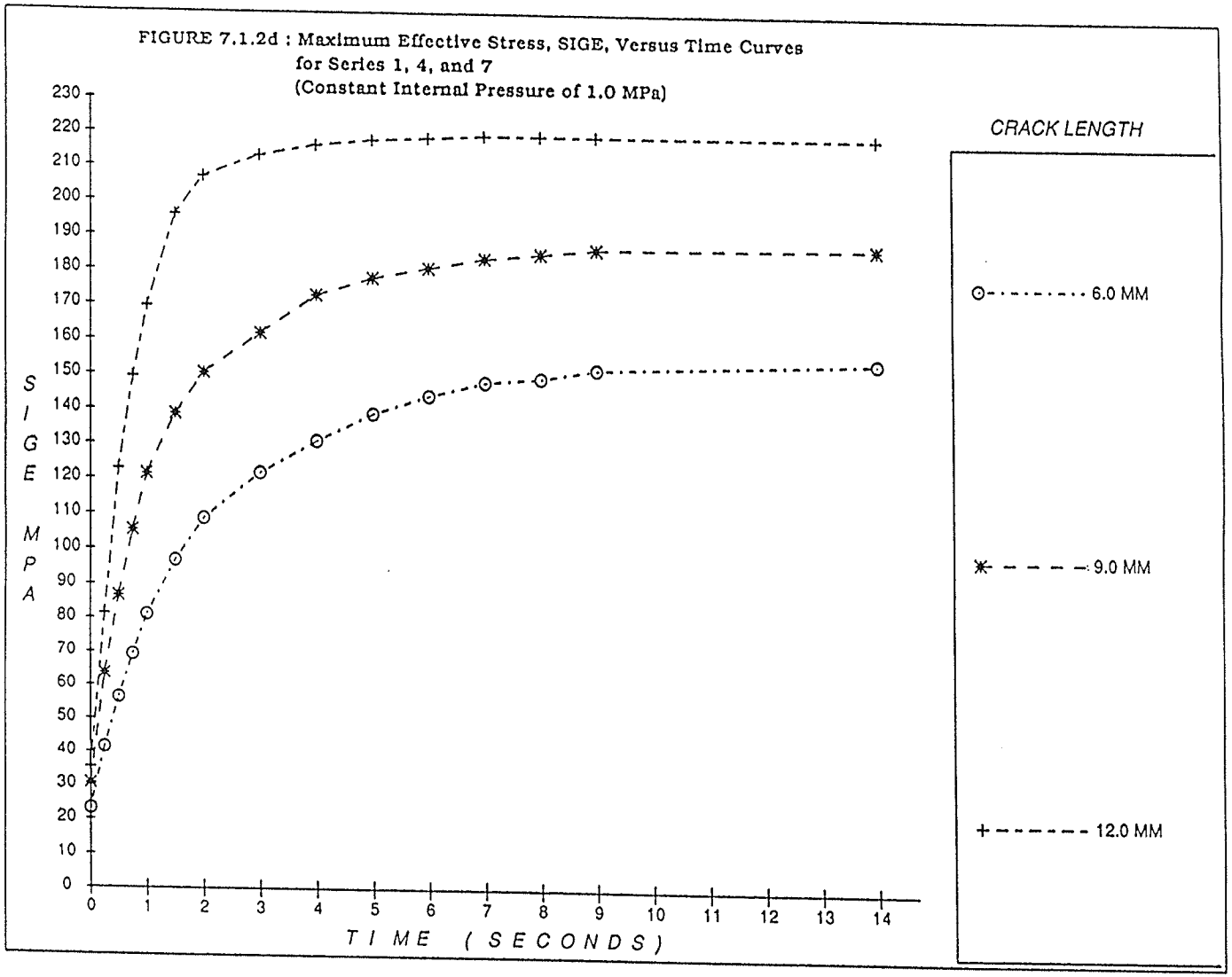

FIGURE 7.1.2d : Maximum Effective Stress, SIGE, Versus Time Curves for Series 1, 4, and 7 (Constant Internal Pressure of 1.0 MPa)

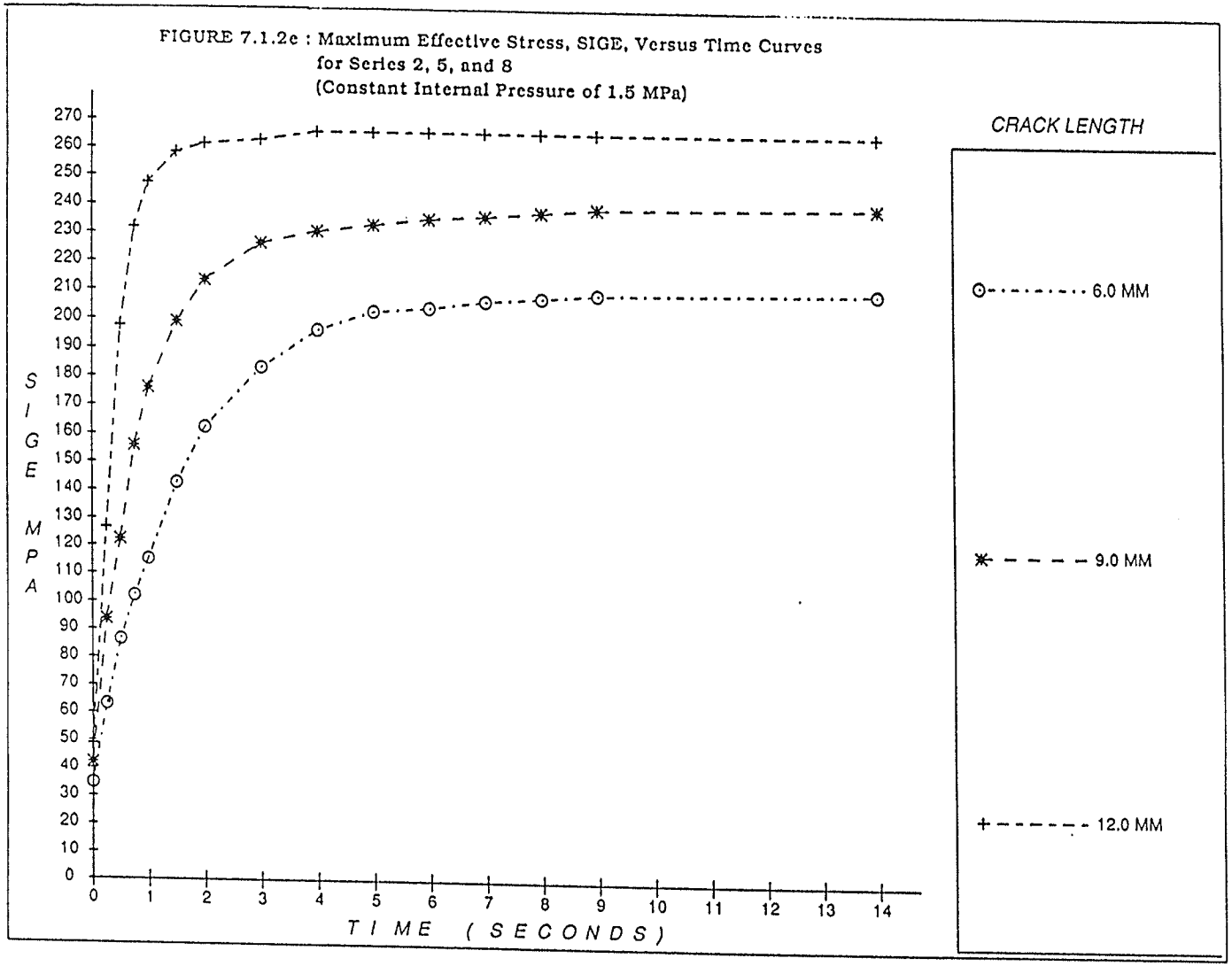
FIGURE 7.1.2e : Maximum Effective Stress, SIGE, Versus Time Curves
for Series 2, 5, and 8
(Constant Internal Pressure of 1.5 MPa)
SIGE MPA
TIME (SECONDS)
CRACK LENGTH
6.0 MM
9.0 MM
12.0 MM

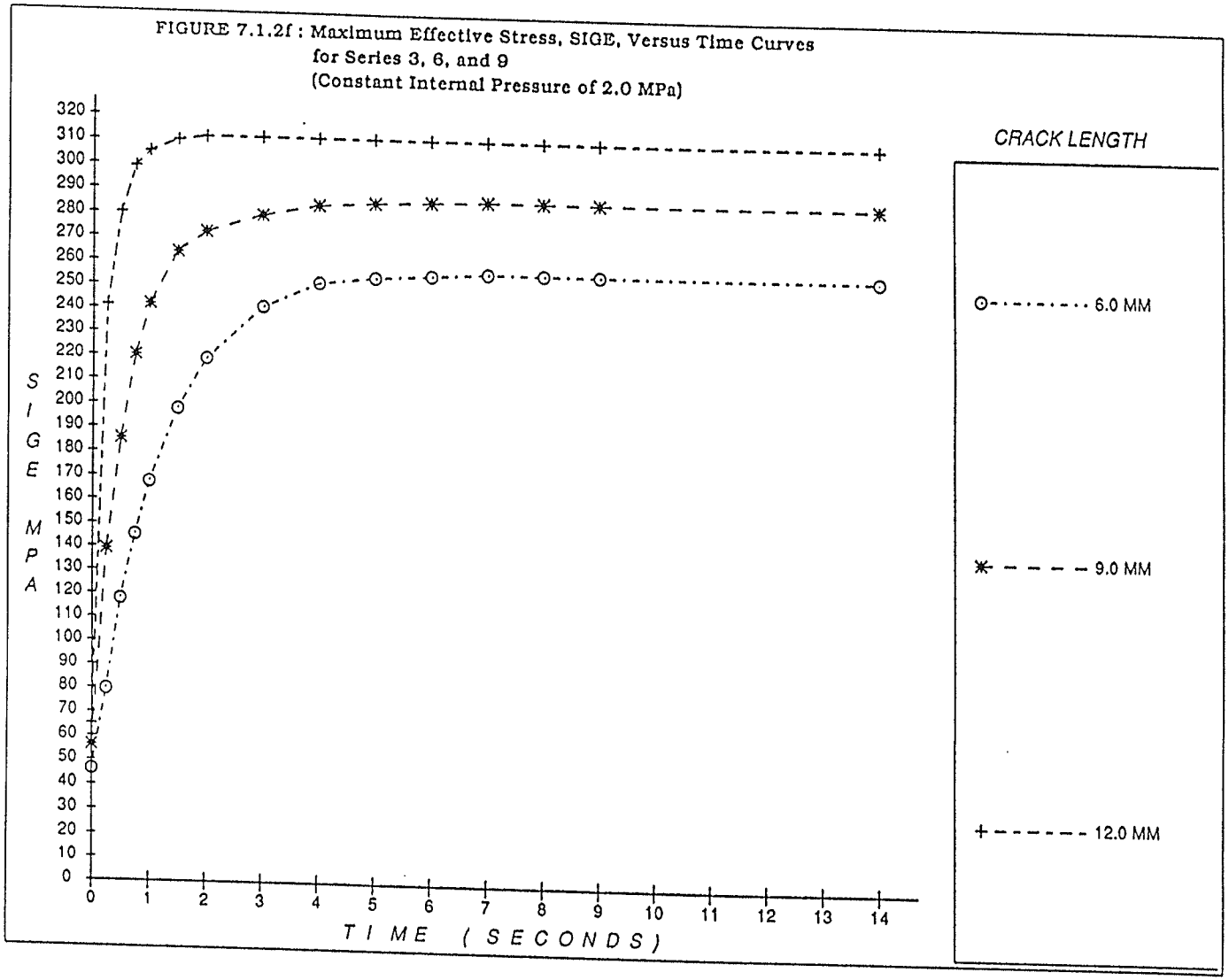

FIGURE 7.1.2f : Maximum Effective Stress, SIGE, Versus Time Curves for Series 3, 6, and 9 (Constant Internal Pressure of 2.0 MPa)

FIGURE 7.1.3a : Effective Stress Distribution (MPa) - Series 1 (time = 14 seconds)

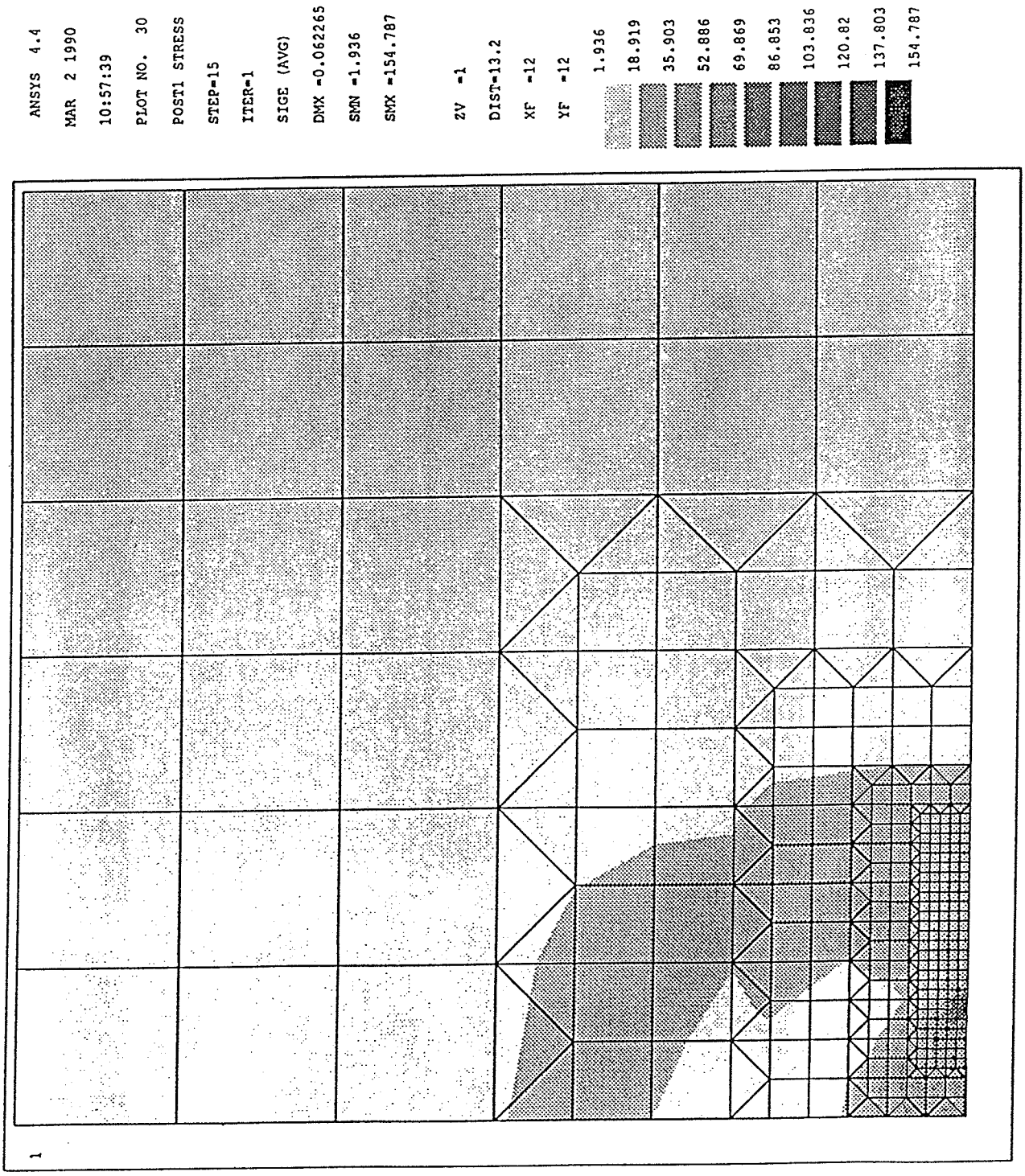

FIGURE 7.1.3b : Effective Stress Distribution (MPa) - Series 2 (time = 14 seconds)

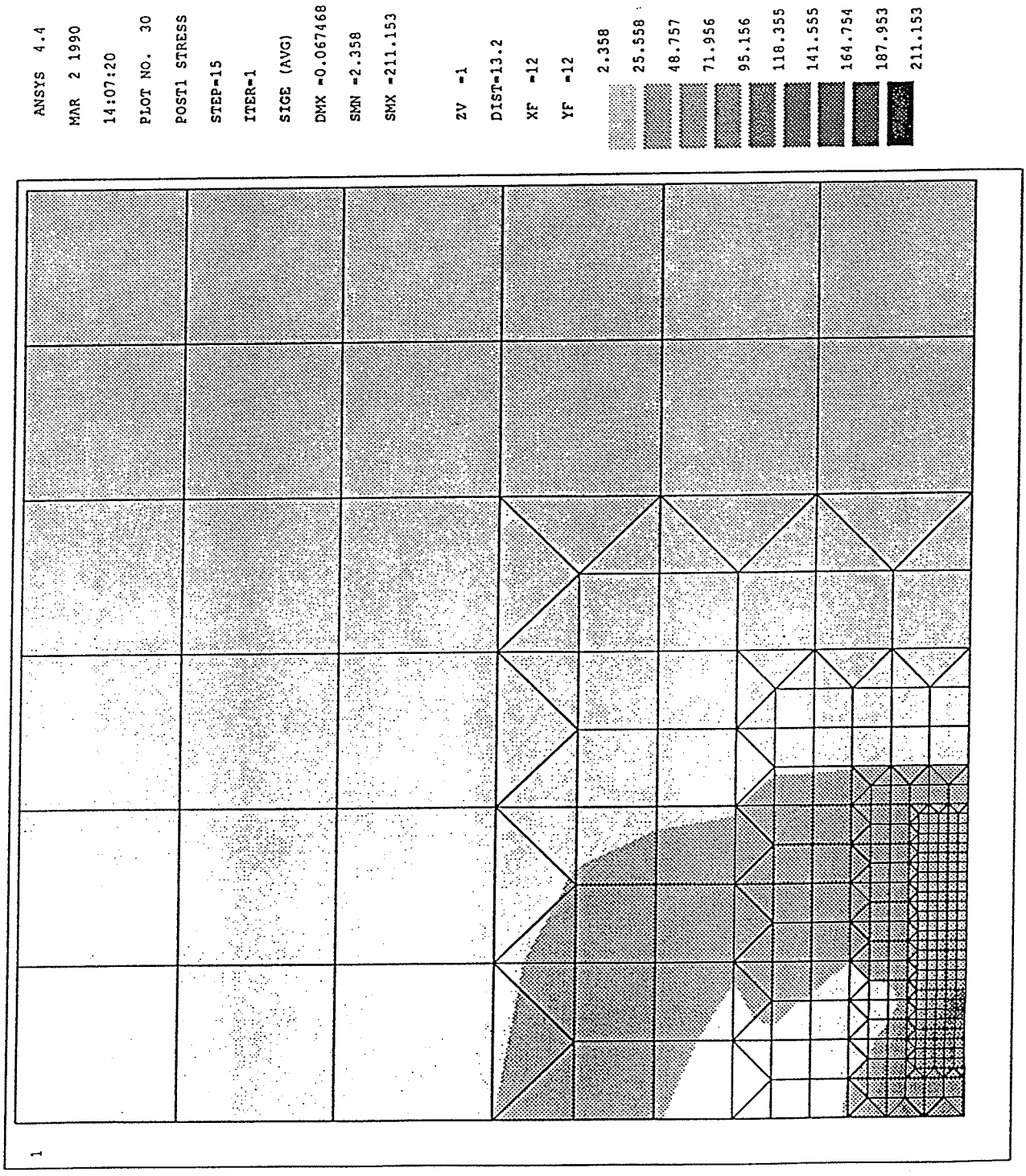

FIGURE 7.1.3c : Effective Stress Distribution (MPa) - Series 3 (time = 14 seconds)

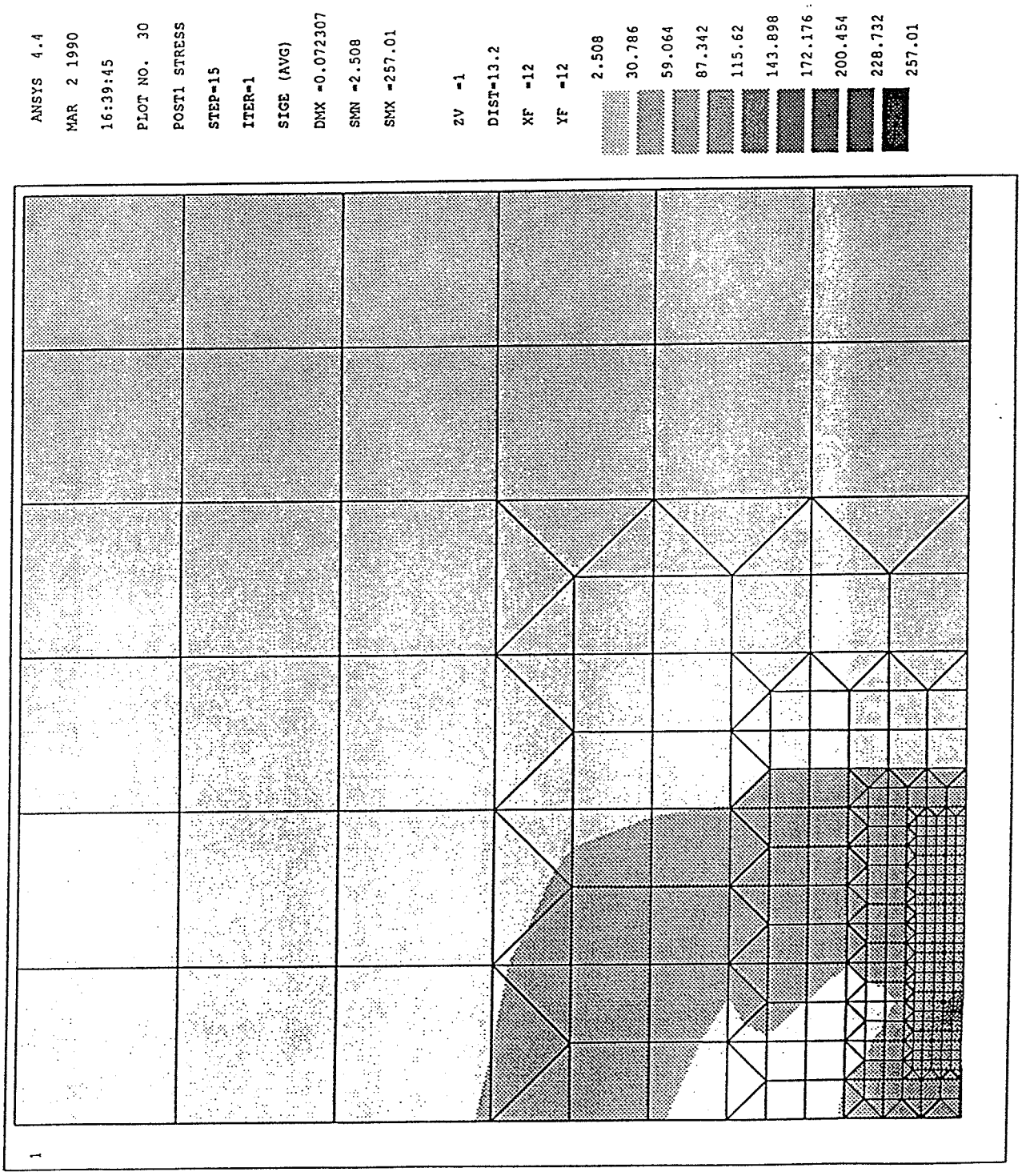

FIGURE 7.1.3d : Effective Stress Distribution (MPa) - Series 4 (time = 14 seconds)

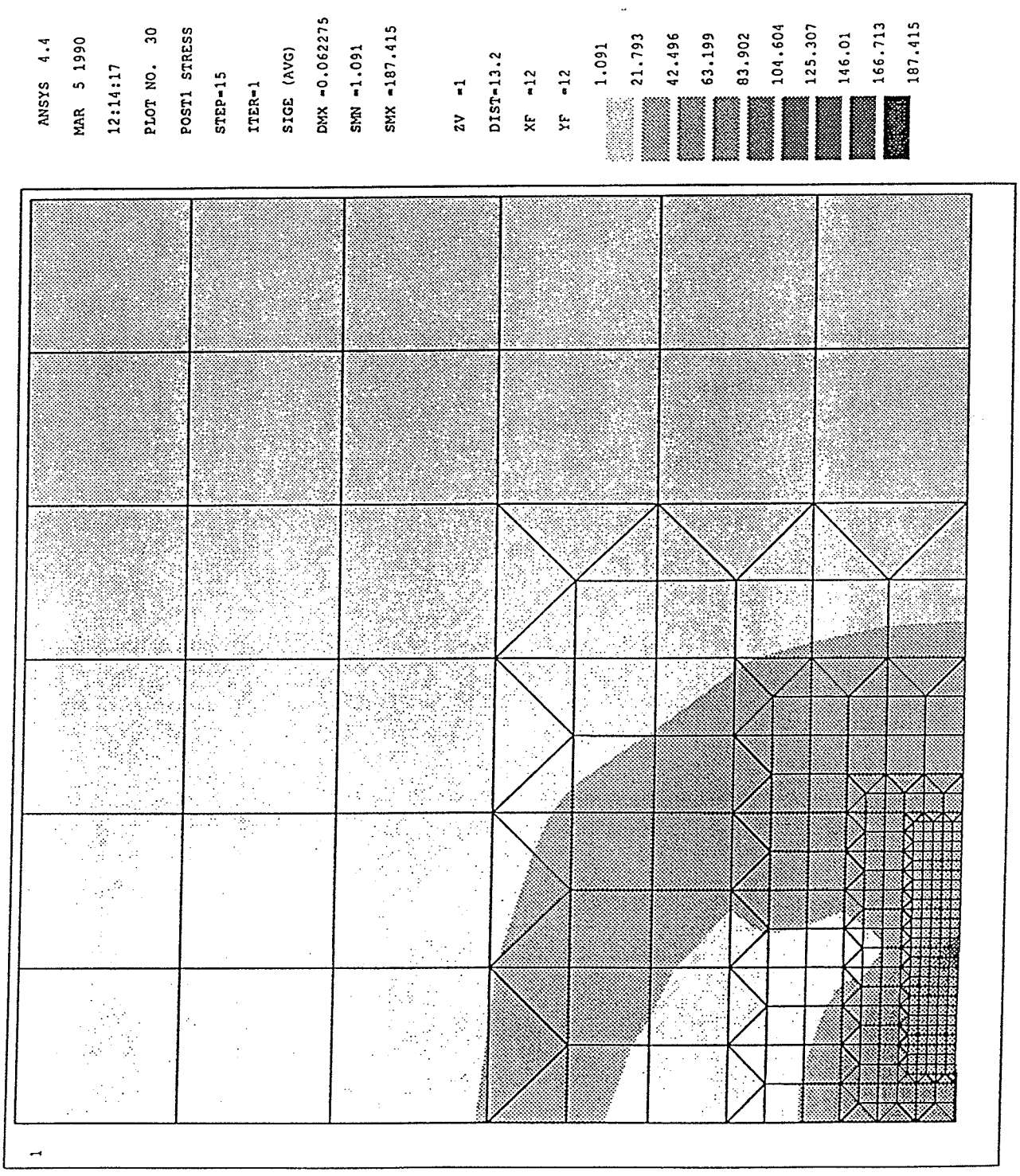

FIGURE 7.1.3e : Effective Stress Distribution (MPa) - Series 5 (time = 14 seconds)

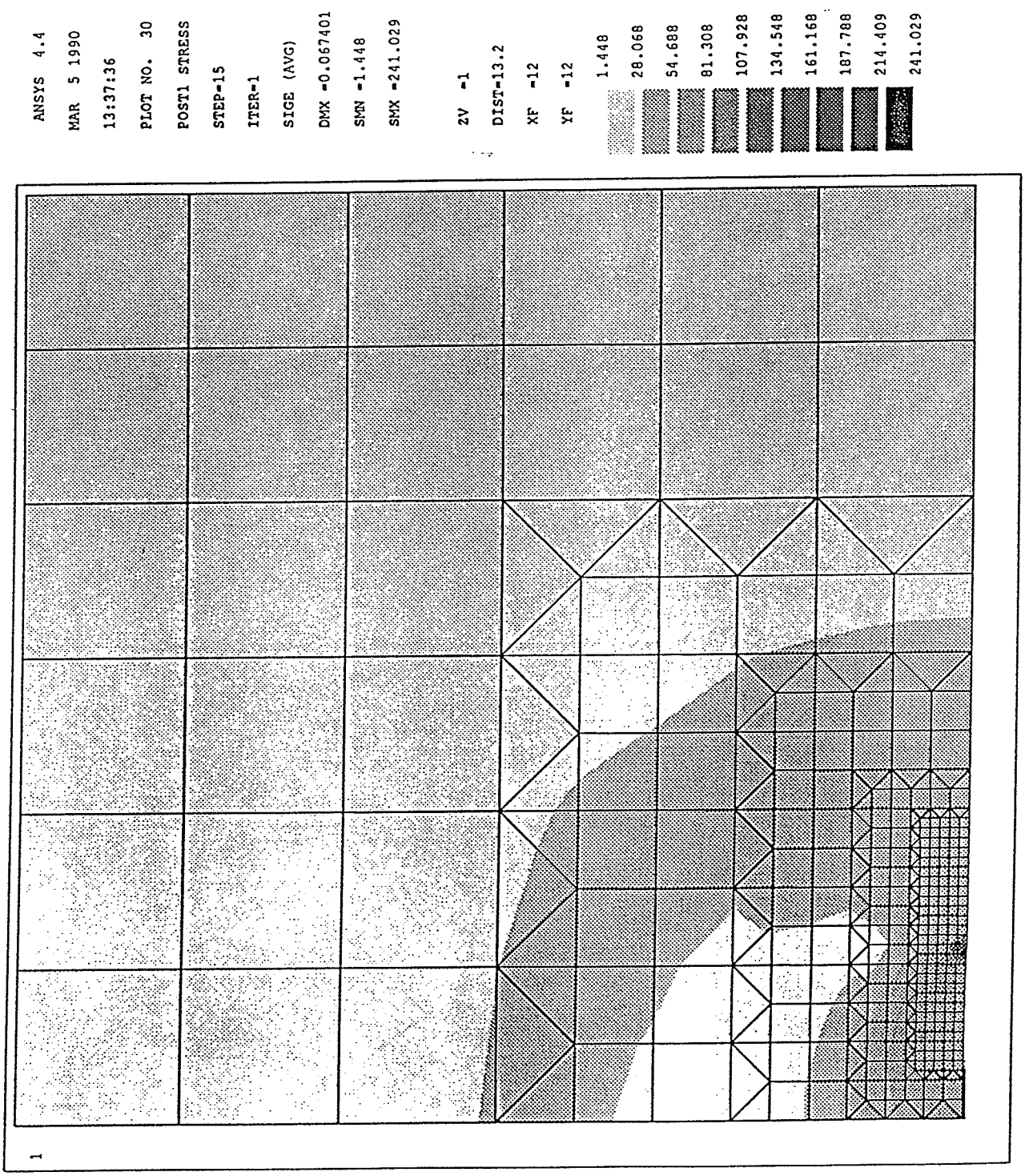

FIGURE 7.1.3f : Effective Stress Distribution (MPa) - Series 6 (time = 14 seconds)

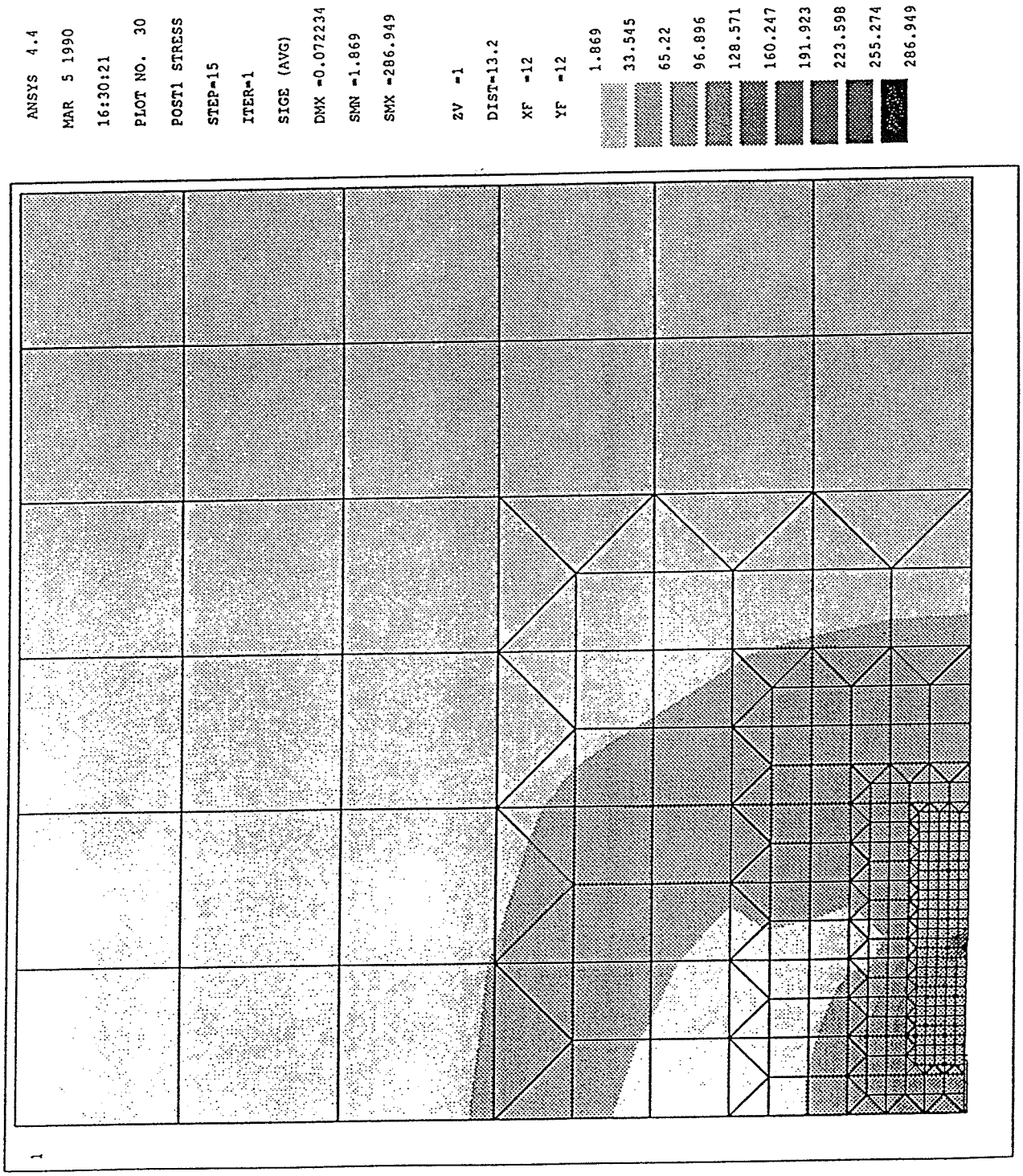

FIGURE 7.1.3g : Effective Stress Distribution (MPa) - Series 7
(time = 14 seconds)

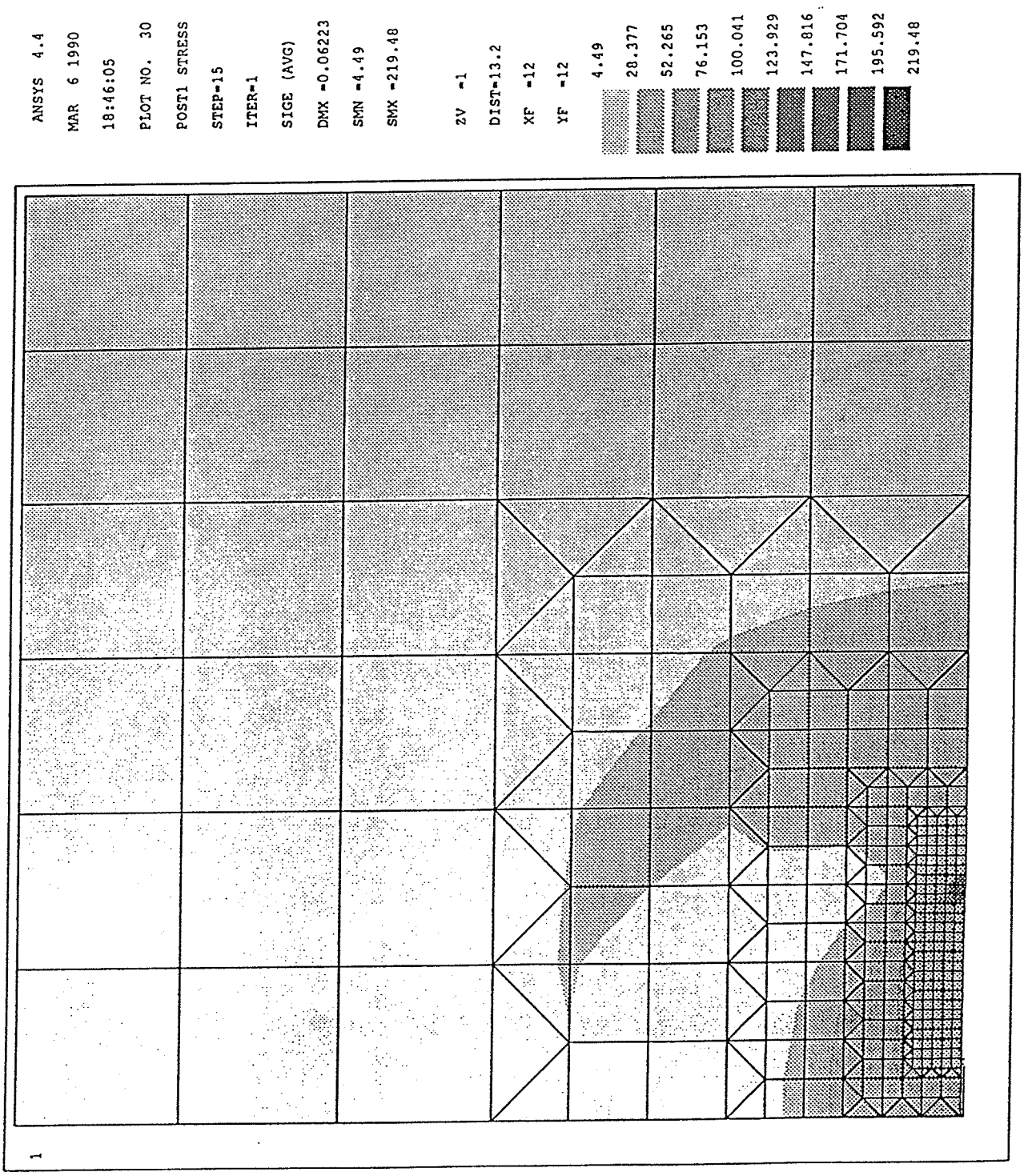

FIGURE 7.1.3h : Effective Stress Distribution (MPa) - Series 8
(time = 14 seconds)

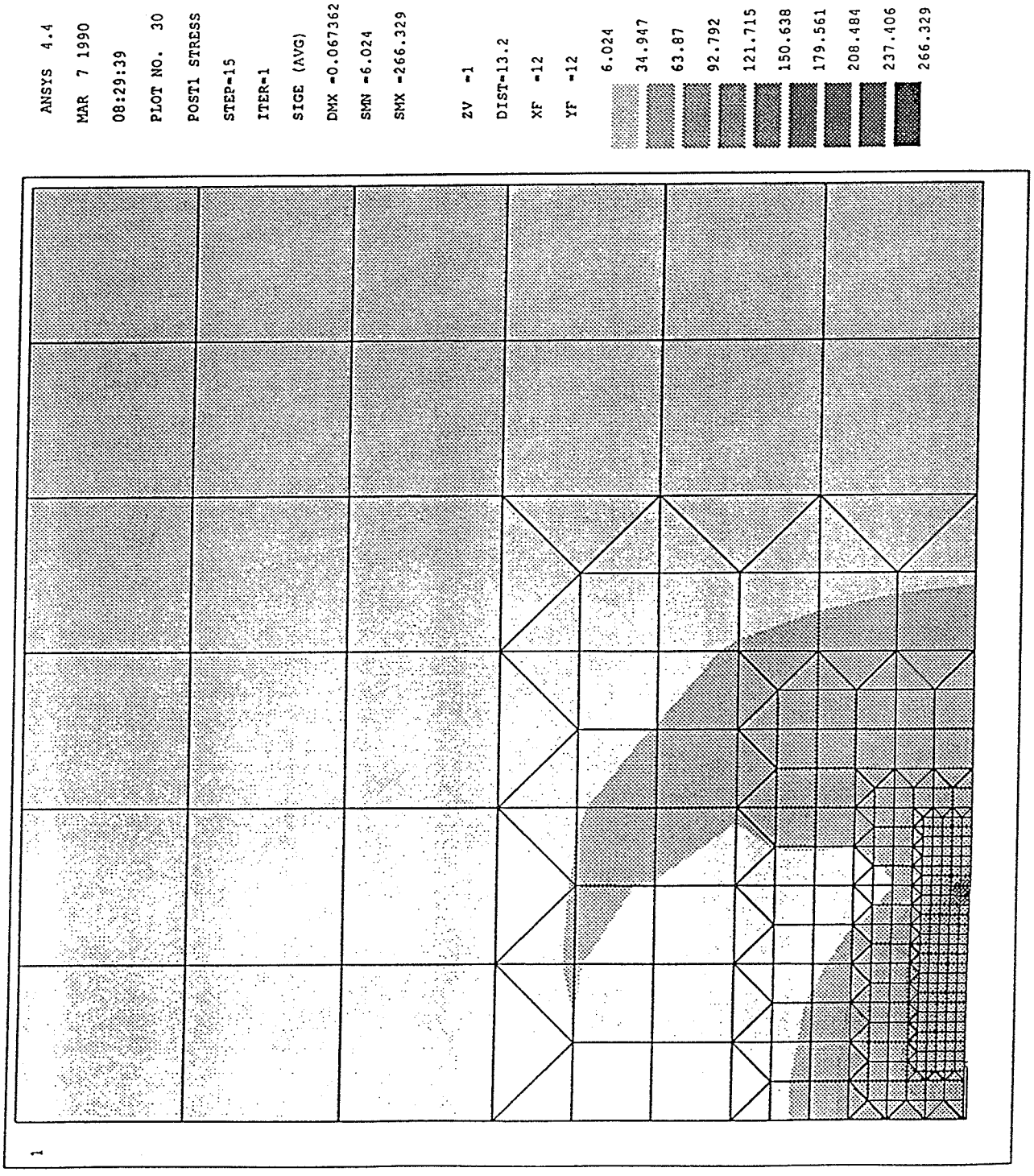

FIGURE 7.1.3i : Effective Stress Distribution (MPa) - Series 9 (time = 14 seconds)

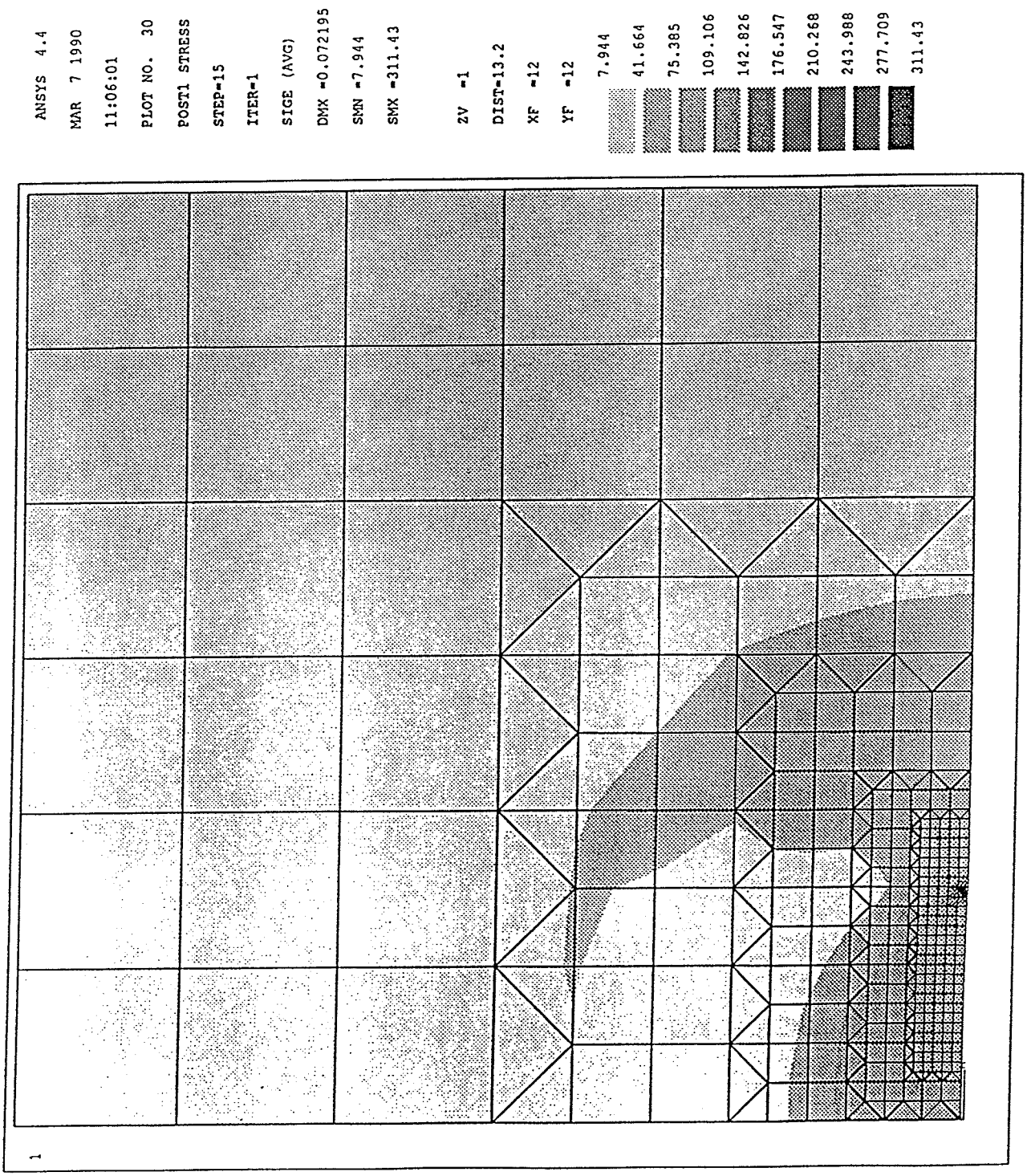

FIGURE 7.1.4a : Temperature Distribution (°C) - Series 1 (time = 14 seconds)

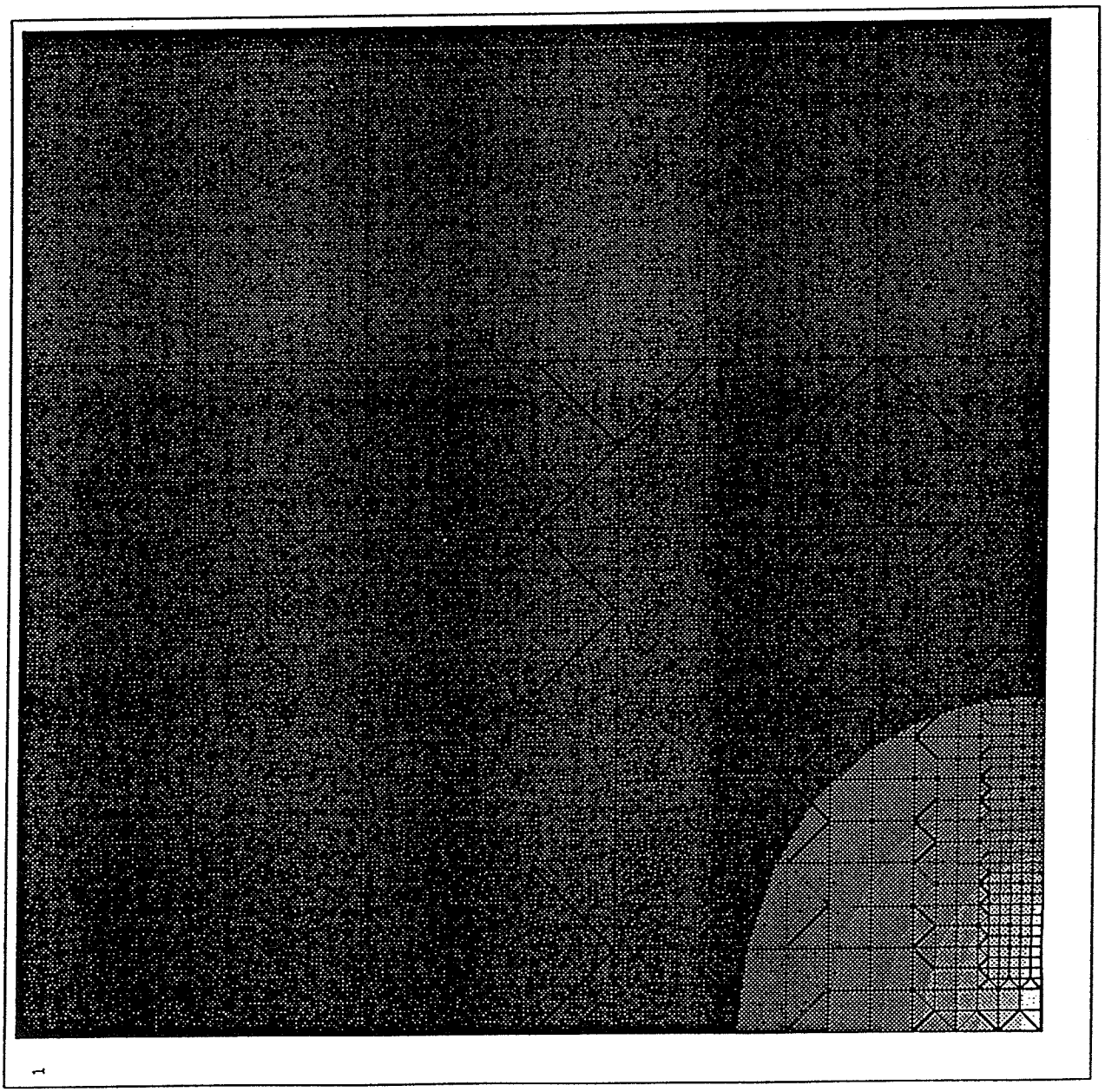

FIGURE 7.1.4b : Temperature Distribution (°C) - Series 2
(time = 14 seconds)

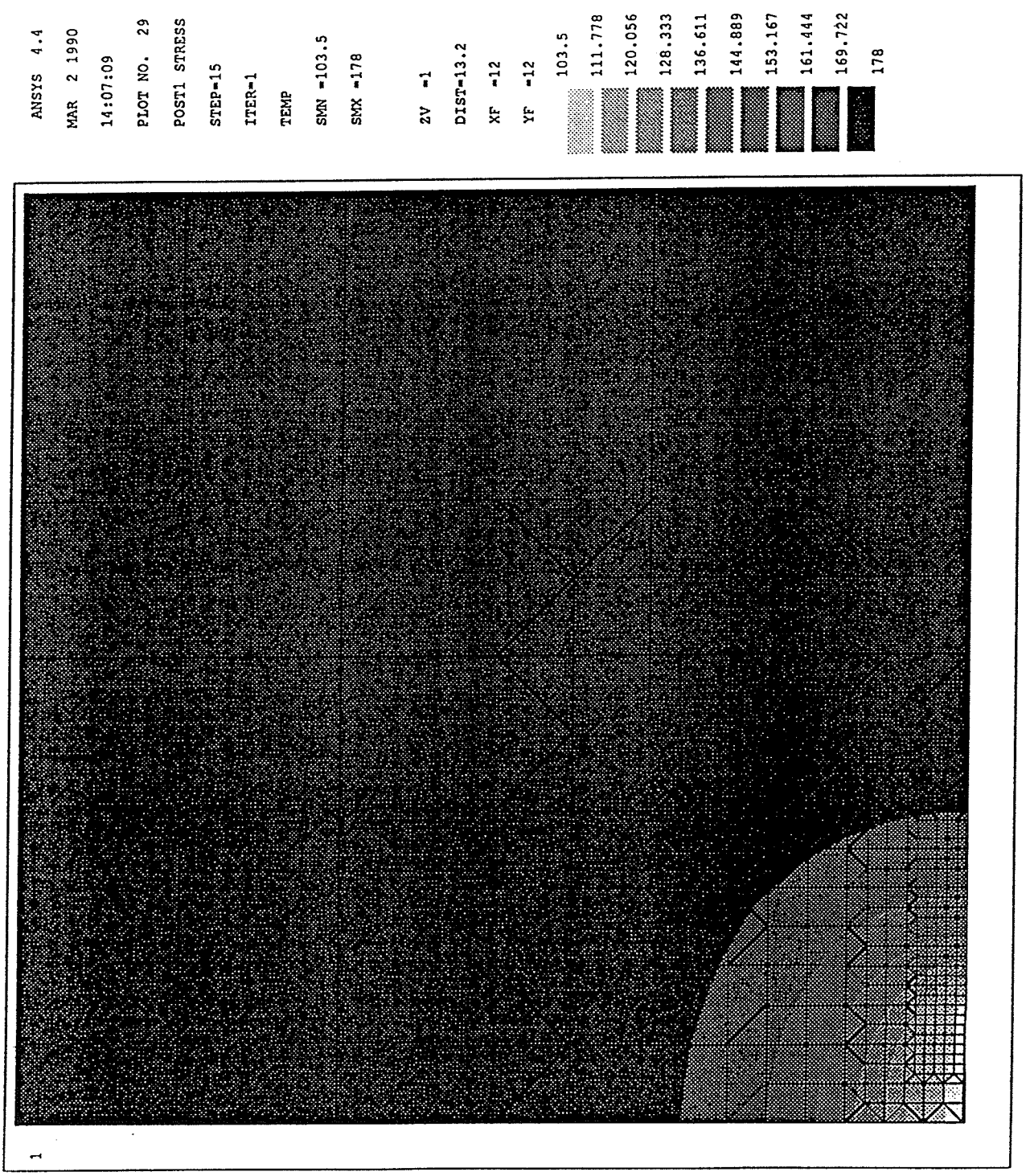

FIGURE 7.1.4c : Temperature Distribution (°C) - Series 3 (time = 14 seconds)

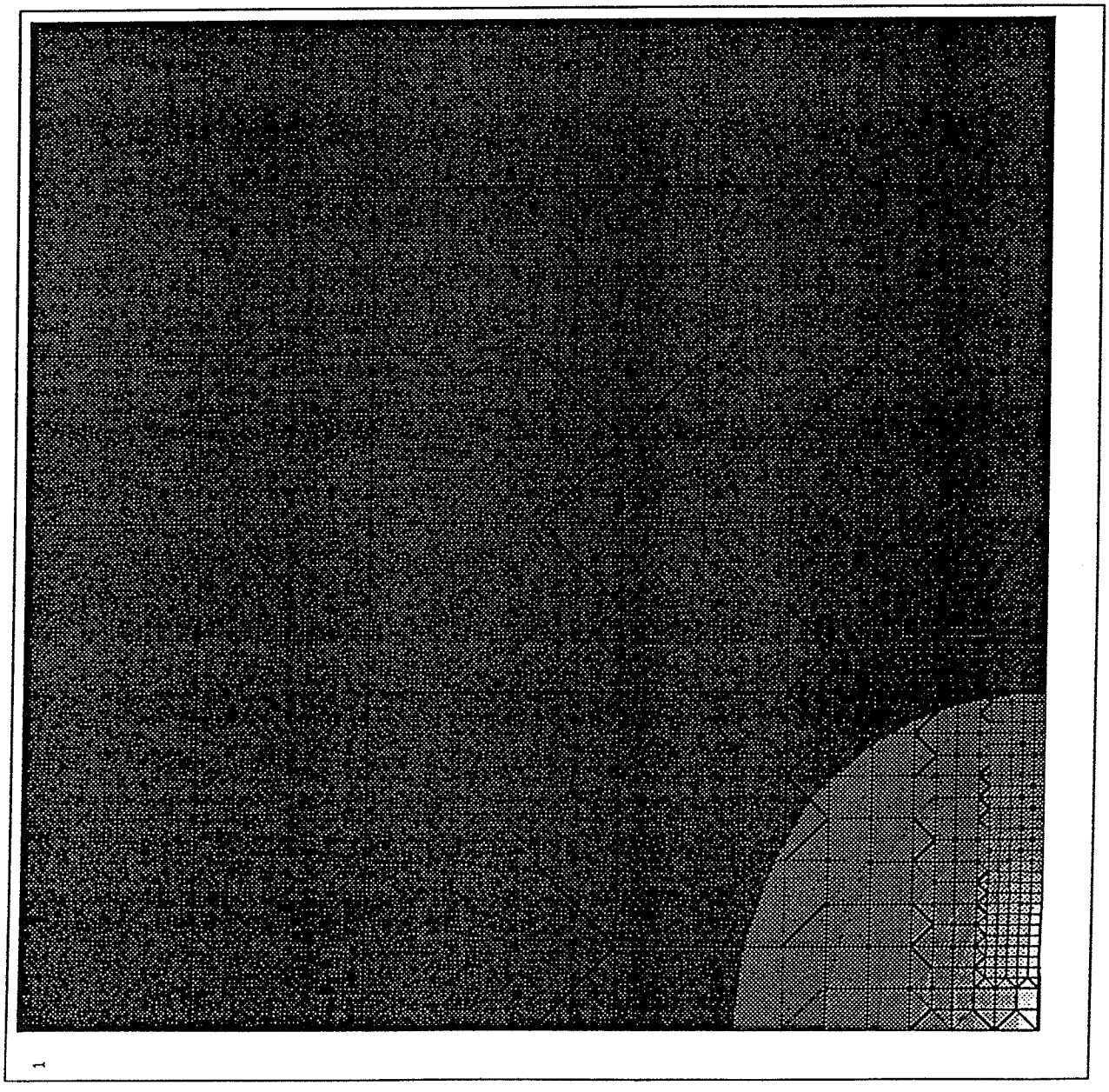

FIGURE 7.1.4d : Temperature Distribution (°C) - Series 4 (time = 14 seconds)

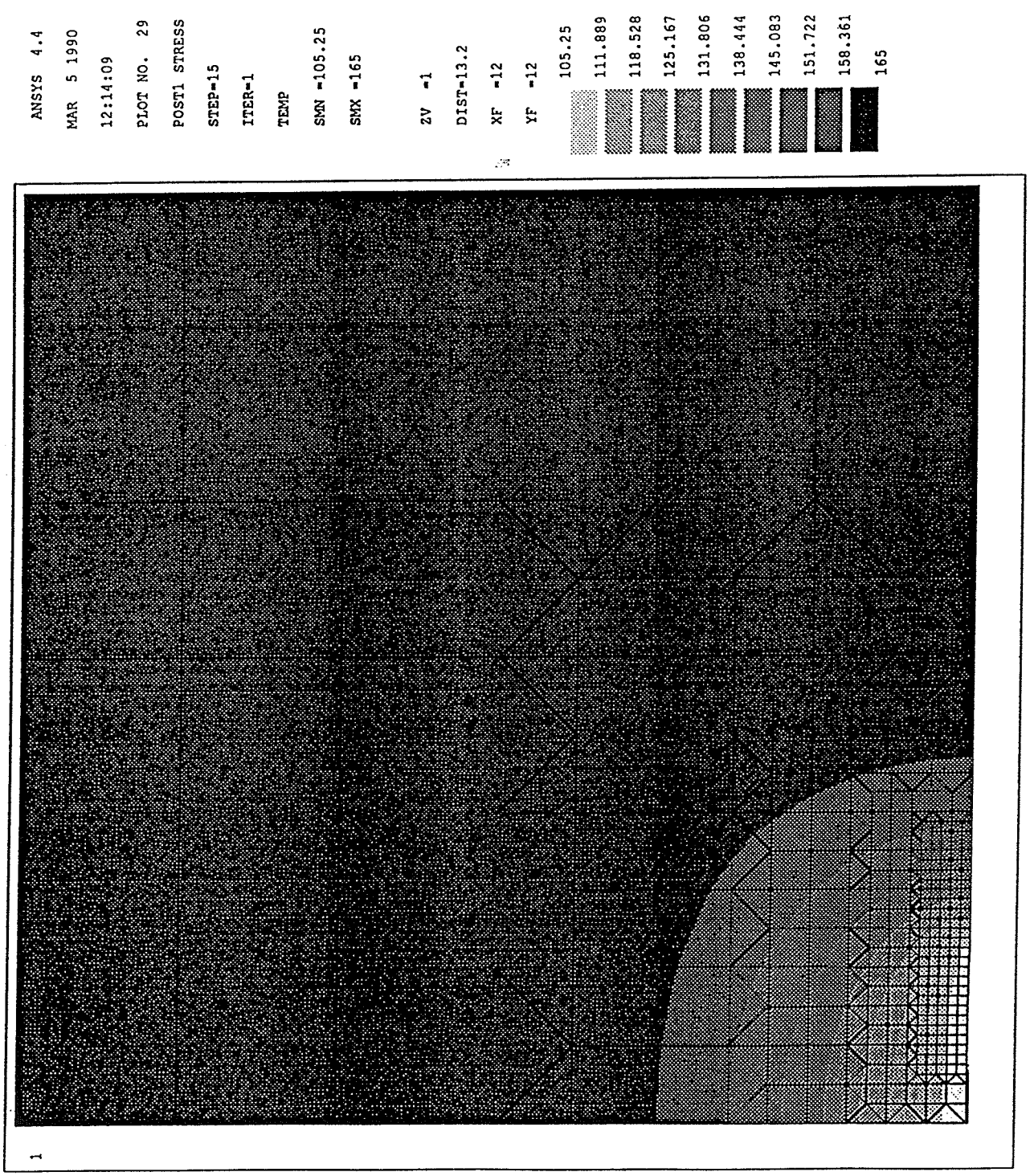

FIGURE 7.1.4e : Temperature Distribution (°C) - Series 5
(time = 14 seconds)

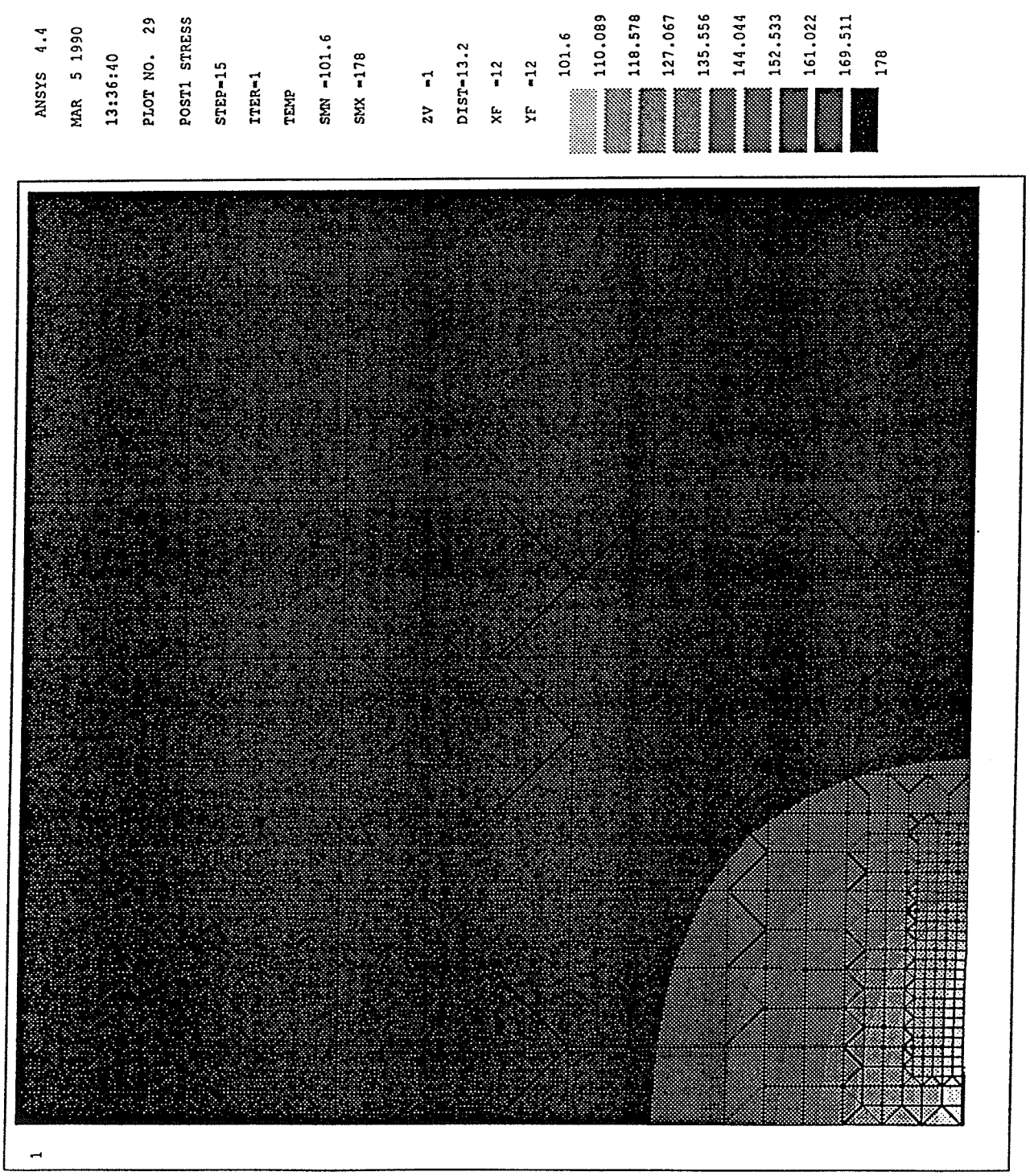

FIGURE 7.1.4f : Temperature Distribution (°C) - Series 6 (time = 14 seconds)

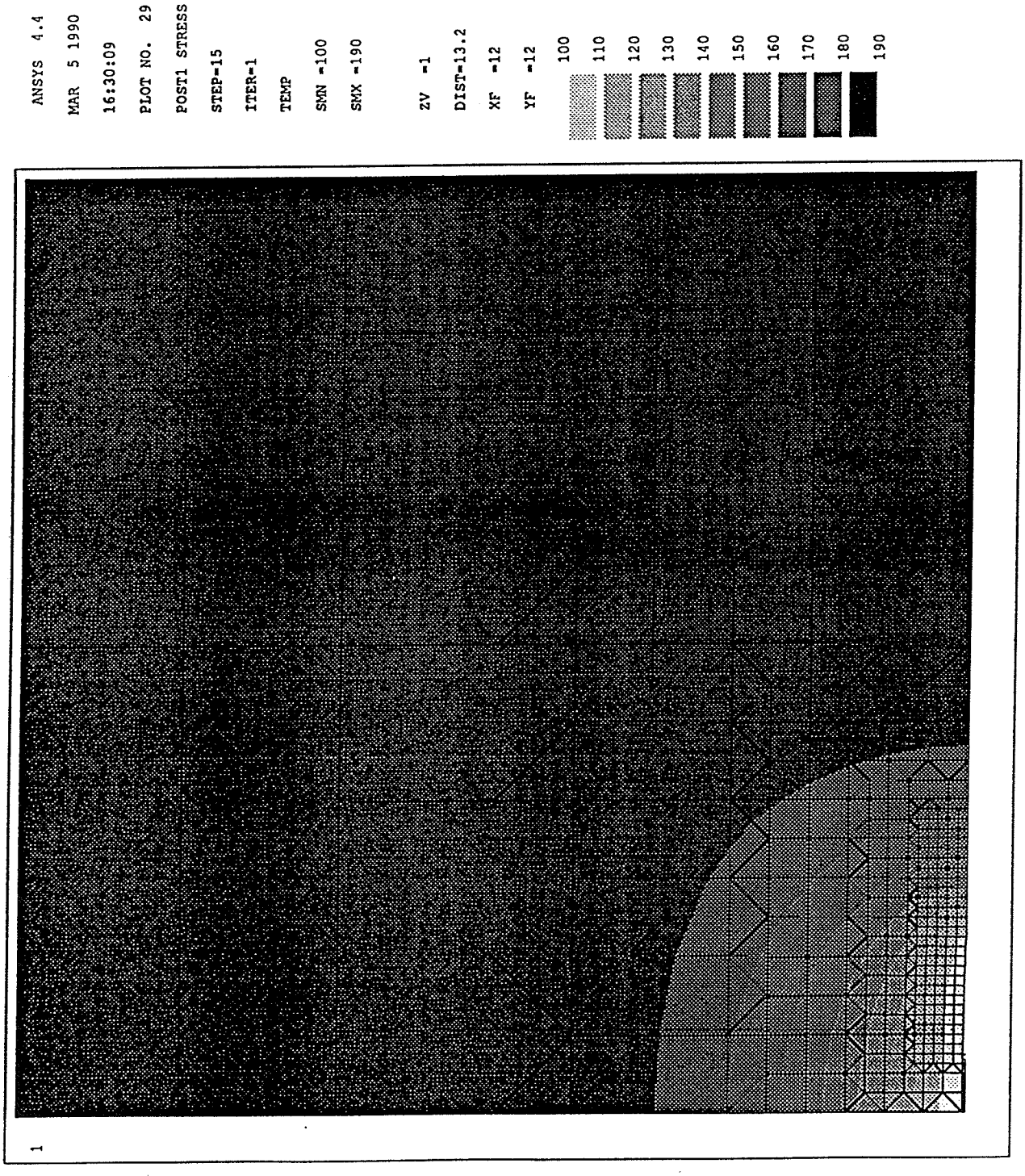

FIGURE 7.1.4g : Temperature Distribution (°C) - Series 7
(time = 14 seconds)

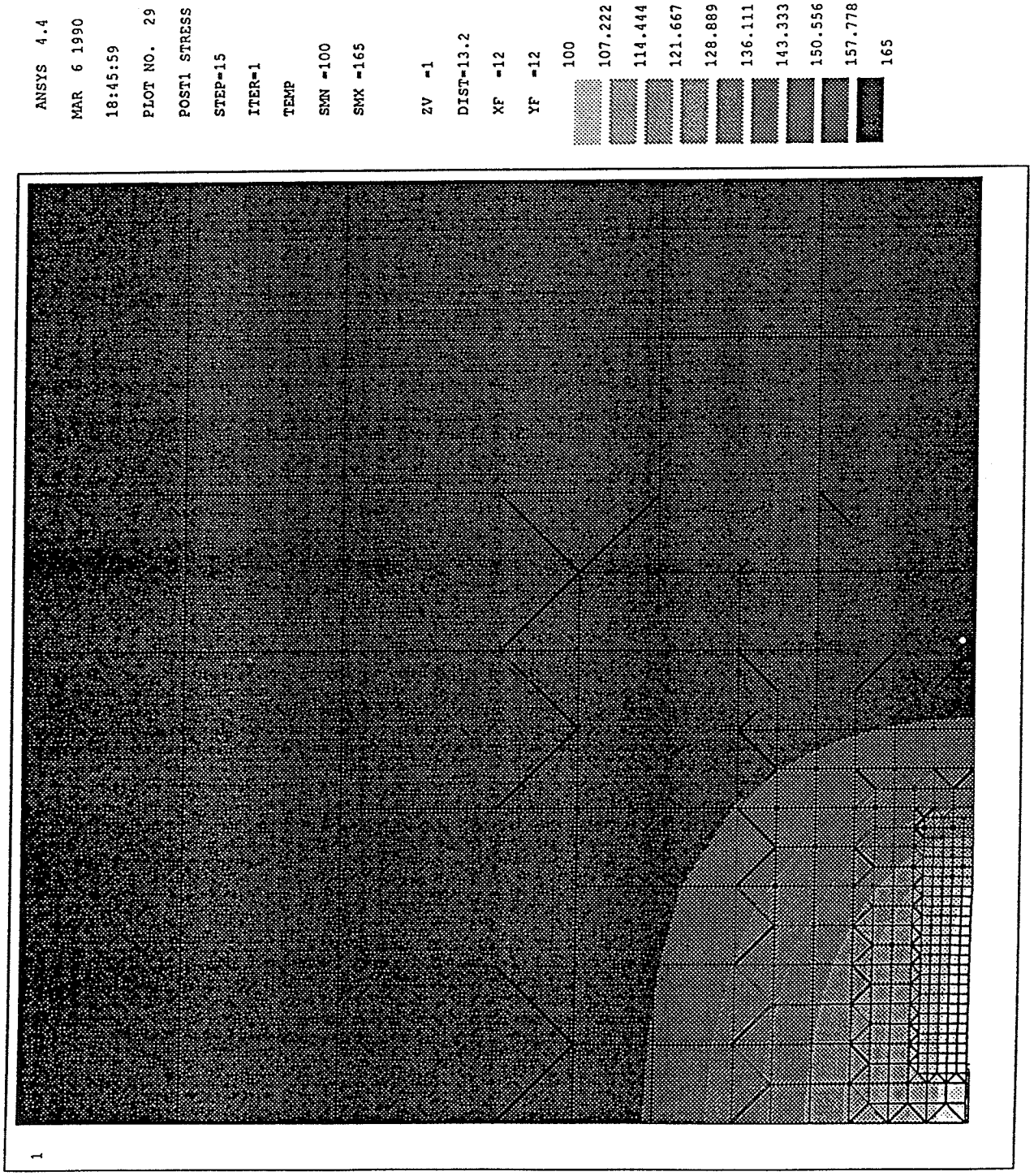

FIGURE 7.1.4h : Temperature Distribution (°C) - Series 8
(time = 14 seconds)

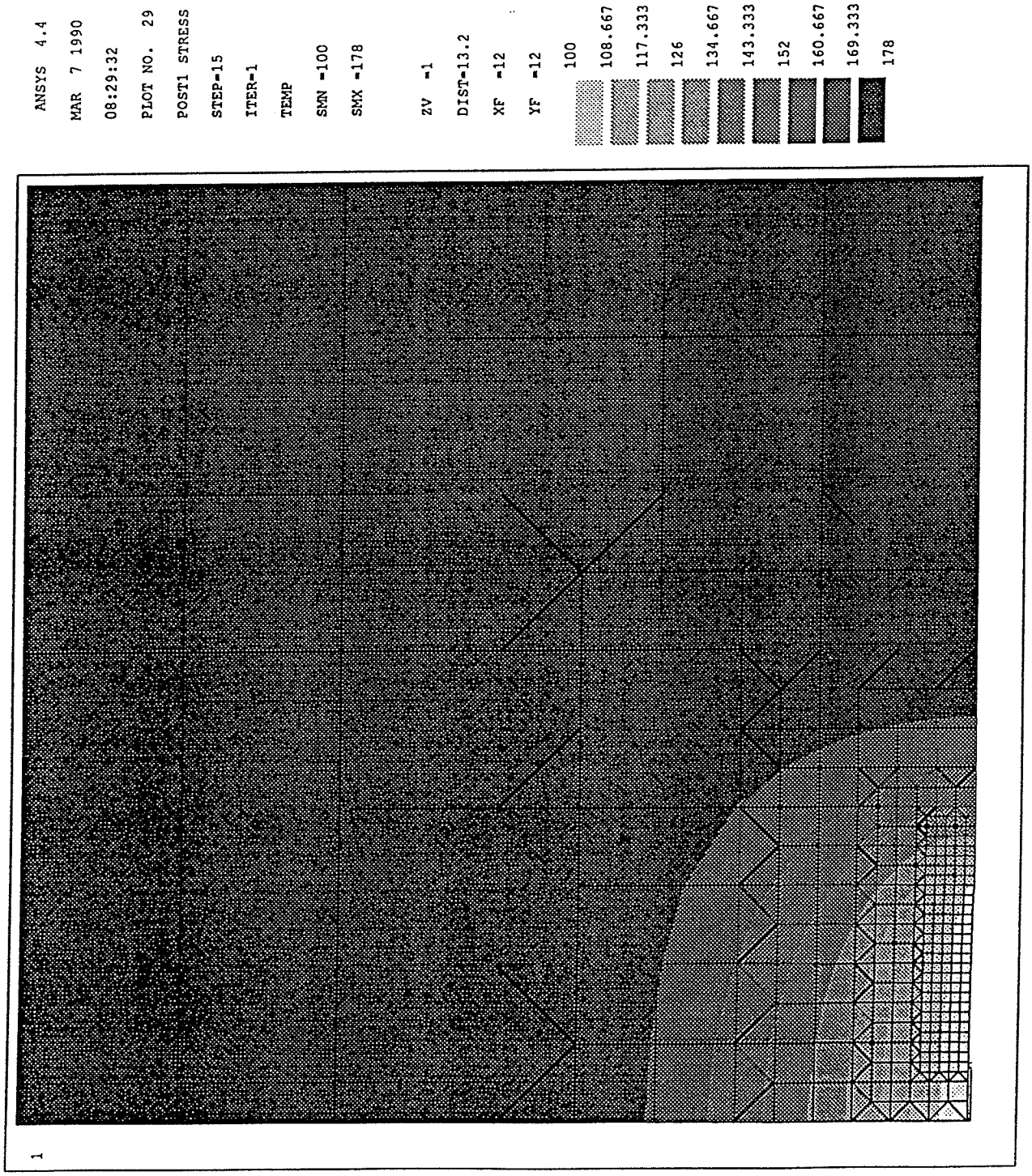

FIGURE 7.1.4i : Temperature Distribution (°C) - Series 9
(time = 14 seconds)

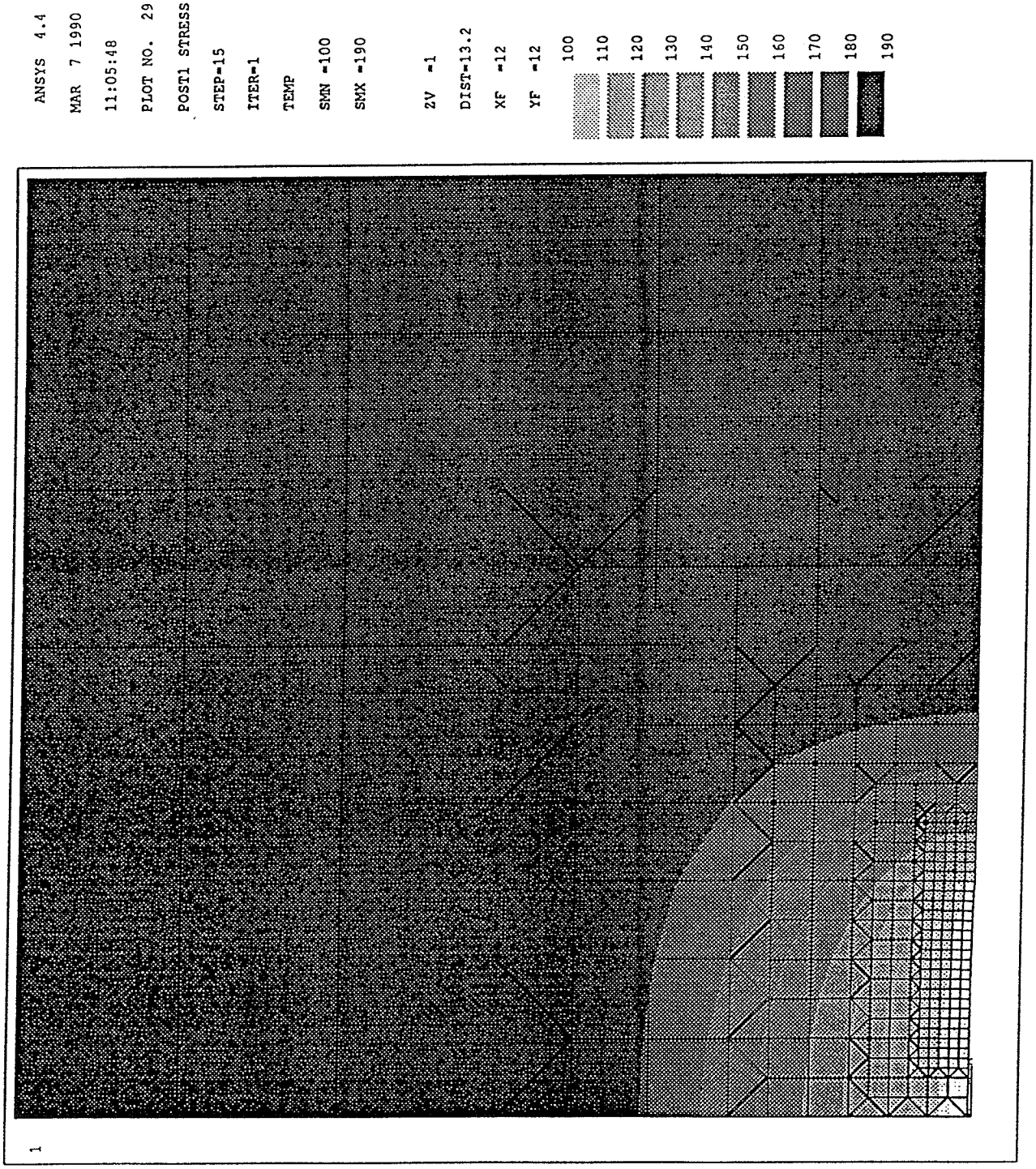

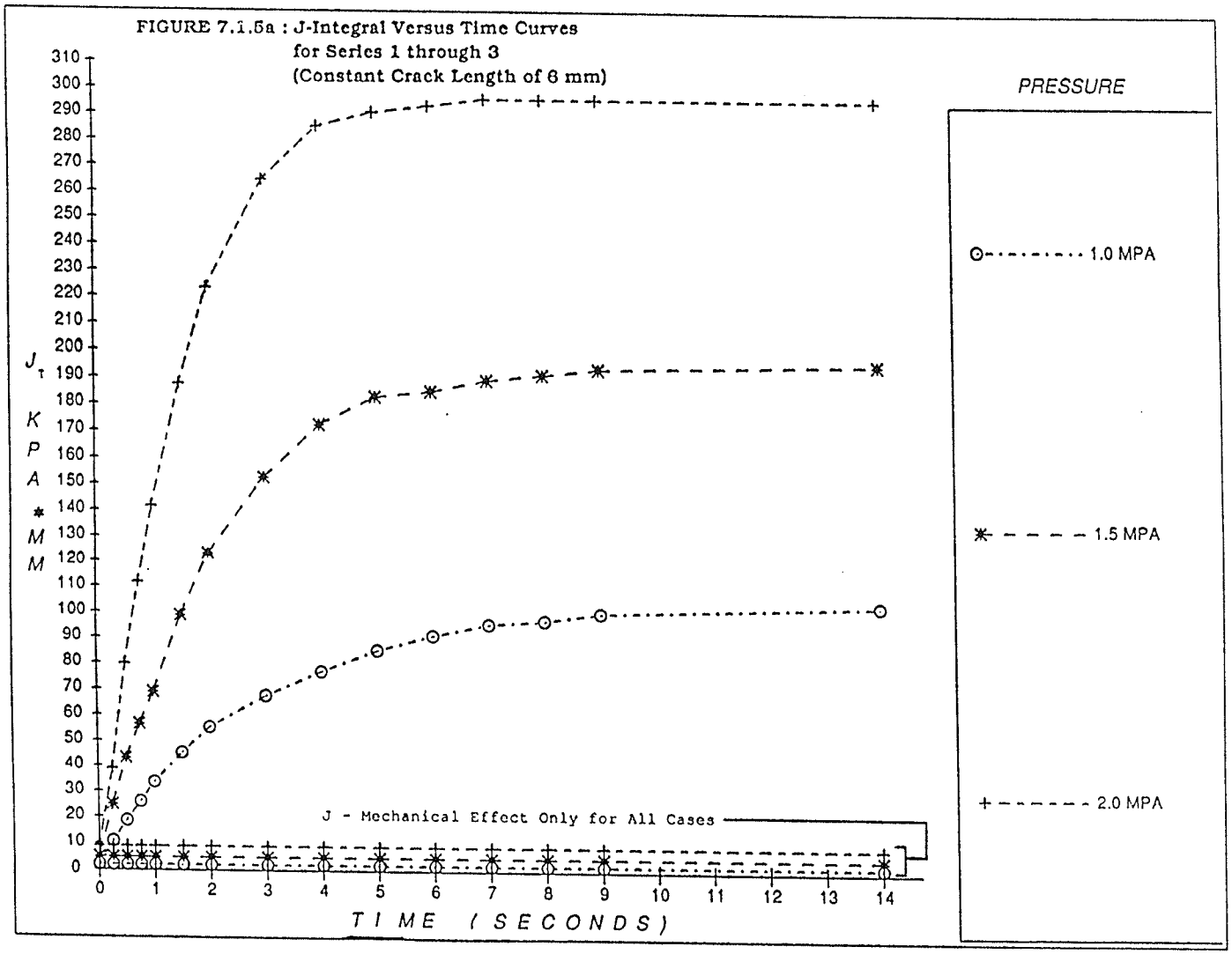
FIGURE 7.1.5a : J-Integral Versus Time Curves
for Series 1 through 3
(Constant Crack Length of 6 mm)
PRESSURE
1.0 MPA
1.5 MPA
2.0 MPA
J - Mechanical Effect Only for All Cases
J_τ KPA * MM
TIME (SECONDS)
310
300
290
280
270
260
250
240
230
220
210
200
190
180
170
160
150
140
130
120
110
100
90
80
70
60
50
40
30
20
10
0
0
1
2
3
4
5
6
7
8
9
10
11
12
13
14

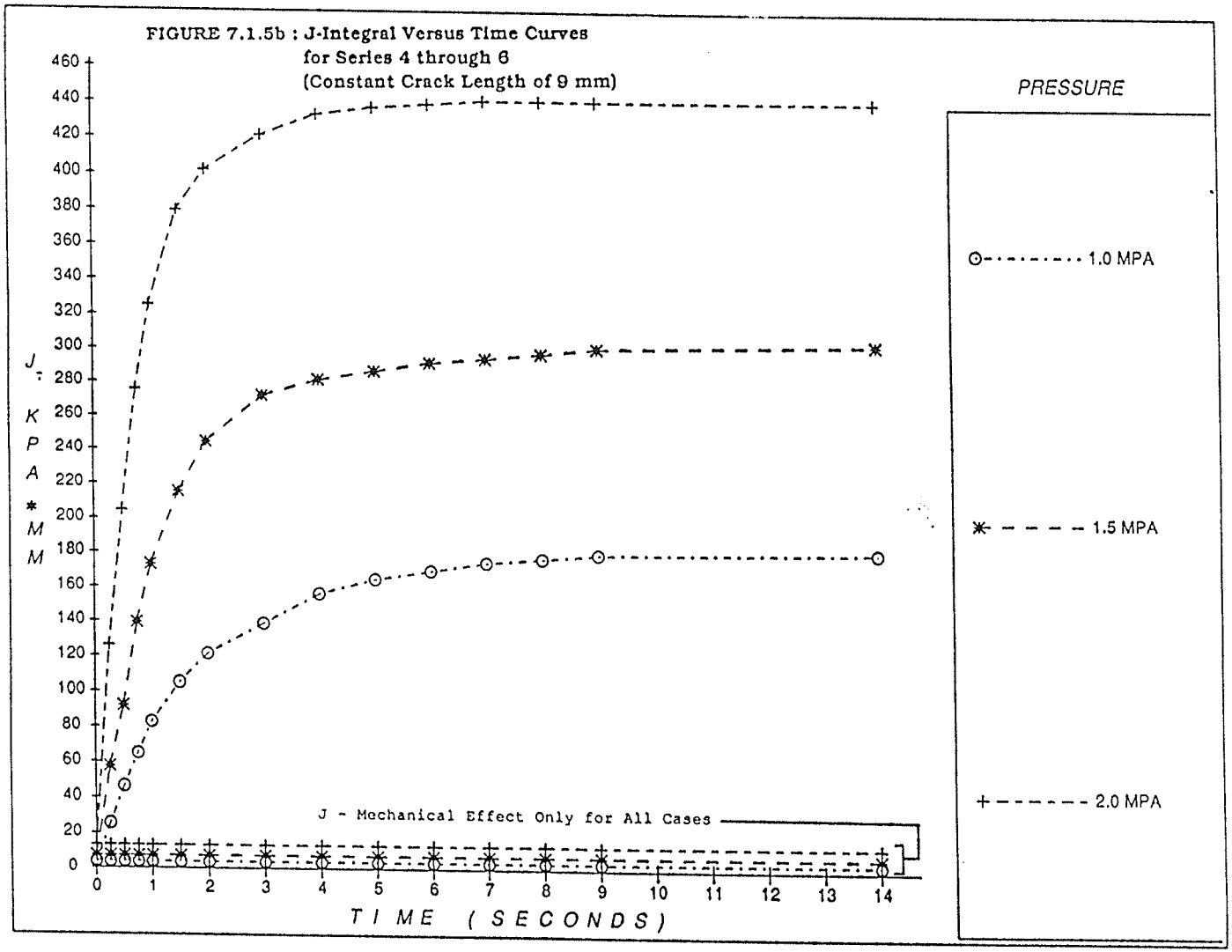
FIGURE 7.1.5b : J-Integral Versus Time Curves
for Series 4 through 6
(Constant Crack Length of 9 mm)
J : KPA * MM
460
440
420
400
380
360
340
320
300
280
260
240
220
200
180
160
140
120
100
80
60
40
20
0
0
1
2
3
4
5
6
7
8
9
10
11
12
13
14
TIME (SECONDS)
J - Mechanical Effect Only for All Cases
PRESSURE
1.0 MPA
1.5 MPA
2.0 MPA

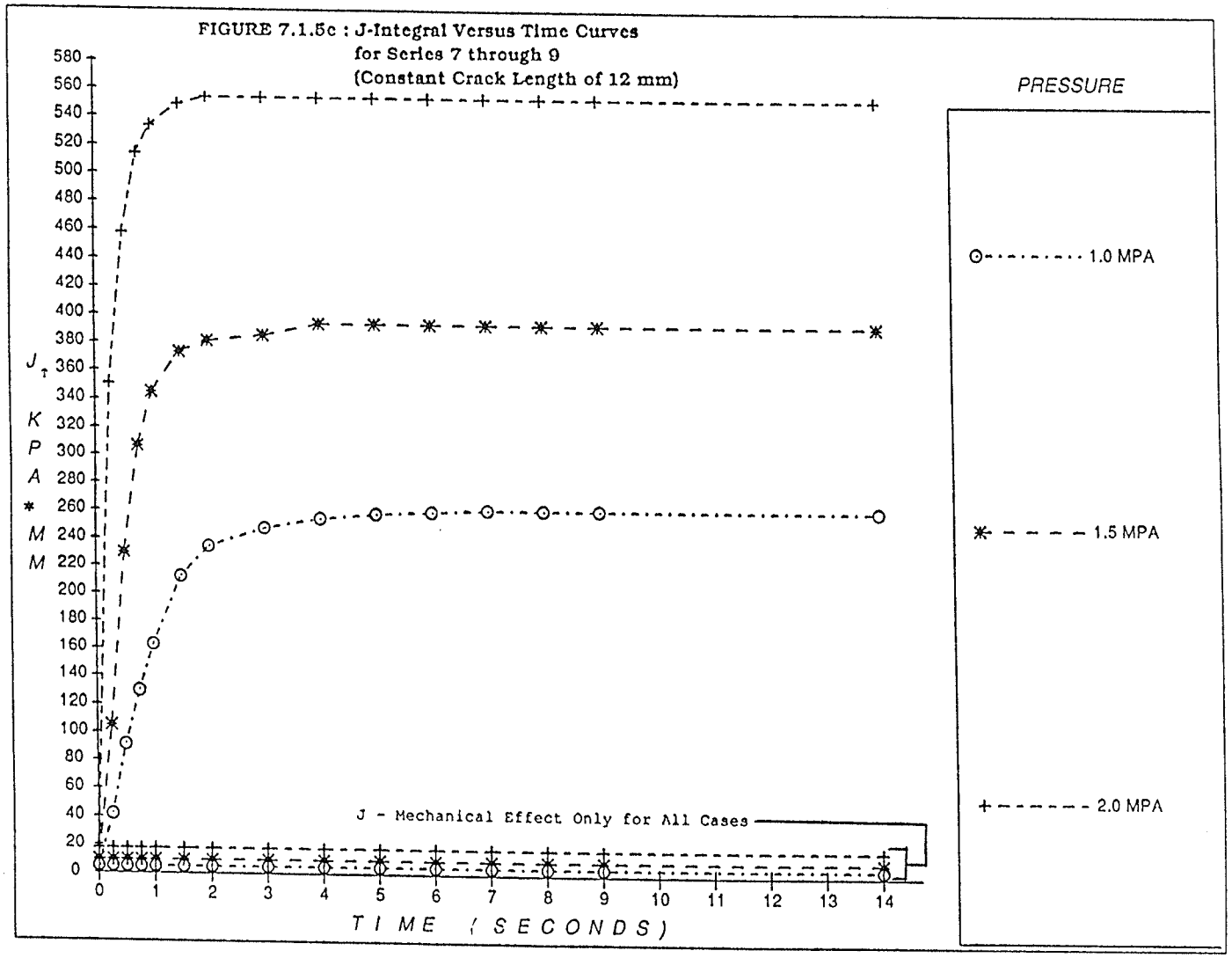
FIGURE 7.1.5c : J-Integral Versus Time Curves
for Series 7 through 9
(Constant Crack Length of 12 mm)
PRESSURE
1.0 MPA
1.5 MPA
2.0 MPA
J - Mechanical Effect Only for All Cases
J_τ K P A * M M
TIME (SECONDS)
0 20 40 60 80 100 120 140 160 180 200 220 240 260 280 300 320 340 360 380 400 420 440 460 480 500 520 540 560 580
0 1 2 3 4 5 6 7 8 9 10 11 12 13 14

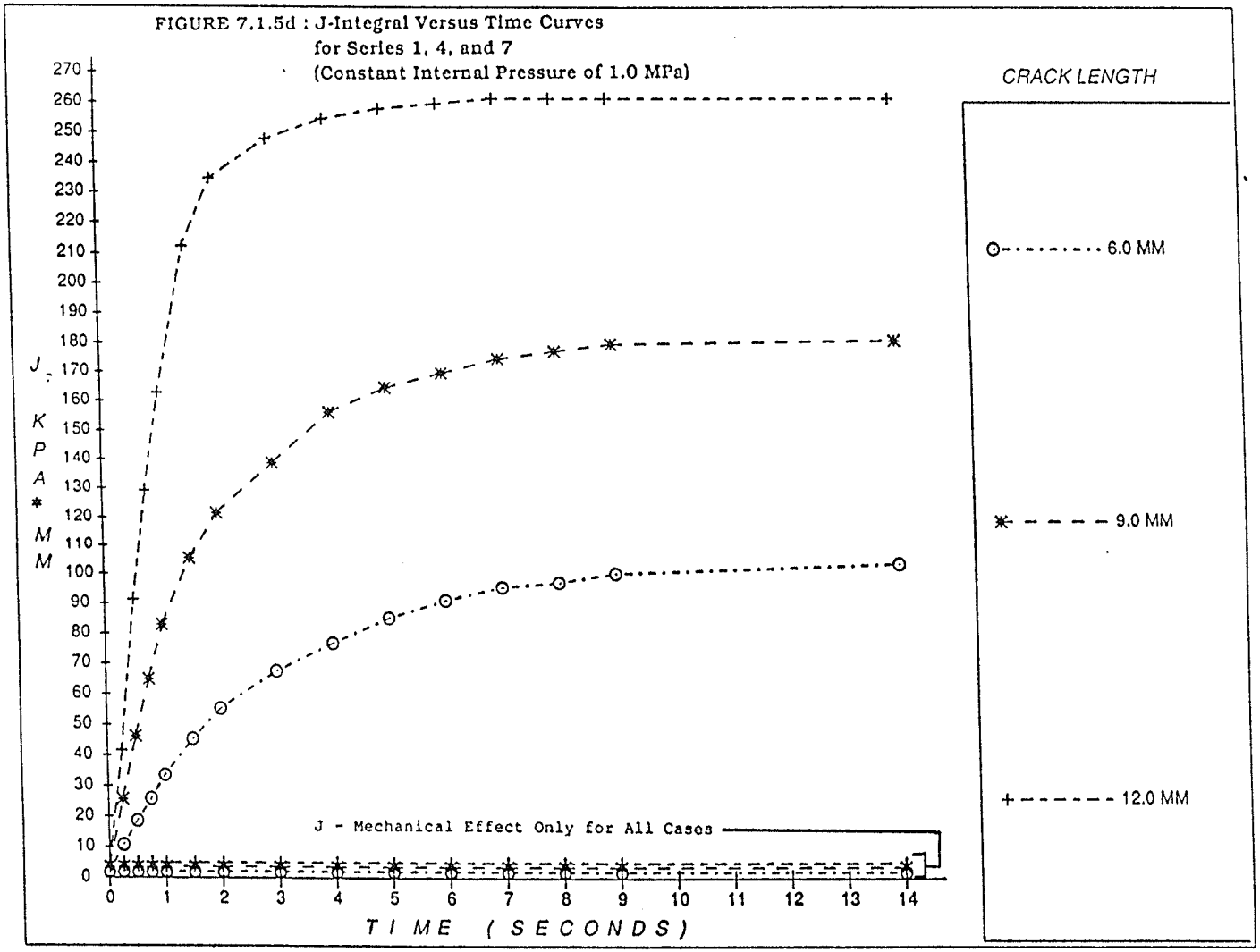
FIGURE 7.1.5d : J-Integral Versus Time Curves
for Series 1, 4, and 7
(Constant Internal Pressure of 1.0 MPa)
CRACK LENGTH
6.0 MM
9.0 MM
12.0 MM
J - Mechanical Effect Only for All Cases
J, KPA*MM
TIME (SECONDS)
0
10
20
30
40
50
60
70
80
90
100
110
120
130
140
150
160
170
180
190
200
210
220
230
240
250
260
270
0
1
2
3
4
5
6
7
8
9
10
11
12
13
14

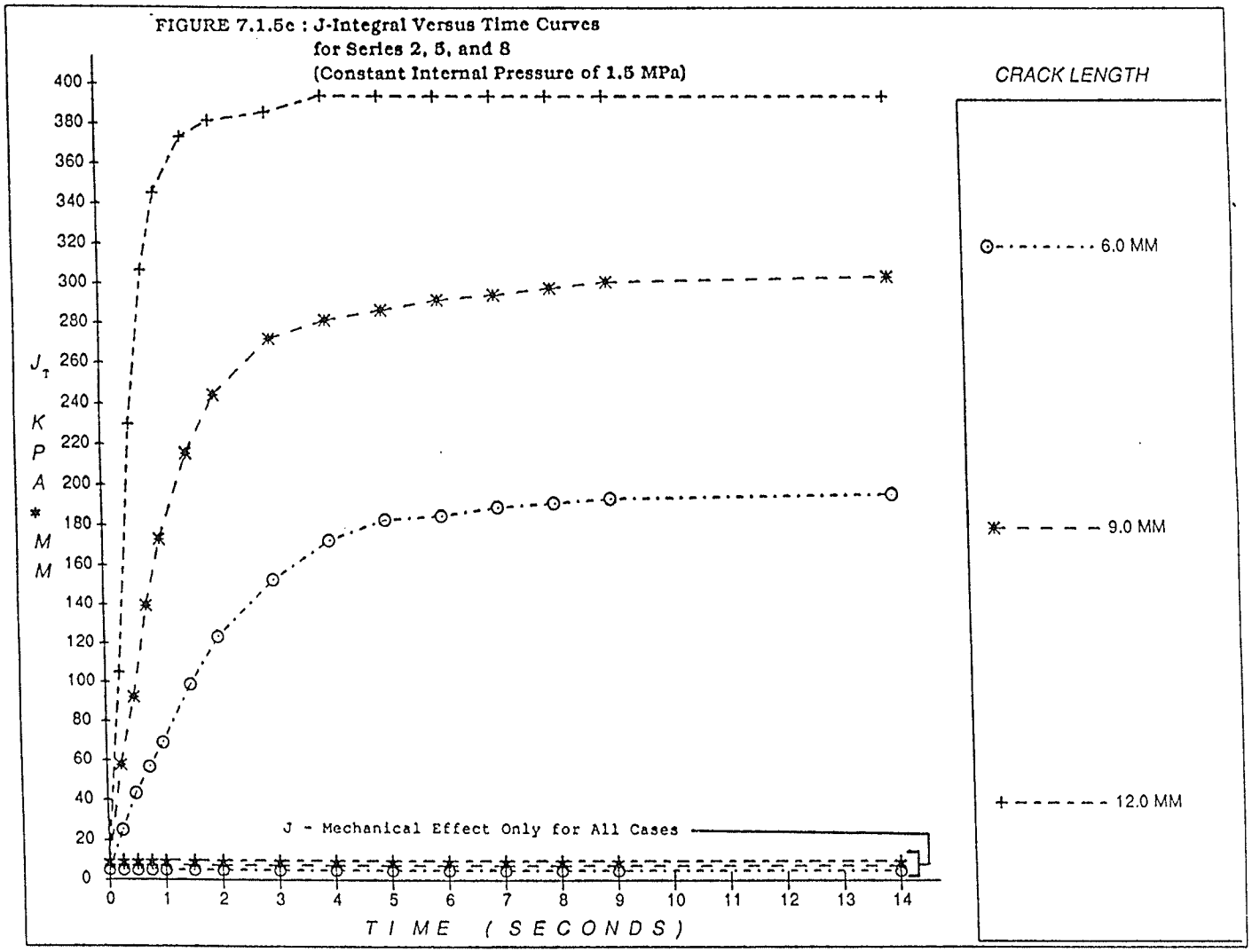
FIGURE 7.1.5c : J-Integral Versus Time Curves
for Series 2, 5, and 8
(Constant Internal Pressure of 1.5 MPa)
CRACK LENGTH
6.0 MM
9.0 MM
12.0 MM
J - Mechanical Effect Only for All Cases
J_T KPA * MM
TIME (SECONDS)
0
20
40
60
80
100
120
140
160
180
200
220
240
260
280
300
320
340
360
380
400
0
1
2
3
4
5
6
7
8
9
10
11
12
13
14

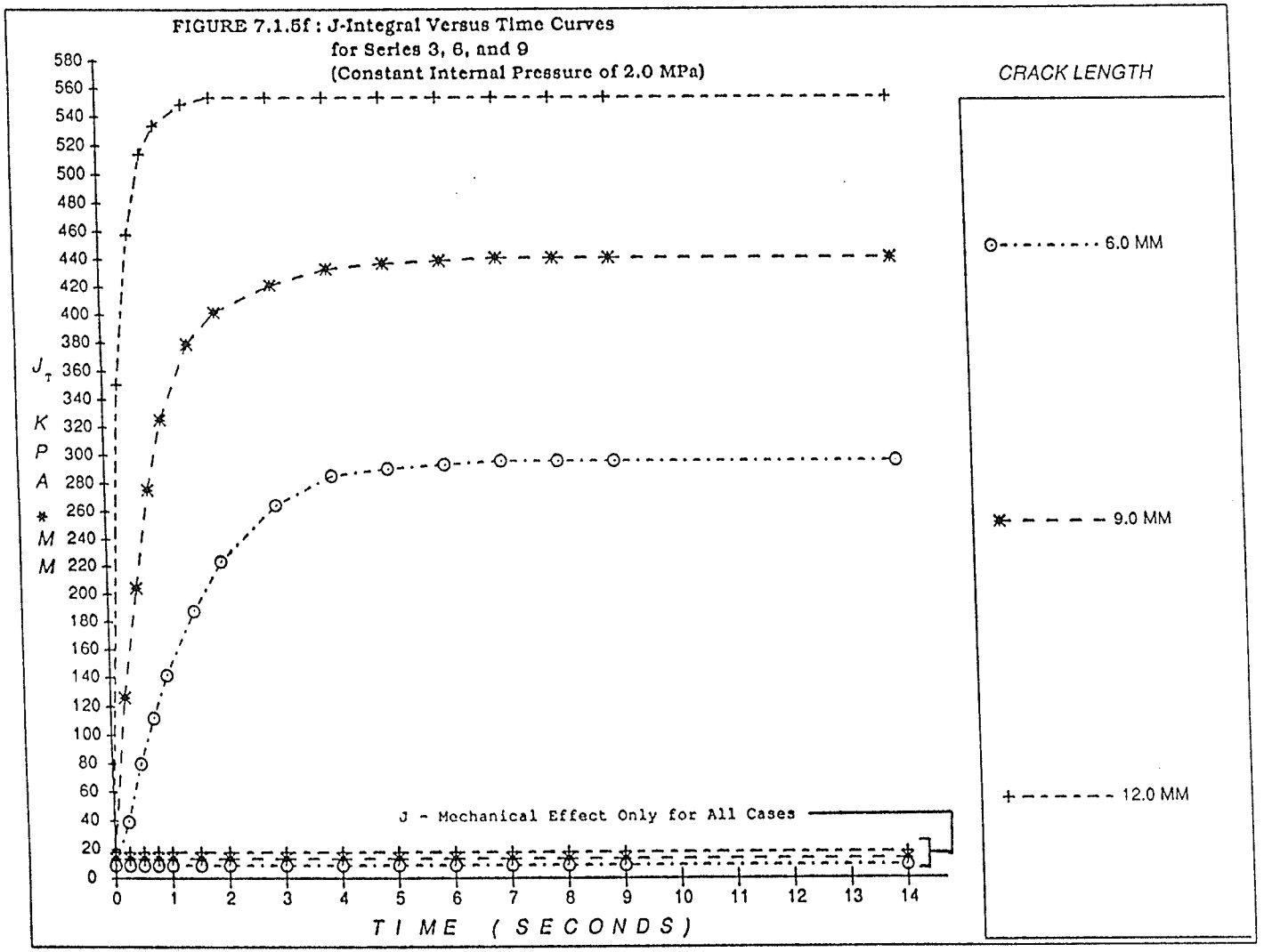
FIGURE 7.1.5f : J-Integral Versus Time Curves
for Series 3, 6, and 9
(Constant Internal Pressure of 2.0 MPa)
CRACK LENGTH
6.0 MM
9.0 MM
12.0 MM
J - Mechanical Effect Only for All Cases
J_T K P A * M M
TIME (SECONDS)
0 20 40 60 80 100 120 140 160 180 200 220 240 260 280 300 320 340 360 380 400 420 440 460 480 500 520 540 560 580
0 1 2 3 4 5 6 7 8 9 10 11 12 13 14

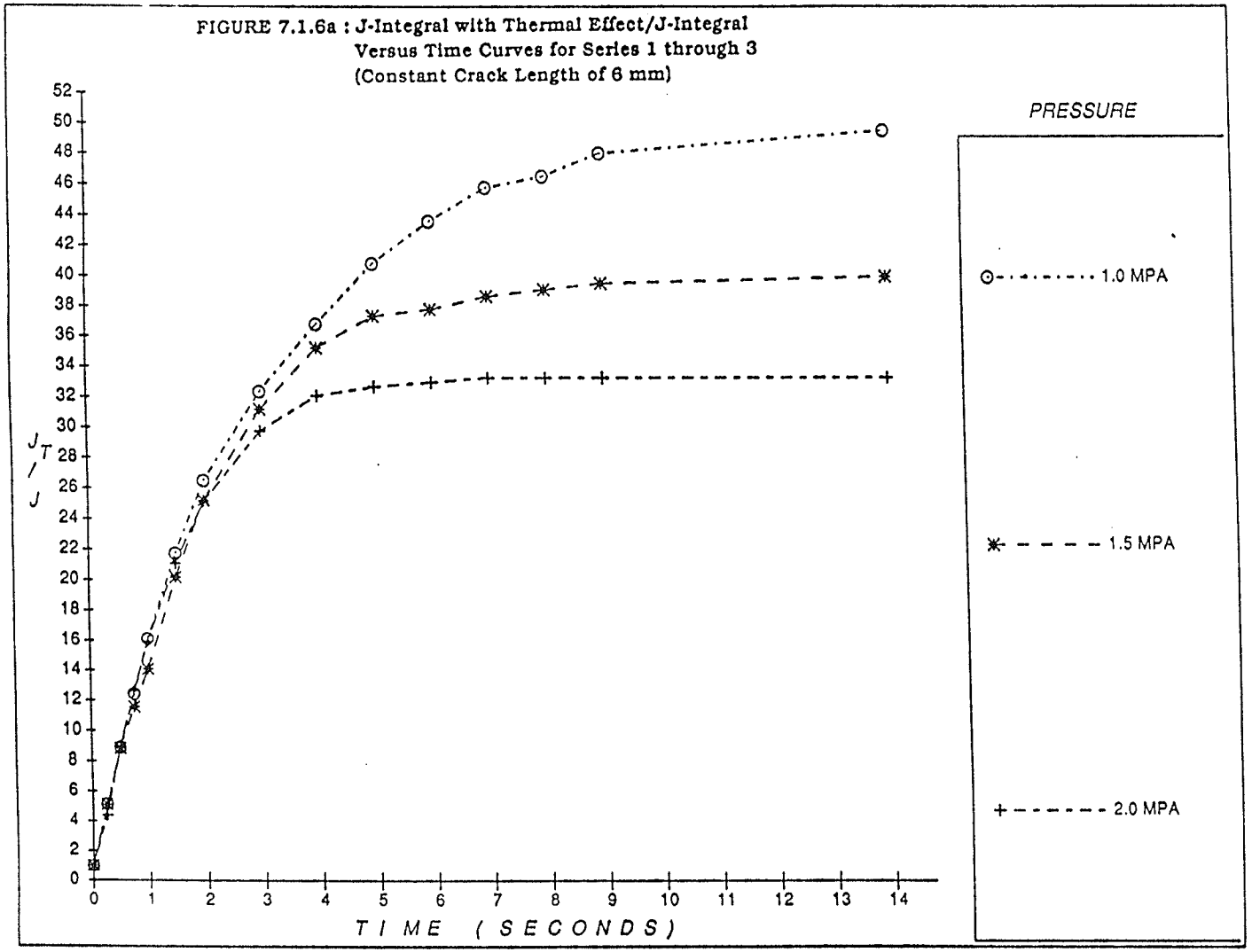

FIGURE 7.1.6a : J-Integral with Thermal Effect/J-Integral Versus Time Curves for Series 1 through 3 (Constant Crack Length of 6 mm)

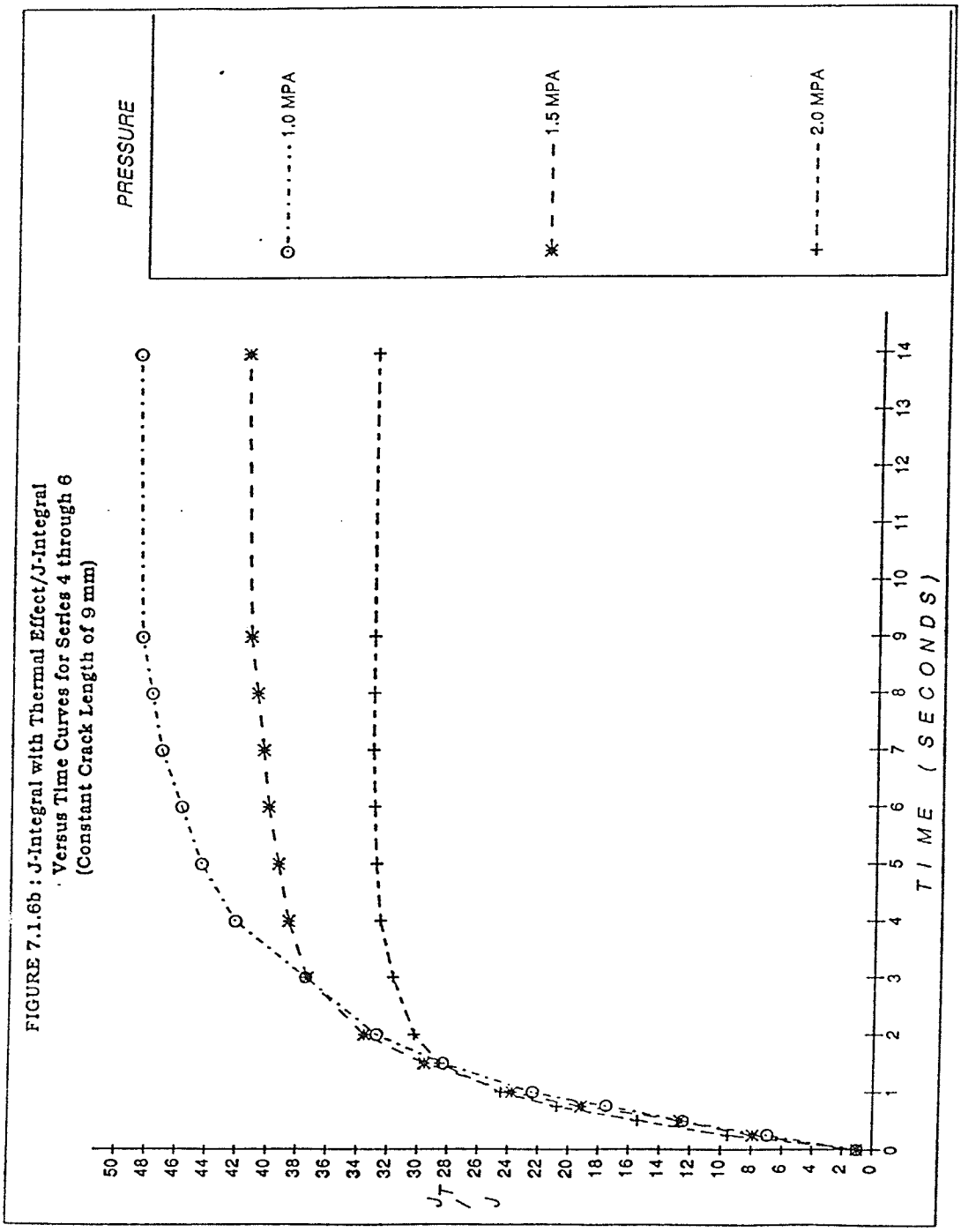

FIGURE 7.1.6b : J-Integral with Thermal Effect/J-Integral Versus Time Curves for Series 4 through 6 (Constant Crack Length of 9 mm)

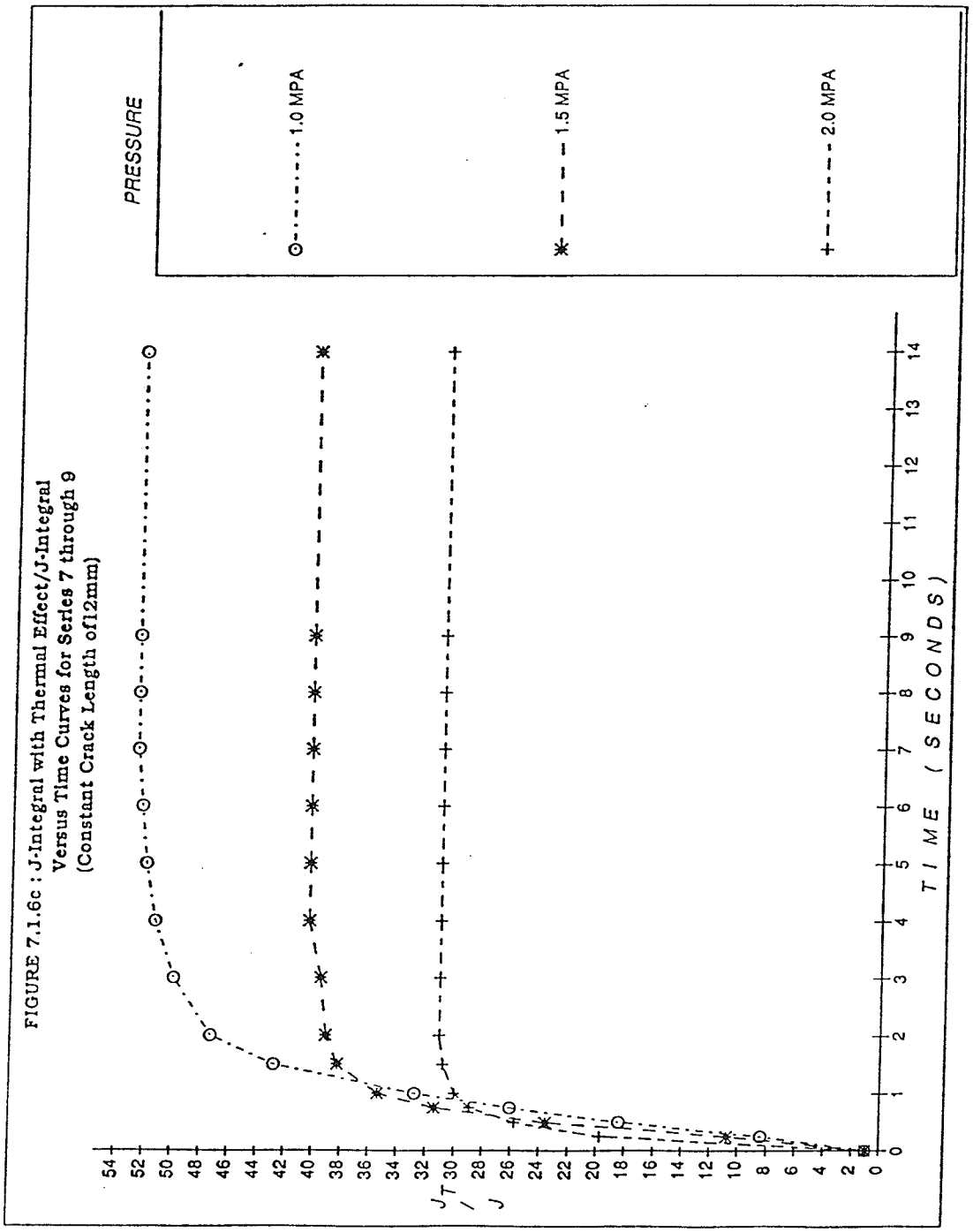

FIGURE 7.1.6c : J-Integral with Thermal Effect/J-Integral Versus Time Curves for Series 7 through 9 (Constant Crack Length of12mm)

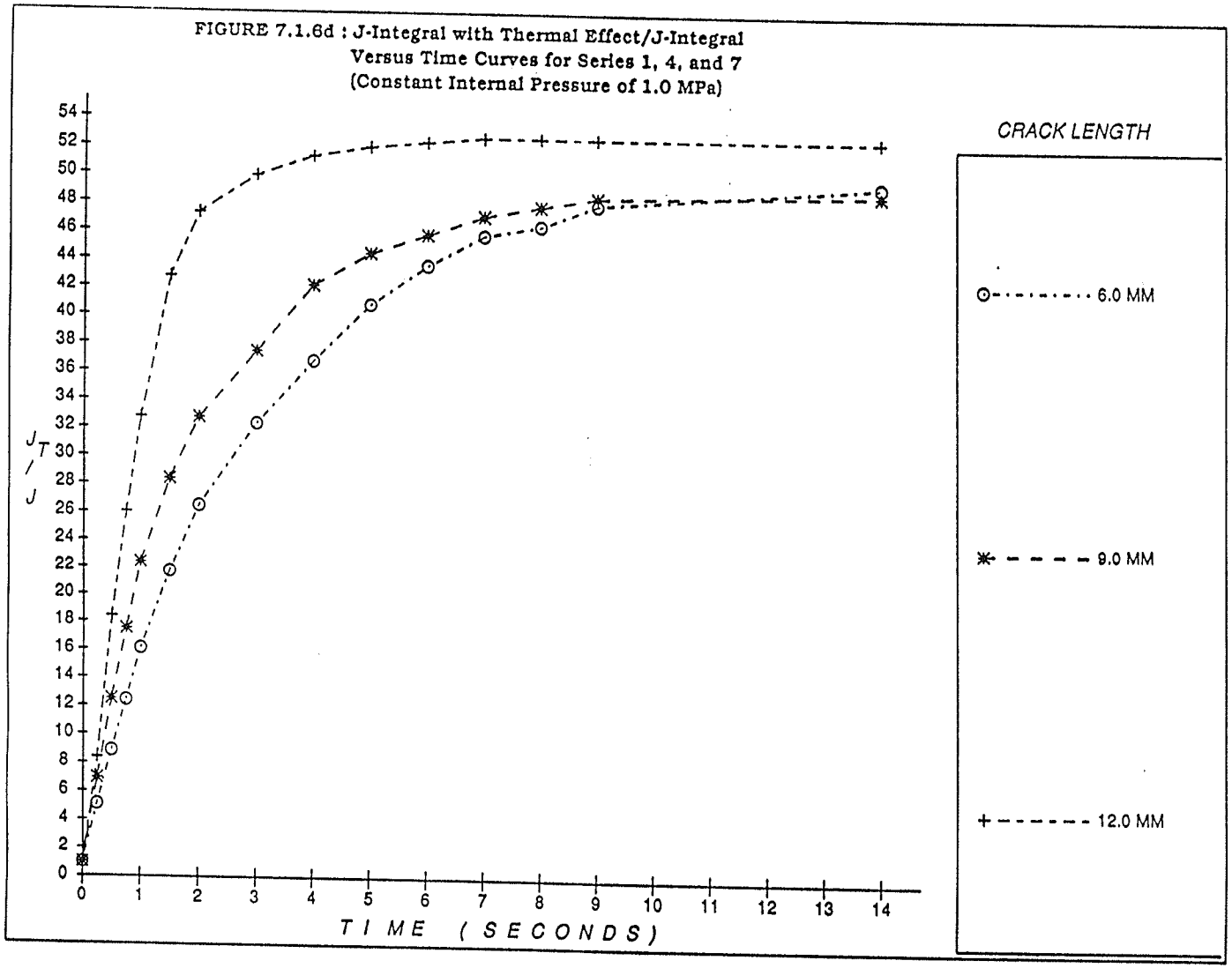

FIGURE 7.1.6d : J-Integral with Thermal Effect/J-Integral Versus Time Curves for Series 1, 4, and 7 (Constant Internal Pressure of 1.0 MPa)

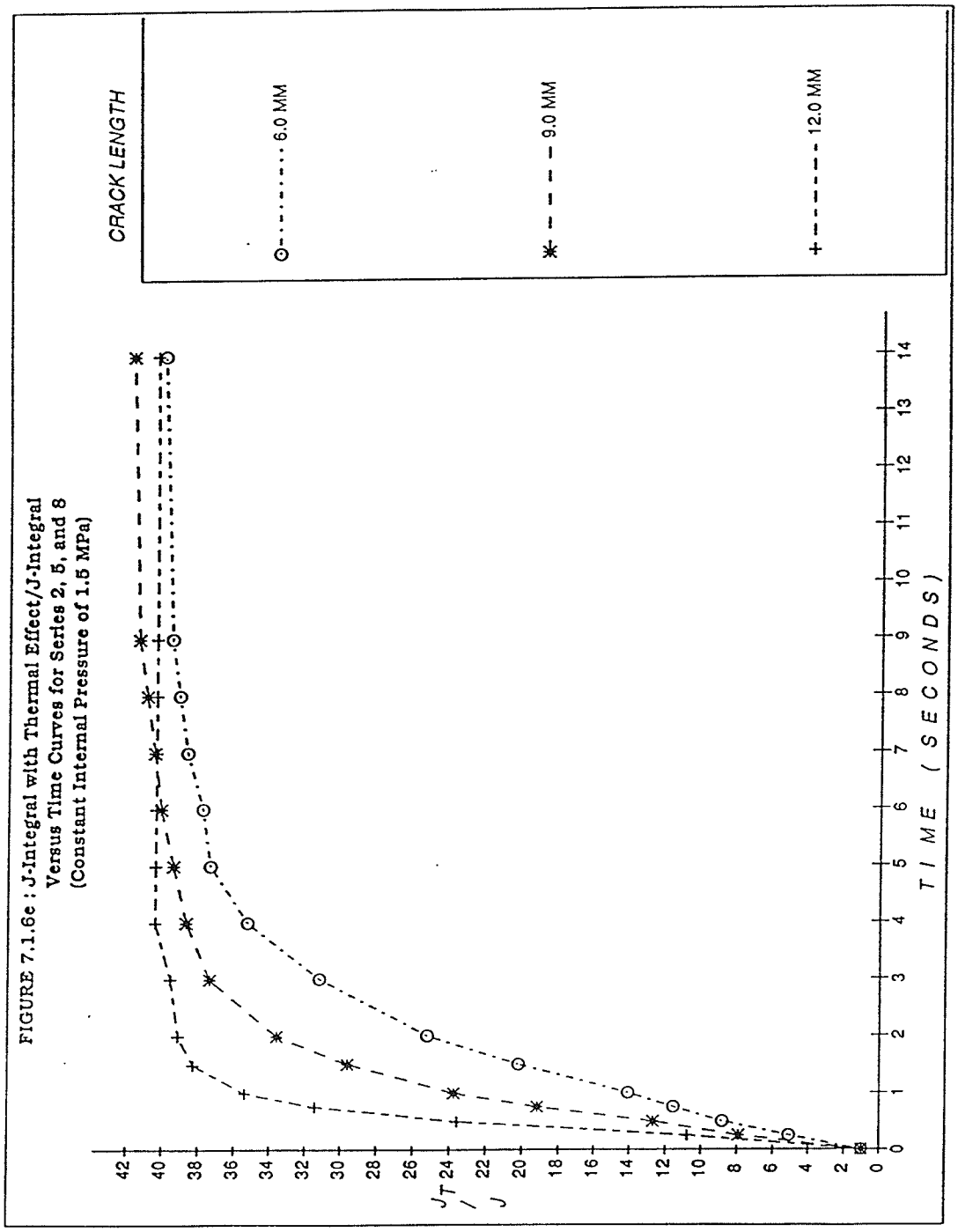

FIGURE 7.1.6e : J-Integral with Thermal Effect/J-Integral Versus Time Curves for Series 2, 5, and 8 (Constant Internal Pressure of 1.5 MPa)

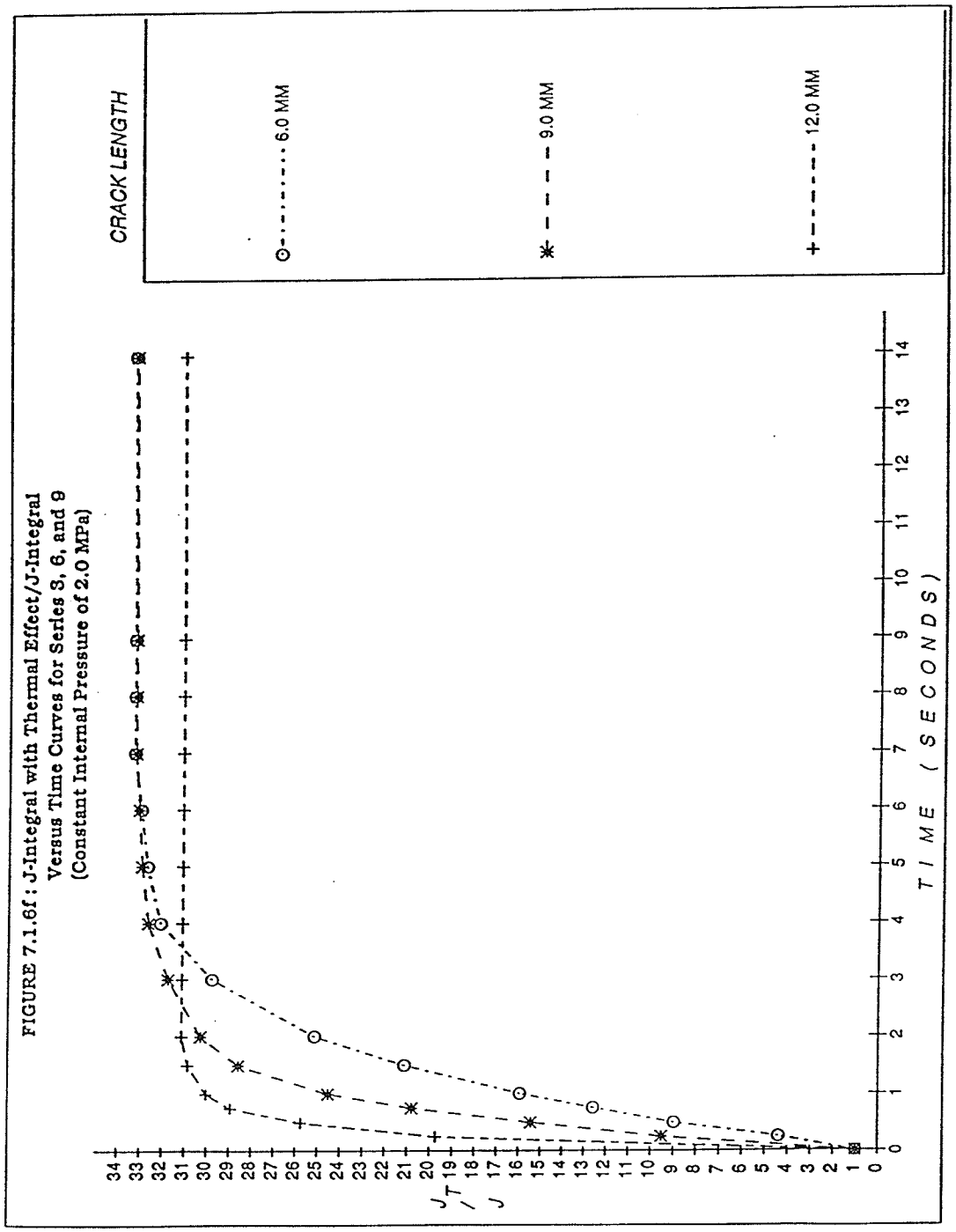

FIGURE 7.1.6f : J-Integral with Thermal Effect/J-Integral Versus Time Curves for Series 3, 6, and 9 (Constant Internal Pressure of 2.0 MPa)

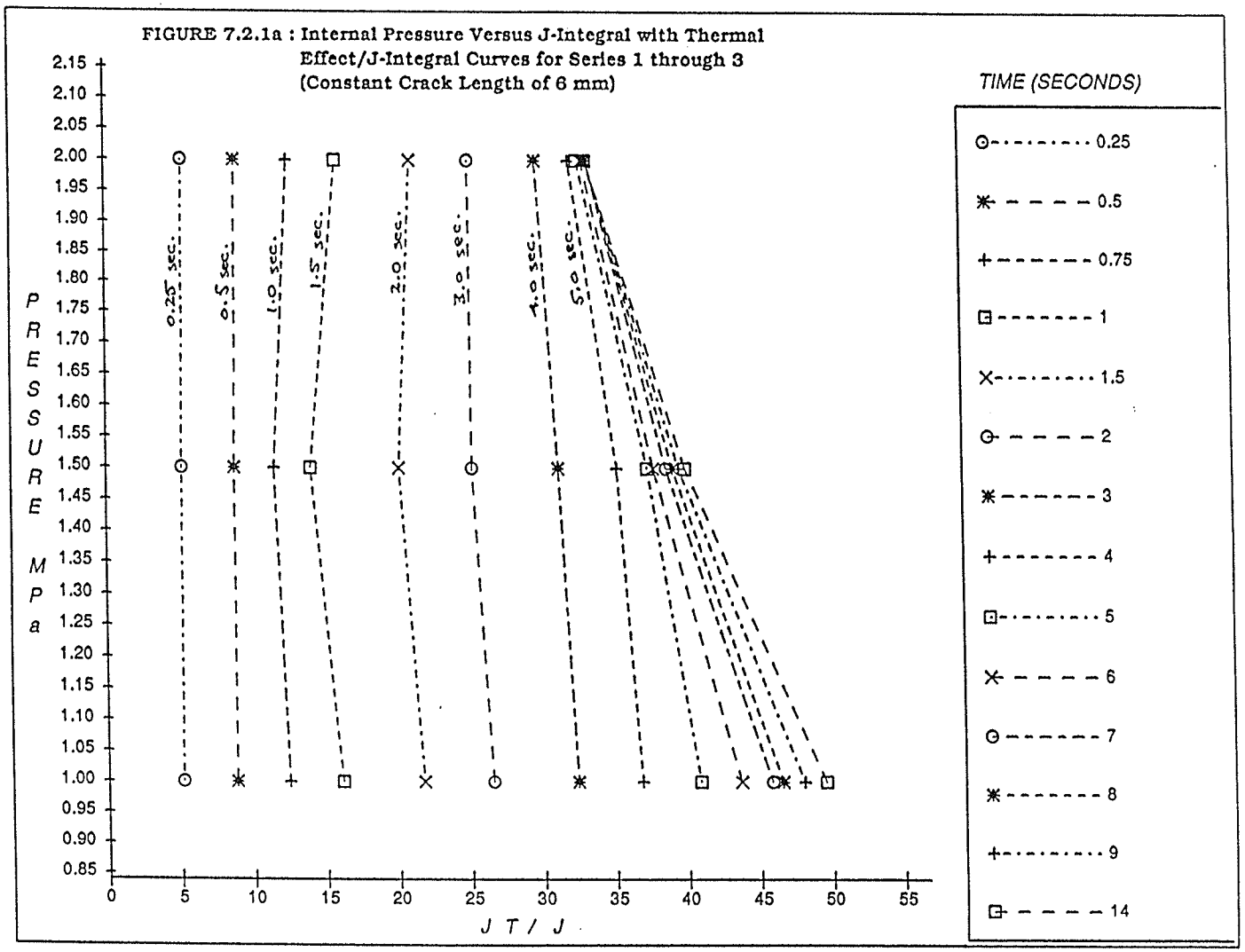
FIGURE 7.2.1a : Internal Pressure Versus J-Integral with Thermal Effect/J-Integral Curves for Series 1 through 3 (Constant Crack Length of 6 mm)
PRESSURE MPa
2.15
2.10
2.05
2.00
1.95
1.90
1.85
1.80
1.75
1.70
1.65
1.60
1.55
1.50
1.45
1.40
1.35
1.30
1.25
1.20
1.15
1.10
1.05
1.00
0.95
0.90
0.85
0
5
10
15
20
25
30
35
40
45
50
55
J T / J
0.25 sec.
0.5 sec.
1.0 sec.
1.5 sec.
2.0 sec.
3.0 sec.
4.0 sec.
5.0 sec.
TIME (SECONDS)
0.25
0.5
0.75
1
1.5
2
3
4
5
6
7
8
9
14

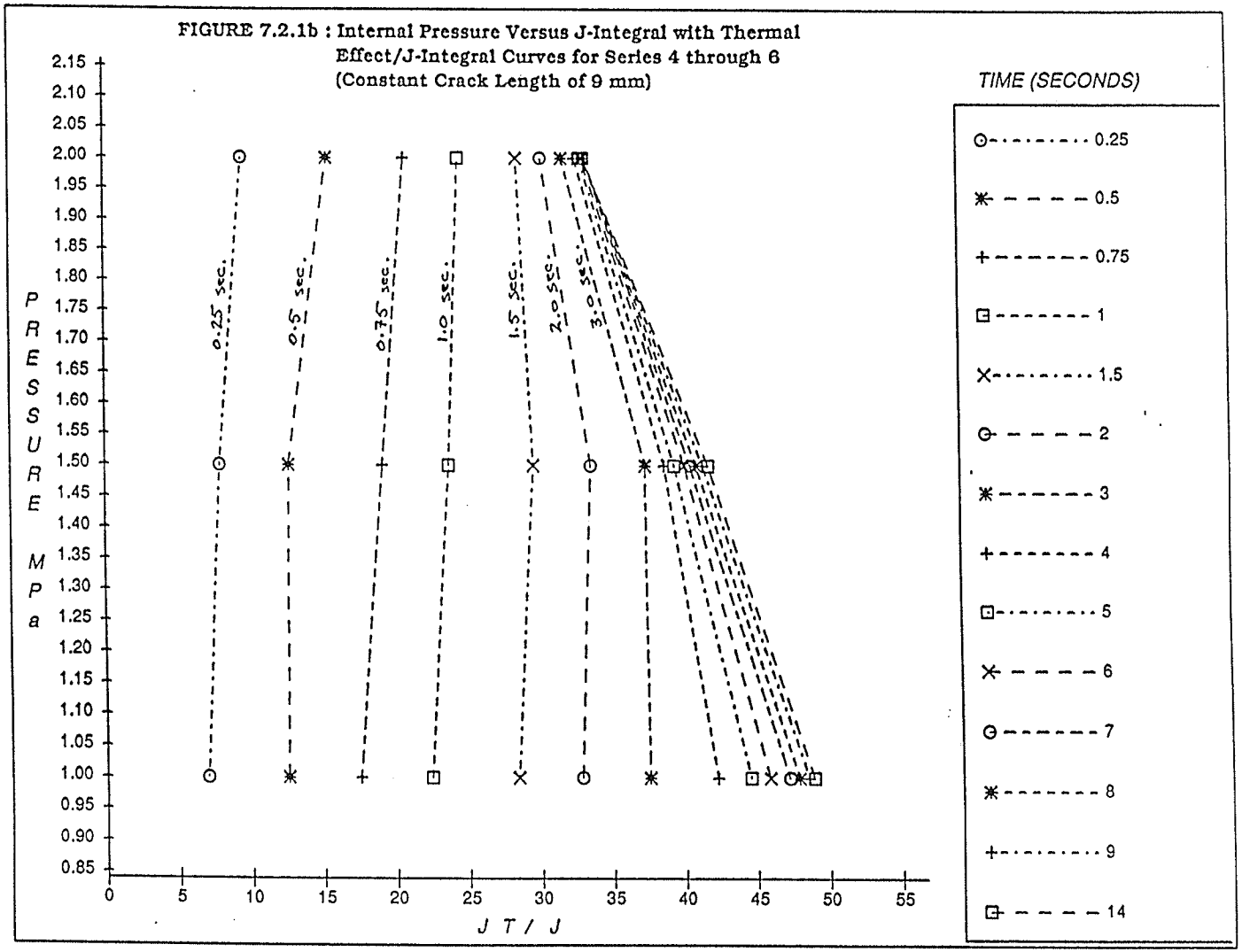

FIGURE 7.2.1b : Internal Pressure Versus J-Integral with Thermal Effect/J-Integral Curves for Series 4 through 6 (Constant Crack Length of 9 mm)

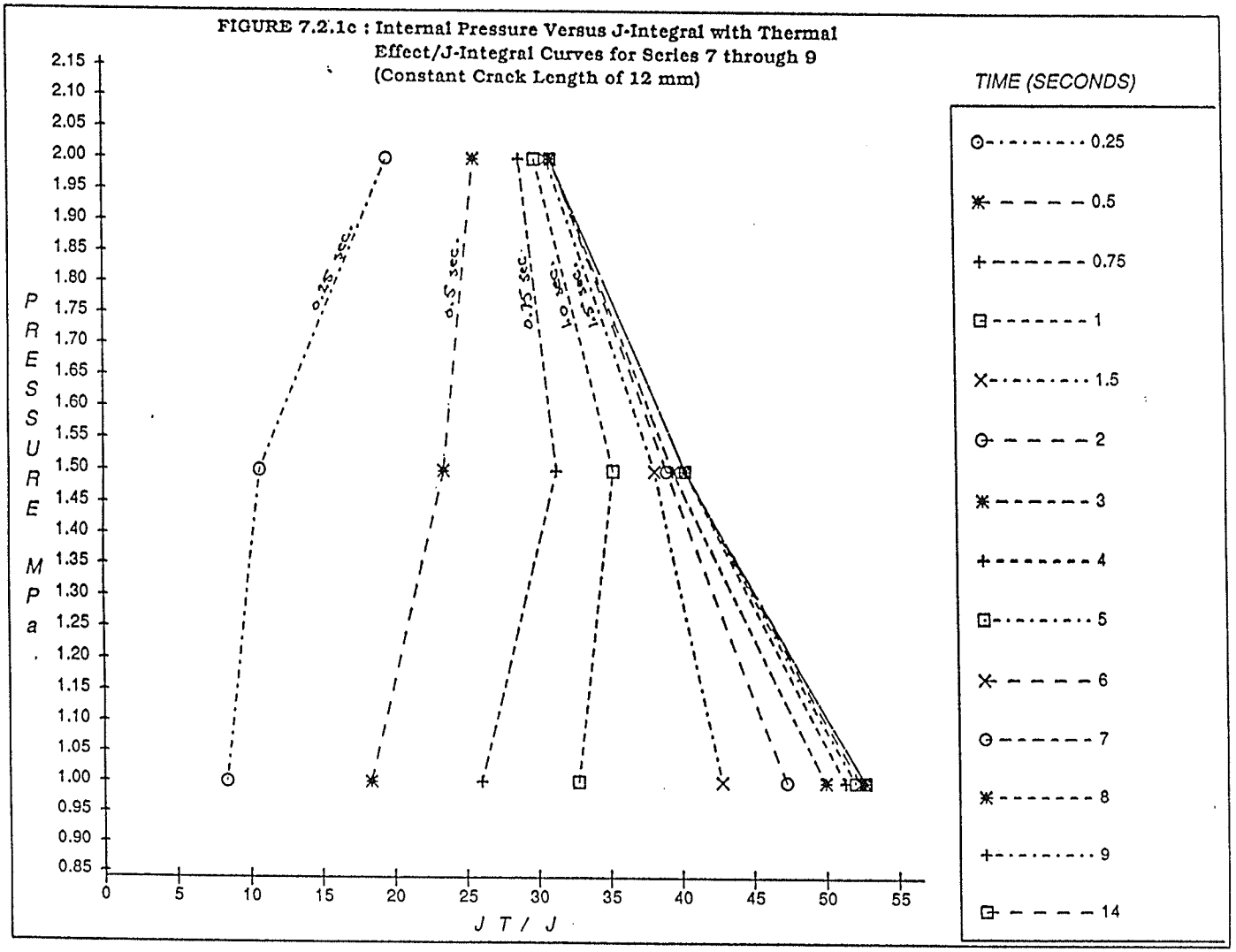
FIGURE 7.2.1c : Internal Pressure Versus J-Integral with Thermal Effect/J-Integral Curves for Series 7 through 9 (Constant Crack Length of 12 mm)
TIME (SECONDS)
0.25
0.5
0.75
1
1.5
2
3
4
5
6
7
8
9
14
PRESSURE MPa
J T / J
0.25 sec.
0.5 sec.
0.75 sec.
1.0 sec.
1.5 sec.

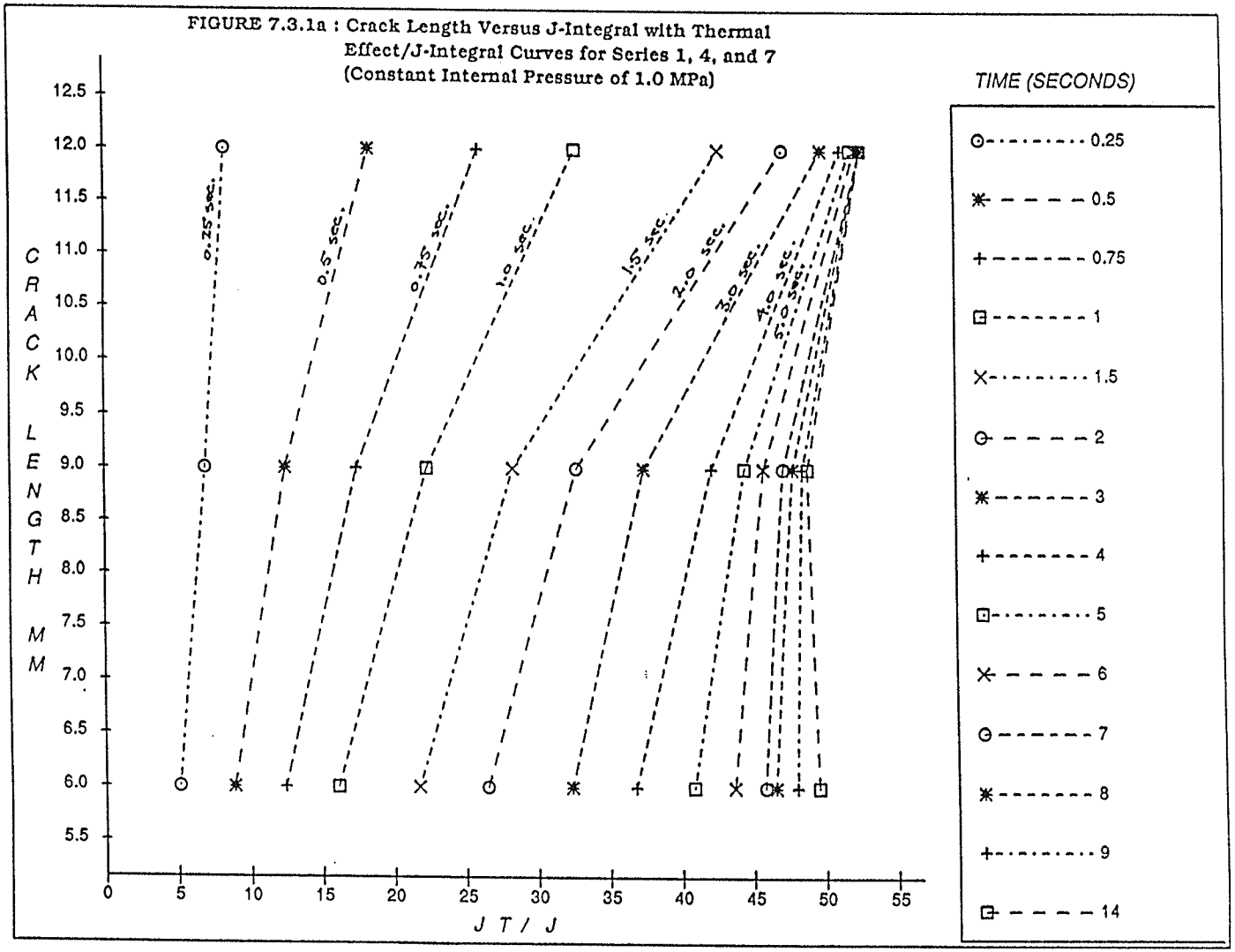
FIGURE 7.3.1a : Crack Length Versus J-Integral with Thermal Effect/J-Integral Curves for Series 1, 4, and 7 (Constant Internal Pressure of 1.0 MPa)
CRACK LENGTH MM
J T / J
TIME (SECONDS)
0.25
0.5
0.75
1
1.5
2
3
4
5
6
7
8
9
14
0.25 sec.
0.5 sec.
0.75 sec.
1.0 sec.
1.5 sec.
2.0 sec.
3.0 sec.
4.0 sec.
5.0 sec.
6.0 sec.

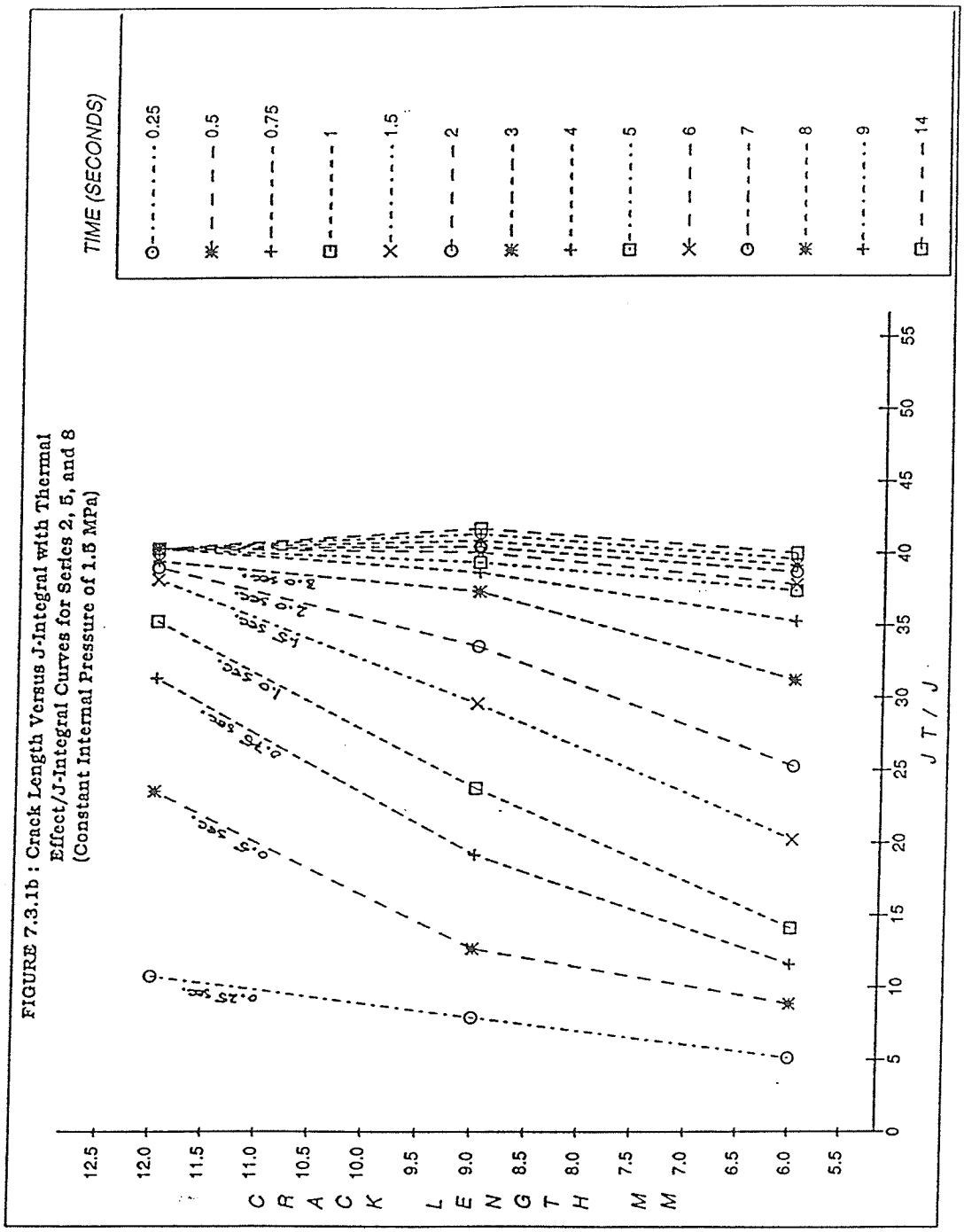

FIGURE 7.3.1b : Crack Length Versus J-Integral with Thermal Effect/J-Integral Curves for Series 2, 5, and 8 (Constant Internal Pressure of 1.5 MPa)

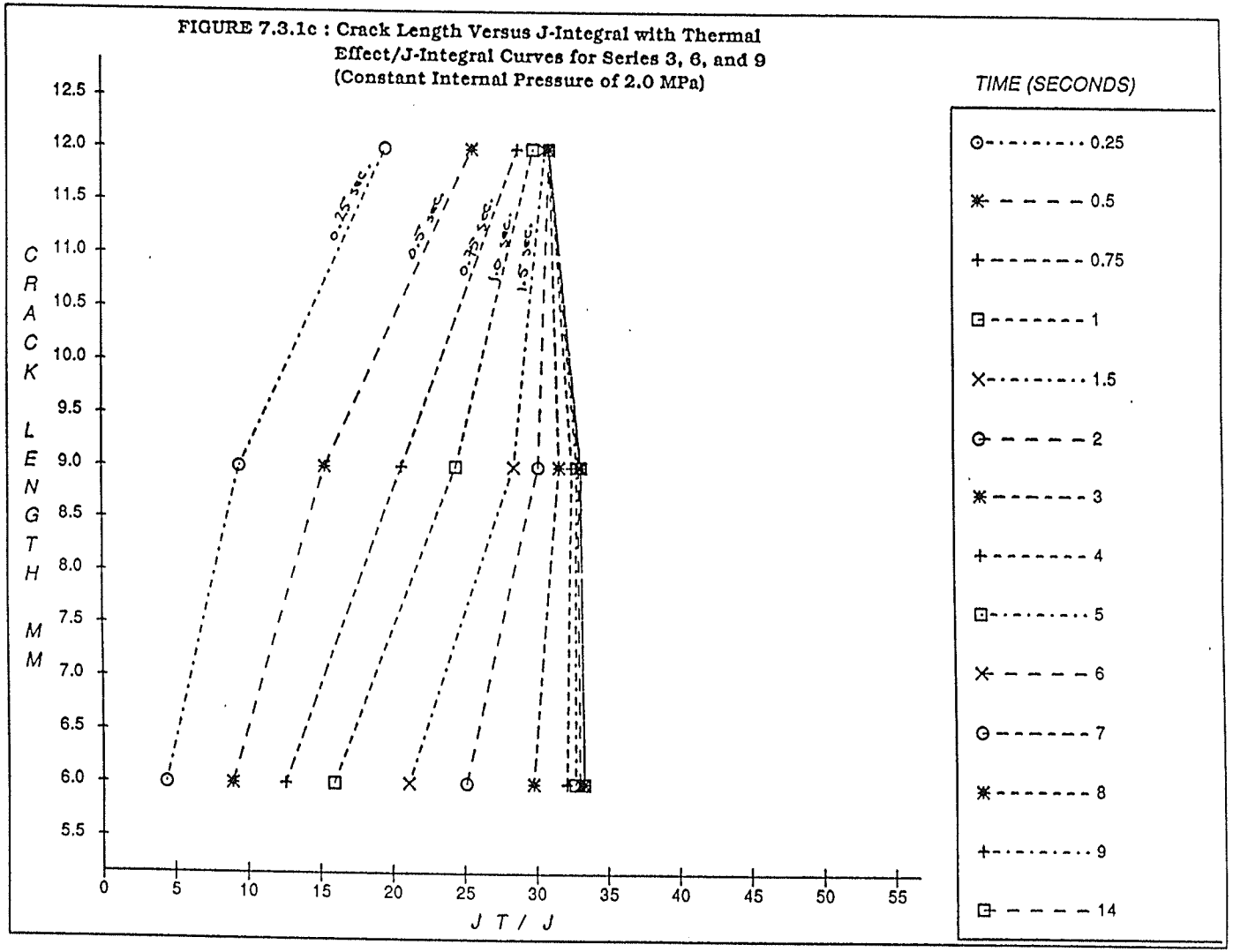

FIGURE 7.3.1c : Crack Length Versus J-Integral with Thermal Effect/J-Integral Curves for Series 3, 6, and 9 (Constant Internal Pressure of 2.0 MPa)

CHAPTER 8. CONCLUSIONS AND RECOMMENDATIONS

The results presented in this thesis (Chapter 7) clearly show that increases in internal pressure and crack length, coupled with the thermal effect due to leaking, magnify the thermal J-integral and thus the possibility of catastophic failure upon leaking.

The maximum thermal J-integral/mechanical J-integral ratio (J_T/J) values reached in the later stages of leaking were found to decrease by approximately 30 percent for 50 percent increases in pressure, independent of crack length. However, in the early stages of leaking, for example at time, t=0.25 seconds, the J_T/J ratio was found to increase . At t=0.25 seconds, for pressures of 1.0, 1.5 and 2.0 MPa, the thermal J-integral increased to approximately 8, 11 and 20 times the purely mechanical J-integral , respectively, for a worst case crack length of 12 mm. At t=0.25 seconds, for crack lengths of 6, 9 and 12 mm, the thermal J-integral increased to approximately 4, 10 and 20 times the purely mechanical J-integral, respectively, for a worst case internal pressure of 2.0 MPa. Therefore, in the initial stages of leaking, as pressure and crack length increase, J_T/J increases, and the thermal effect is significant.

The Leak-Before-Break theory will thus overestimate the critical crack size for catastophic failure, since it does not take into consideration the thermal effect of leaking. However, further research, beyond the scope of this thesis, is required to more accurately determine the extent of the thermal effect due to leaking. Some recommendations for further research are;

(a) to gauge the effect of different pipe wall thicknesses and internal radii on the thermal J-integral,

(b) to conduct tests at higher pressures,

(c) to conduct tests using different piping materials,

d) to develop a dimensionless parameter relating all aspects of the pipe geometry to the thermal J-integral. In effect introducing an alternative to the Leak-Before-Break determination of a critical crack length, and finally,

(e) to conduct tests using different actuating media. Although this thesis considered only saturated water, the Joules-Thompson effect will also occur for other actuating media such as natural gas or liquid nitrogas.

9. REFERENCES

1. Irwin, G.R., Kraft, J.M., Paris, P.C., and Wells, A.A., "Basic Aspects of Crack Growth and Fracture", NRL REPORT 6559, Washington, D.C., November 1967.

2. Hsu, T.R., Chen, G.G., Gong, Z.L., and Sun, N.S., "On Thermofracture Behavior of Leaking Thin-wall Pipes",Int. J. Pres. Ves. & Piping, 24 (1986), p.269.

3. Rice, J.R., "A Path Independent Integral and the Approximate Analysis of Strain Concentration by Notches and Cracks", J. Appl. Mech., Trans.ASME, 35 (1968), p.379.

4. Hahn, G.T., Sarrate, M., and Rosenfield, A.R., "Criteria for Crack Extension in Cylindrical Pressure Vessels", Int. J. of Frac. Mech., Vol.5, No.3, September 1969, p.187.

5. Folias, E.S., "On the Effect of Initial Curvature on Cracked Flat Sheets", Int. J. of Frac. Mech., Vol.5, No.4, December 1969, p.327.

6. Blackburn, W.S., and Jackson, A.D., "An Integral Associated with the State of a Crack Tip in a Non-elastic Material", Int. J. of Frac., Vol.13, No.2, April 1977, p.183.

7. Wilson, W.K., and Yu, I.W., "The Use of the J-Integral in Thermal Stress Crack Problems", Int. J. of Frac., Vol.15, No.4, August 1979, p.377.

8. Kishimoto, K., Aoki, S., and Sakata, M., "On the Path Independent Integral-J", Eng. Frac. Mech., Vol.13, p.841.

9. Ainsworth, R.A., neal, B.K., Hellen, T.K., "Fracture Behavior in the Presence of thermal Strains", Proc. of Conf. on tolerance of flaws in pressurized components, Institute of Mech. Eng., May 1978,p. 171.

10. Chell, G.G., "A J Estimation Procedure for Combined Mechanical, Thermal and Residual Stresses", Int J. Pres. Ves. & Piping, 23 (1986), p.187.

11. Liebowitz, H., Lee, J.D., and Eftis, J., "Bi-axial Load Effects in Fracture Mechanics", Eng. Frac. Mech., Vol.10, 1978, p.315.

12. Hsu, T.R., Chen, G.G., and Gong, Z.L., "A Numerical Evaluation of J-Integral for a Center-Cracked Plate Subject to Biaxial Thermomechanical Load", SMIRT-8, Paper G2/9, August 1985.

13. Hellen, T.K., Cesari, F., and Maitan, A., "The Application of Fracture Mechanics in Thermally Stressed Structures", Int. J. Pres. Ves. & Piping, 10 (1982), p.181.

14. Bloom, J.M., "A Procedure for the Assessment of the Structural Integrity of Nuclear Pressure Vessels", J. Pres. Ves. Tech., Vol.105, 1983, p.28.

15. Gruter, L., Zeibig, H., Percie du Sert, B., and Bhandari, S., "Leak-before-break Considerations for LMFBR Structures", Int. J. Pres. Ves. & Piping, 24 (1986) p.337.

16. Hutin, J.P., and Billon, F., "Flaw Analysis in Steam Generator Tubes", Int. J. Pres. Ves. & Piping, 25 (1986), p.267.

17. Mukherjee, B., "The J-resistance Curve Leak-before-Break Test Program on Material for the Darlington Nuclear Generating Station", Int. J. Pres. Ves. & Piping, 31 (1988), p.363.

18. Wang, W., and Zhang, K.D., "A Fracture Behavior Investigation of Lower Carbon Seamless Tube with longitudinal Crack", Int. J. Pres. Ves. & Piping, 31 (1988), p.3.

19. Hsu, T.R., Chen, C.C., Gong, Z.L. and Sun N.S., "A Hybrid Experimental-Numerical Approach to the Determination of J-Integral in a Leaking Pipe", Numerical Methods in Fracture Mechanics, 1986.

20. Griffith, A.A., "The Phenomena of Rupture and Flow in Solids", Philosophical Transactions, Royal Society of London, A221, 1920, p.163.

21. Rolfe, Stanley T., and Barsom, John M., "Fracture and Fatigue Control in Structures, Applications of Fracture Mechanics", Prentice-Hall Inc., Englewood Cliffs, New Jersey.

22. Liu, H.W., "On the Fundamental Basics of Fracture Mechanics", Eng. Frac. Mech., Vol.17, No.5, 1983, p.425.

23. Westergaard, "Bearing Pressures and Cracks", J. Appl. Mech., 61, 1939, p.A49.

24. Wells, A.A., "Unstable Crack Propagation in Metals : Cleavage and Fast Fracture", Crack Propagation Symposium, Cranfield, England, 1961.

25. Burdekin, F.M., and Stone, D.E.W., "COD Approach to Fracture Mechanics in Yielding Materials", J. Strain Analysis 1, 1966, p.145.

26. Tracey, D.M., "Finite Element Solutions for Crack-Tip Behavior in Small-Scale Yielding", J. Eng. Mat. Tech., Trans. ASME, Vol.98, 1976, p.146.

27. Rice, J.R., and Sorensen, E.P., "Continuing Crack-Tip Deformation and Fracture for Plane-strain Crack Growth in Elastic-Plastic Solids", J. of the Mech. and Physics of Solids, Vol.26, 1978, p.163.

28. de Koning, A.U., "A Contribution to the Analysis of Quasi-Static Crack Growth in Sheet Materials", Fracture 1977, Vol.3, ICF4, Waterloo, Canada, June 19-24, p.25.

29. Green, G., and Knott, J.F., "On Effects of Thickness on Ductile Crack Growth in Mild Steel", J. of the Mech. and Physics of Solids, Vol.23, 1975, p.167.

30. Kanninen, M.F., Rybicki, E.F., Stonesifer, R.B., Brock, D., Rosenfield, A.R., Marschall, C.W. and Hahn, G.T., "Elastic-Plastic Fracture Mechanics for Two-Dimensional Stable Crack Growth and Instability Problems", Elasic-Plastic Fracture, eds. J.D. Landes, J.A. Begley and G.A. Clarke, ASTM STP 668, March 1979, p.121.

31. Rice, J.R., Drugan, W.J. and Sham, T.L., "Elastic-Plastic Analysis of Growing Cracks", Fracture Mechanics, ASTM STP 700, 1979, p.189.

32. Dowling, A.R., and Townley, C.H.A., "The Effects of Defects on Structural Failures : A Two-Criteria Approach", Int. J. Pres. Ves. & Piping, Vol.3, 1975, p.77.

33. Harrison, R.P., Loosemore, K. and Milne, I., "Assessment of the Integrity of Structures Containing Defects", CEGB Report No. R/H/R6, Central Electricity Generating Board, 1976. Updated Revision 2, April 1980.

34. Bloom, J.M. and Hechmer, J.L., "Limits of Linear Elastic Fracture Mechanics", J. Pres. Ves. Tech.. Vol.106, 1984, p.196.

35. Hutchinson, J.W., "Singular Behavior at the End of a Tensile Crack in a Hardening Material", J. of Mech. and Physics of Solids, Vol. 16, pp.13-31, 1968.

36. Rice, J.R., and Rosengren, G.F., "Plane Strain Deformation Near a Crack Tip in a Power-Law Hardening Material", J. of Mech. and Physics of Solids, Vol.16, pp.1-12, 1968.

37. Hsien, J.S., "Principles of Thermodynamics", McGraw-Hill, New York, 1975.

38. Swanson Analysis Systems Inc., ANSYS User's Manuals I and II, Version 4.4, 1989.

39. Hsu, T.R., "The Finite Element Method in Thermomechanics", George Allen & Unwin, London, 1986.

40. Cook, Robert D., Concepts and Applications of Finite Element Analysis, Second Edition, John Wiley & Sons Inc., 1981.

41. Busby, H.R., and Trujillo, D.M., "Numerical Solution to a Two- Dimensional Inverse Heat Conduction Problem", International Journal for Numerical Methods in Engineering, Vol.21, pp.349-359, 1985.

42. Cubberley, W.H., Bardes, B.P., Baher, H., Benjamin, D., Unterweiser, P.M., and Kirkpatrick, C.W., "Metals Handbook", 9th Edition, Vol.1, American Society for Metals, 1978.

43. Tecmar DT701 Data Acquisition Board Manual.

44. ASME Boiler and Pressure Vessel Code, Section XI.

45. Shih, C.F., Andrews, W.R., German, M.D., Van Stone, R.H., and Wilkinson, J.P.D., "Methodology for Plastic Fracture", EPRI Contract RP 601-2, Combined 7th and 8th Quarterly Report prepared by General Electric Company, July 31, 1978.

APPENDIX I : Basic Formulations of the Finite Element Method

Since the Finite Element Method is widely documented [39,40], only the basic formulations will be outlined here. Prior knowledge of matrix algebra and elementary theory of elasticity is assumed.

Consider an element of surface area, S, and volume, V, as shown in Figure AI.1. The Principle of Virtual Work, PVW, states that ,

$$U' + W' = 0 \qquad \text{(AI.1)}$$

where U' is the stored strain energy for a virtual displacement, u', applied to a displacement, u, of an existing equilibrium state,

$$U' = \int_v (\varepsilon')^T \sigma \, dV \qquad \text{(AI.2)}$$

where ε' is the strain evaluated at u',

σ is the stress condition.

W' is the work done by the applied forces, F, required to produce u',

$$W' = - \int_v (u')^T F \, dV \qquad \text{(AI.3)}$$

Using the following well-known transformations,

$\{ u\} = [N] \{ \delta\}$ - general displacements to nodal displacements

$\{ \varepsilon\} = [B] \{ \delta\}$ - strains to nodal displacements (AI.4)

$\{ \sigma\} = [D] \{ \varepsilon\}$ - stresses to strains

$\{ \sigma\} = [D][B]\{ \delta\}$ - stresses to nodal displacements

where [N] is the interpolation functions which relate the element quantities to those at the nodes, [B] is obtained by differentiation of [N] with respect to the local coordinates, and [D] relates stress, $\{\sigma\}$, and strain, $\{\varepsilon\}$, through Hooke's Law.

The stress condition, with an initial strain condition such as a temperature change within the element, is,

$$\{\sigma\} = [D]\{\varepsilon\} - [D]\{\varepsilon o\} \qquad \text{(AI.5)}$$

Substituting equation (AI.5) and appropriate equations from equations (AI.4) into equation (AI.2) ;

$$U' = \int_v \lfloor \delta' \rfloor [B]^T [D] [B] \{\delta\} \, dV - \lfloor \delta' \rfloor \int_v [B]^T [D] \{\varepsilon o\} \, dV \qquad \text{(AI.6)}$$

or, setting $[K] = \int_v [B]^T [D] [B] dV$, and $\{Po\} = \int_v [B]^T [D] \{\varepsilon o\} \, dV$,

$$U' = \lfloor \delta' \rfloor [K] \{\delta\} - \lfloor \delta' \rfloor \{Po\} \qquad \text{(AI.7)}$$

where [K] is the stiffness matrix,

{Po} are the work equivalent nodal forces for initial strains.

Similarly, dividing F into body forces, {Fb}, and traction, {Fs}, equation (AI.3) becomes,

$$W' = \int_v (u')^T \{Fb\} \, dV - \int_s (u')^T \{Fs\} \, dS \qquad \text{(AI.8)}$$

where $\{Fb\} = [\rho] \{\ddot{u}\}$, where ρ is the mass density and $\{\ddot{u}\}$ acceleration.

Substituting the above equation for {Fb} and appropriate equations from equations (AI.4) into (AI.8) yields,

$$W' = \int_v \lfloor \delta' \rfloor [N]^T [\rho] [N] \{\ddot{\delta}\} \, dV - \int_s \lfloor \delta' \rfloor [N]^T \{Fs\} \, dS \qquad \text{(AI.9)}$$

or setting $[M] = \int_v [N]^T [\rho] [N] \, dV$, and $\{Ps\} = \int_s \lfloor \delta' \rfloor [N]^T \{Fs\} \, dS$ in equation (AI.9), where [M] is the element consistent-mass matrix, and {Ps} are the work equivalent nodal forces for the surface traction,

$$W' = \lfloor \delta' \rfloor [M] \{\ddot{\delta}\} - \lfloor \delta' \rfloor \{Ps\} \qquad \text{(AI.10)}$$

Therefore, substituting equations (AI.7) and (AI.10) into U' = -W',

$$\lfloor \delta' \rfloor [K] \{\delta\} - \lfloor \delta' \rfloor \{Po\} = - \lfloor \delta' \rfloor [M] \{\ddot{\delta}\} + \lfloor \delta' \rfloor \{Ps\} \qquad \text{(AI.11)}$$

or , setting {Ps} + {Po} = {Fn}, the element nodal-force vector,

$$[K] \{\delta\} + [M] \{\ddot{\delta}\} = \{Fn\} \qquad \text{(AI.12)}$$

The elements mass is lumped at the nodes, and the element matrices are assembled to form the global system of the equations of motion, which can be represented as in equation (AI.12).

Equation (AI.12) may be written in incremental form as,

$$[K] \{\Delta u_t\} + [M] \{\Delta \ddot{u}_t\} = \{\Delta F_t\} \qquad \text{(AI.13)}$$

where $\Delta u_t = \Delta u_{t+\Delta t} - u_t$, ...etc.

The Newmark- β method approximates the displacements and velocities at t+Δt by,

$$\{\Delta u_{t+\Delta t}\} = \{u_t\} + \Delta t \{\dot{u}_t\} + \Delta t^2 (((1/2)- \beta) \{\ddot{u}_t\} + \beta \{\Delta \ddot{u}_{t+\Delta t}\}) \qquad \text{(AI.14a)}$$

$$\{\Delta \dot{u}_{t+\Delta t}\} = \{\dot{u}_t\} + \Delta t ((1- \gamma) \{\ddot{u}_t\} + \gamma \{\Delta \ddot{u}_{t+\Delta t}\}) \qquad \text{(AI.14b)}$$

where β and γ dictate the assumed variation of the acceleration over the time step, Δt. Equation (AI.14a), in incremental form, becomes,

$$\{\Delta u_t\} = \Delta t \{\dot{u}_t\} + \Delta t^2 (\{1/2\}\{\ddot{u}_t\} + \beta \{\Delta \ddot{u}_t\}) \qquad \text{(AI.15)}$$

This equation can be rearranged to yield,

$$\{\Delta \ddot{u}_t\} = \{1/\beta\} (\{1/\Delta t^2\}\{\Delta u_t\} - \{1/\Delta t\}\{\Delta \dot{u}_t\} - (1/2)\{\ddot{u}_t\}) \qquad \text{(AI.16)}$$

Substituting equations (AI.15) and (AI.16) into (AI.13) and rearranging yields,

$$([K] + \frac{1}{\beta\Delta t^2}[M])\ \{\Delta u_t\} = \{\Delta F_t\} + [M]\ (\frac{1}{\beta\Delta t}\{\dot{u}_t\} + \frac{1}{2\beta}\{\ddot{u}_t\}) \qquad \text{(AI.17)}$$

$$\text{or,} \quad [K']\{\Delta u_t\} = \{\Delta F'_t\}\ , \qquad \text{(AI.18)}$$

where [K'] is the equivalent stiffness matrix, and $\{\Delta F'_t\}$ is the equivalent force matrix .

Equation (AI.18) represents a set of linear algebraic equations at discrete time instants, t. Matrix inversion, Cholesky decomposition, or Gaussian elimination can used to determine the primary unknwon quantities, $\{u_t\}$ at each node.

Equation (AI.13) is a set of second order differential equations, requiring two initial conditions to begin the time-integration procedure . The initial conditions chosen are $\{\dot{u}_{t=0}\}$ and $\{u_{t=0}\}$, which, when substituted into equation (AI.13), is used to solve for $\{\ddot{u}_{t=0}\}$ by,

$$\{\ddot{u}_{t=0}\} = [M]^{-1}\ (\{F_{t=0}\} - [K]\ \{u_{t=0}\}. \qquad \text{(AI.19)}$$

Incremental nodal displacements at all remaining time instants can be found by solving equation (AI.18). Incremental element strains and stresses can be found from equations (AI.4). The total displacements, strains and stresses can be determined by adding the respective incremental values.

The extension of the above formulations from elastic analysis to elastic-plastic analysis is detailed in reference [39], Chapter 3. The necessary

modifications to the elastic formulations are summarized as follows.

The nodal displacements are calculated by the cummulation of the incremental values computed from each loading step;

$$\{u\} = \{u\} + \{\Delta u\} \tag{AI.20}$$

with the incremental displacement components calculated from;

$$[Ko]\ \{\Delta u\} = \{\Delta F\} \tag{AI.21}$$

where [Ko] is the overall current elastic-plastic stiffness matrix;

$$[\,Ko] = \sum_{1}^{M} [Kep] \tag{AI.22}$$

where [Kep] is the current elastic-plastic stiffness matrix,

[ΔF] is the incremental load matrix, and

M is the number of elements in the model.

[Kep] is evaluated by replacing [D] in equation (AI.5) by [Cep] derived in reference [39] (equation 3-70 for isotropic hardening and equation 3-91 for kinematic hardening).

Incremental strain components are obtained by,

$$\{\Delta\varepsilon\} = [B]\ \{\Delta u\} \tag{AI.23}$$

and the incremental stresses by the constitutive equations in reference [39] (equation 3-53 for isotropic hardening, and equation 3-90 for kinematic hardening).

The total stresses and strains are then calculated from the corresponding incremental values.

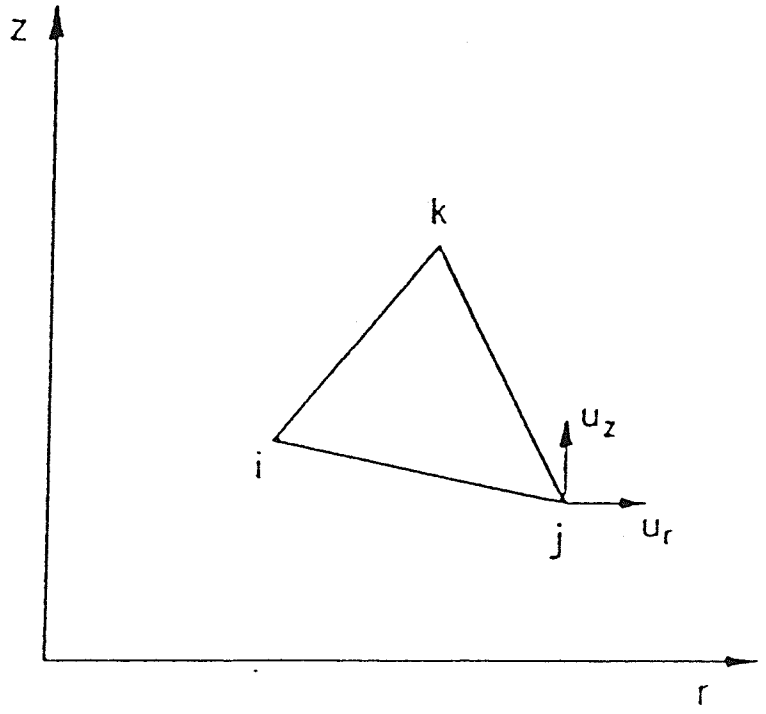

FIGURE AI.1 : A Typical Triangular Finite Element

APPENDIX II : Experimental Equipment Specifications

Water Tank : Model 507, Serial 3-69, Style 266-4
Working Pressure 500 psi
Temprite Products Corporation, Troy, Michigan, U.S.A.

Flanges : CCTF-KOF 4 150 STD B16 A105-85N 641 Specification

Heaters : 1500 W, 120 V, Straight Water Heaters

Pressure Gage : 0-600 psi, USG U.S. GAUGE
Tube-sst 316, Conn-sst 316

Data Acquisition Board : Tecmar DT701 Data Translation
See following pages

DATA TRANSLATION INC
4 Strathmore Rd., Natick MA 01760
(617) 655-5300 Telex 948474

UNIVERSAL SCREW TERMINAL SIGNAL CONDITIONING PANEL, MICROCOMPUTER COMPATIBLE DT701

FEATURES

- Reliable connection points for microcomputer analog I/O & digital I/O signals
- Standard 19" width RETMA Rack Mounting
- Standard ribbon cable connection to many Data Translation analog interface boards
- Designed printed circuit mounting space for analog input components:
  - current loop resistors
  - noise filters
  - voltage dividers
  - open circuit thermocouple detection
  - protection fuses
- Thermocouple cold reference junction compensation on board
- Barrier-strip screw terminals
- Flexible mounting assembly option with protective cover

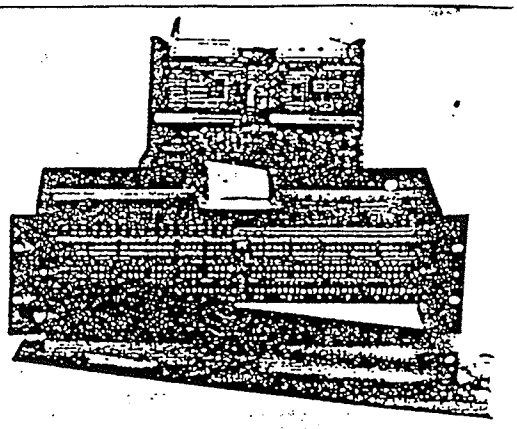

Fig. 1.
DT701-50-T-MA is the universal screw terminal signal conditioning panel with a 50 pin connector for direct plug-in connection to the microcomputer analog input board. Also shown on the panel at the center is the thermocouple cold reference junction compensation circuit.

DESCRIPTION

The DT701 Universal Screw Terminal Signal Conditioning Panel is a convenient connection scheme for microcomputer analog and digital input/output signals. It consists of a heavy gauge printed circuit board with barrier-strip screw terminals. It provides ease of connection of analog or digital signals to the complete line of Data Translation interface boards or to any interface board requiring a means of connection from the microcomputer to the outside world. The unit mounts in a standard 19" width RETMA rack and is available as a direct mounting printed circuit board or with an optional mounting assembly. The mounting assembly is a complete subassembly with sheet metal enclosure and protective cover.

The DT701 will provide connection for up to 50 separate inputs with up to 13 separate screws for the connection of common or ground signals. A specially designed area is set aside using a standard matrix pattern to allow the user to mount his own passive signal conditioning or protection circuits. Such circuits include current loop resistors, noise filters, protection circuits open thermocouple detection circuits. Voltage dividers or any circuit required which mates with the standard pattern.

A unique feature of the DT701 is the inclusion of a thermocouple cold reference junction compensation circuit. This on-board circuit allows direct connection of thermocouples to the DT701 and provides the proper compensation to the analog interface board. Connection to the interface boards is via a standard flat ribbon cable or a flat twisted pair cable. These cables are also available from Data Translation.

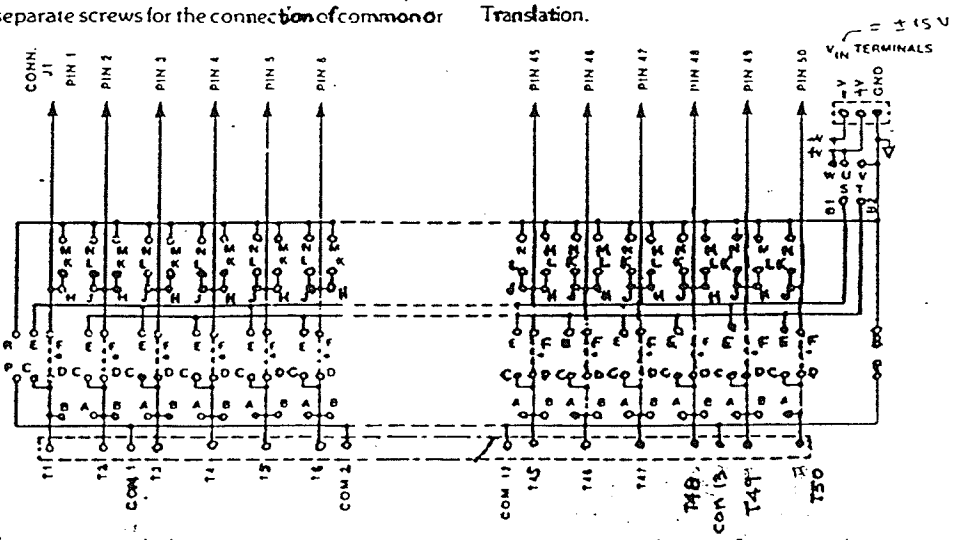

Fig. 2.
Schematic shows screw terminal connectors and standard matrix pattern on DT701

MODEL CONFIGURATION

DT701 consists of a 19 inch rack mount printed circuit board with screw terminals and standard matrix for user configuration of signal conditioning.

Options

- 50 - consists of a 50 Pin 3M connector for connection of DT701 to flat ribbon cable or flat twisted pair cable. 3M connector type 3433 or equivalent.
- 40 - consists of 40 Pin 3M connector for connection of DT701 to flat ribbon or flat twisted pair cable. 3M connector type 3432 or equivalent.
- 20 - consists of 2 - 20 Pin 3M connectors for connection of DT701 to flat ribbon or flat twisted pair cables. 3M connector type 3492 or equivalent.
- MA - consists of a Standard RETMA 19" mounting assembly with plexiglass cover. To provide protected recessed mounting.
- T - Thermocouple reference junction compensation circuit.

SPECIFICATIONS DT701

Size

The panel consists of heavy duty printed circuit board designed to mount in a standard RETMA 19" rack. 19"W x 5.00" H. (482.6mm x 127.0mm)

Printed Circut Board

0.125 in. (3.17mm) thick, (FR4 Material)

Screw Terminal

The panel contains 63 screw terminals. 50 terminals are connected to the standard matrix pattern and 13 are used for user common connections.

Number of Signal Inputs

50 signal input lines or 25 pair maximum. For analog inputs this means 50 single-ended (SE) or 25 differential (DI) inputs.

Barrier-Strip Screw Size

3-56 panhead screws with captive wire clamping plate.

Barrier-Strip Screw Spacing

0.250 in. (6.35mm)

Barrier-Strip Screw Material

Brass

Barrier-Strip Material - Polyester

U.L. grade 94V-0, 130°C operating

Acceptable Wire Size

18 to 22 AWG

Acceptable Lug Size

0.250 in (6.35mm) Wide Wire Lugs

Barrier-Strip Rating

5A. 300V

OPTIONS

T Option - Ambient Temperature Compensation

The DT701 can be configured with the -T option. This option provides a thermocouple reference junction compensation circuit. This circuit consists of a solid state temperature transducer mounted at the physical center of the screw terminal assembly. The transducer output is buffered and normalized to provide 10mV/°C output (See Fig. 6)

The T option outputs are brought out on two solder pads on the DT701 panel (Hi, Lo). These two pads can be wired to any set of screw terminal inputs for use as an input channel or to provide automatic compensation with -T option interface boards.

Ambient Temperature Compensation Circuit

When the thermocouple wire is connected to copper wire at the barrier strip an additional thermocouple is made with an output that would cancel the measurement thermocouple's output if the barrier strip was at the same temperature.

To compensate for this error an integrated circuit temperature transducer is mounted at the center of the barrier strip. The output at pin + as shown is -1 microampere per degree Kelvin. Following this, the amplifier is utilized to remove the -2.7 volt offset due to ambient temperature and reference the output to 0°C with +10 millivolts per +degree C and -10 millivolts per -degree C. (See Fig. 6.)

Compensation Selection

The compensation for various thermocouples can now be determined by calculating the value of the scaling resistor (R). This is accomplished by the formula:

$$R = \left[\left(\frac{10mV}{V_{COMP}} \right) - 1 \right] \times 100$$

Where COMP = the output of the given thermocouple type in uV/°C.

R = Scaling resistor in ohms

K.

T OPTION SPECIFICATION

Accuracy

±1°C

Output Impedance

Amplifier Output .1 ohm, 100 ohm Divider

Output Drive

Amplifier ±5mA

Adjustment Capability

Adjustible from -20mV to +30mV output @ 25°C (Nominally +25mV)

Temperature Range (Operating)

0°C to 55°C

The DT701 can be supplied with a sheet metal assembly to provide recessed mounting in a standard 19" RETMA rack. Also provided is a plexiglass cover for additional protection. See Fig. 4a.

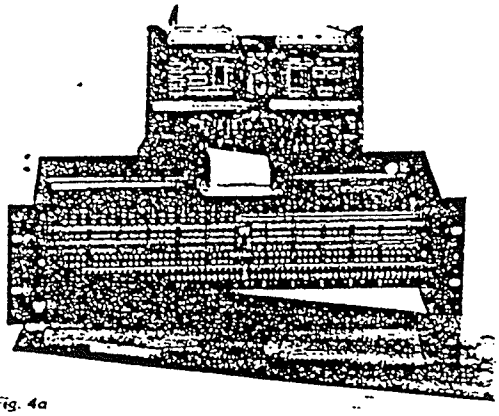

Fig. 4a
The mounting assembly allows the DT701 to be mounted separately in any 19 inch rack.

MA Material

16 gauge steel, Finish - black semi-gloss

Size

19"W x 5.25"H (482.6mm x 133.35mm)

Cover Material

0.125 in. (3.17mm) thick plexiglass

Connection to the Computer Interface

Connections to the computer are via 50 pin or 40 pin flat ribbon cables or two 20 pin cables. This cable assembly can be either flat cable or twisted pair cables.

50 Pin Configuration (-50)

In this configuration the DT701 panel contains a 50 pin connector for connection to standard Data Translation interfaces.

This option is standardly used with all the following analog I/O interface boards: DEC quad LSI-11* series, DEC Unibus* PDP-11 series, and Intel/National Multibus series.

Mating Connector Type for 50 pin

3M Type 3425 or equivalent

20 Pin Configuration (-20)

In this configuration two 20 pin 3M type connectors are utilized to provide compatibility with Data Translation interfaces containing 20 pin connectors.

This option is standardly used with all the following analog I/O interface boards: DEC dual height LSI 11 series and MOSTEK Prolog STD BUS series

Mating Connector Type for 20 pin

3M Type 3421 or equivalent

40 Pin Configuration (-40)

In this configuration the DT701 panel contains a 40 pin connector to provide compatibility with Data Translation interfaces containing 40 pin connectors

*Trademark of Digital Equipment Corp

3M Type 3417 or equivalent

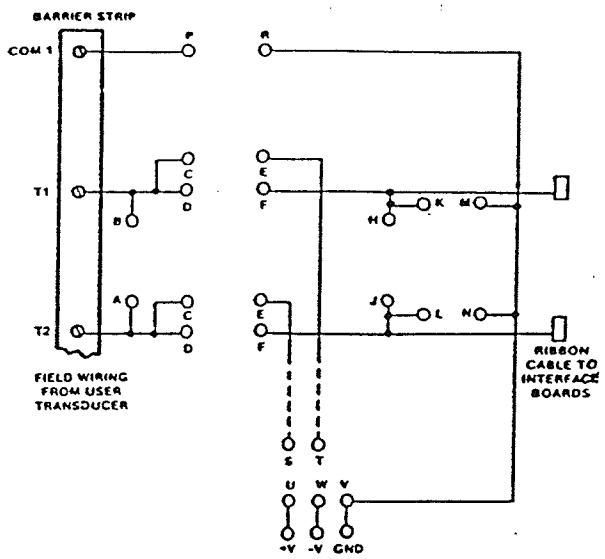

Fig. 3.
DT701 Signal Conditioning Matrix

USER SIGNAL CONDITIONING MATRIX

The standard Matrix pattern is shown in Figure 3. It should be noted that each terminal line has associated with it a standard pattern. Each hole in the pattern is marked with a letter and this pattern is repeated for each terminal.

The printed circuit on the DT701 connects each screw terminal input to the flat ribbon cable connector. A user can jump straight through if he desires (connect jumper D to F). Each input line, however, passes through a specially designed matrix pattern onto which a user may connect components for signal conditioning or protection. This standard matrix is designed to allow easy placement of R-C components for noise filters, resistors for voltage division, fuses for protection or other components as the user's applications may require.

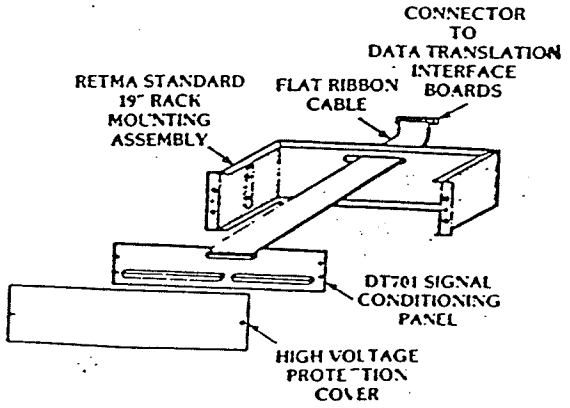

Fig 4b
DT701 Panel with MA (Mounting Assembly)

APPENDIX III : Calculations for Thin Wall Pressure Vessel Assumption and Safety Check

From the ASME Boiler and Pressure Vessel Code, Section VIII [45], a pressurized pipe is thick wall if its wall thickness exceeds 0.1R, where R is the inside radius of the pipe. For the experimental pipe geometry considered in this thesis (Figure 5.3.1), R is 23.25 mm and the wall thickness is 2 mm.

$$0.1R = 0.1\,(23.25) = 2.325 \text{ mm} \geq 2 \text{ mm}$$

Therefore, the pipe is thin walled.

A pipe is considered safe if its wall thickness exceeds the minimum allowable wall thickness, t_f,

$$t_f = \frac{(p)(D)}{2.0\,(f)(e) + p} \qquad \text{(AVI.1)}$$

where p is the maximum design pressure = 2.0 MPa

D is the outside diameter of the pipe = 50.5 mm

e = 1.0 for seamless pipe.

f is the permissible design stress = $\sigma y/2$ = 483MPa/2 = 241.5 MPa,

where σy is the yield stress.

From equation (AVI.1),

$$t_f = \frac{(2.0)(50.5)}{(2)(241.5)(1.0) + 2.0} = 0.208 \text{ mm} \qquad \text{(AV.2)}$$

Therefore, a 2 mm wall thickness is acceptable, with a sufficient safety margin to be sure the pipe will not rupture even with a 12 mm through-wall crack.

APPENDIX IV : Calculation of Plasticity Modulus

The steel material behavior is described by classical bilinear kinematic hardening described by a bilinear stress-strain curve starting at the origin with positive stress and strain values [39]. This curve was calculated from;

$$\sigma = K\varepsilon^n \qquad \text{(AIV.1)}$$

where σ is the stress

ε is the strain, and

n=0.15 for low carbon steel.

From Section 5.3, σ_y = 483 MPa and E=0.2x10^6 MPa, therefore,

$$\varepsilon_y = \sigma_y / E = 483/0.2\text{x}10^6 = 2.415\text{x}10^{-3} \text{ m/m} \qquad \text{(AIV.2)}$$

Therefore,

$$K = \sigma_y/\varepsilon_y^n = 483/(2.415\text{x}10^{-3})^{0.15} = 1192.64 \text{ MPa} \qquad \text{(AIV.3)}$$

Substituting equation (AIV.3) into equation (AIV.1) yields,

$$\sigma = 1192.64\ \varepsilon^{0.15} \qquad \text{(AIV.4)}$$

The stress-strain curve described by equations (AIV.2) and (AIV.4) is shown in Figure AIV.1. The slope of the plastic portion of the curve, past the yield strength yields the plastic modulus, E'.

$$E' = \frac{553.65-498.97}{0.006-0.003} = 1.82\text{x}10^4 \text{ MPa} \qquad \text{(AIV.5)}$$

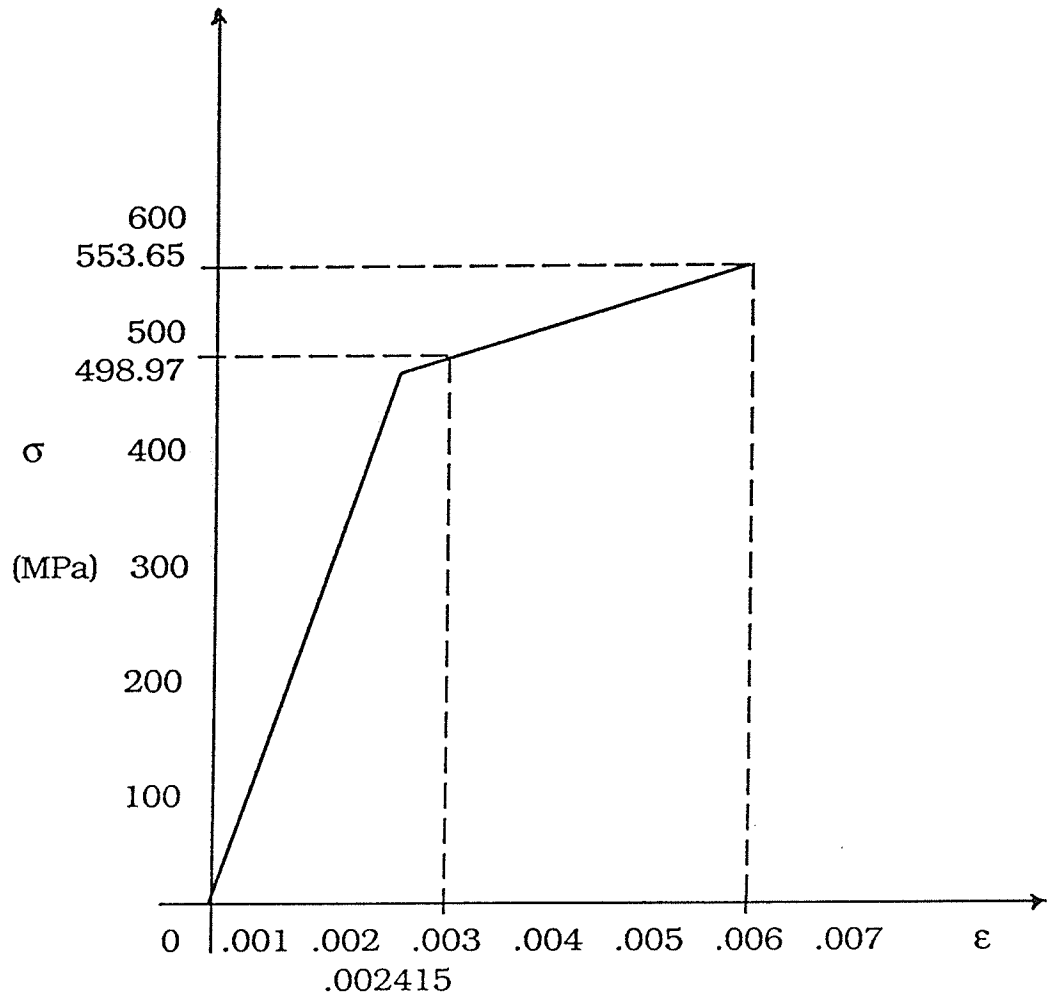

FIGURE AIV.1 : Plasticity Modulus Calculation

APPENDIX V : Proof of Cylinder to Flat Plate Modelling Assumption

Using the experimental specimen geometry in Figure 5.3.1 , from reference [5] ;

$$\lambda = [12\,(1-\nu^2)\,]^{1/4}\,\frac{c}{[Rt\,]^{1/2}} \qquad \text{(AV.1)}$$

where, λ is a dimensionless design variable,

ν is Poisson's Ratio = 0.3,

R is the inside radius of the cylinder = 23.25 mm,

t is the thickness of the cylinder = 2 mm,

c is the half crack length, which is equal to 3, 4.5, and 6 mm for series 1-3, 4-6, and 7-9 experiments, respectively.

For the three half crack lengths, 3, 4.5, and 6 mm, λ is found from equation AV.1 to be 0.8, 1.2, and 1.6, respectively.

The percent error, PE, from assuming a flat plate geometry can then be calculated from [5];

$$PE = 100.0\left[a_1 + b_1\left[\ln\frac{c}{(Rh)^{1/2}}\right]\right]\frac{c^2}{R} \qquad \text{(AV.2)}$$

where a_1 and b_1 are dimensionless design variables found from λ [5], as shown in Table AV.1,

all other variables are defined as in equation (AV.1).

For the three half crack lengths, 3, 4.5, and 6 mm the errors calculated for assuming a flat plate geometry are 3.7, 2.1, and 6.1 percent, respectively, which are within acceptable limits.

TABLE AV.1 : Dimensionless Design Variables a_1 and b_1 for Experimental Half Crack Lengths [5]

Half Crack Length	λ	a_1	b_1
3 mm	0.8	0.04107	0.02659
4.5 mm	1.2	0.06406	0.03985
6 mm	1.6	0.08482	0.04990

APPENDIX VI : ANSYS Optimization File to Calculate Temperature Distributions

```
$set def [demo.jeff.pipex]      * change directory
$ansys44          * load ansys
tp6=150           * variable to be optimized
/prep7            * enter /prep7
/input,28         *** file 28 is created by a cdwrite command
kan,-1            *** in /prep7, base model input for /prep7 is
ktemp,0           *** listed Appendix VII.
hcrl=6.0                * half crack length in mm
to0=165.0               * bulk metal temperature in 'C
to1=125.0               * thermocouple 1 measurement 'C
to2=125.0               * thermocouple 2 measurement 'C
to3=115.0               * thermocouple 3 measurement 'C
to4=125.0               * thermocouple 4 measurement 'C
to5=125.0               * thermocouple 5 measurement 'C
tref,to0                * reference temperature
tunif,to0               * uniform temperature
iter,-5                 * number iterations, -ve for automatic
nall                      time-step optimization
eall
ntdel,all
nsel,y,0
nrsel,x,0,hcrl
nt,all,temp,tp6
nall
nsel,y,9,25
nasel,x,11.5,25
nt,all,temp,to0
nall
eall
lwrite
*** further time steps are added here once previous
*** time step is optimized.
afwrite
finish
/input,27
finish
/post1               *get values required for optimization
set
*get,a1,temp,66
*get,a2,temp,66
*get,a3,temp,116
*get,a4,temp,66
*get,a5,temp,66
e1=(a1-to1)*(a1-to1)
e2=(a2-to2)*(a2-to2)
e3=(a3-to3)*(a4-to3)
e4=(a4-to4)*(a4-to4)
e5=(a5-to5)*(a5-to5)
y1=e1+e2
y2=y1+e3
y3=y2+e4
ymi1=y3+e5        * variable to be minimized
*stat
finish
/opt              * optimize function ymi1
opvar,tp6,dv,100,188
opvar,ymi1,obj
oplist,all,,1
opcopy
oprun,10
finish
/eof
```

APPENDIX VII : Base Model Input and Input File for Transient Thermal Analysis

BASE MODEL RUN FILE

```
$SET DEF [DEMO.JEFF.PIPEi]
$ANSYS44
/PREP7
/INPUT,MAT,DAT
/INPUT,NODE,DAT
/INPUT,ELEM,DAT
/INPUT,DISP,DAT
SAVE
FINISH
/EOF
```

BASE MODEL MATERIAL DATA

```
NL,1,1,0,0,0,0,0,0                  * undefined fields
NL,1,7,0,0,0,0,0,0                  * undefined fields
NL,1,13,10.0,0,0,0,0,0              * 10 is code for bi-linear hardening
NL,1,19,-9999.0,9999.0,0,0,0,0      * temperature range for properties
NL,1,25,483.0,483.0,0,0,0,0         * yield stress
NL,1,31,18200.0,18200.0,0,0,0,0     * plastic modulus
NL,1,37,0,0,0,0,0,0                 * undefined fields
NL,1,43,0,0,0,0,0,0                 * undefined fields
MP,EX,1,0.2E6                       * elastic modulus
MP,ALPX,1,0.11E-4                   * thermal expansion coefficient
MP,GXY,1,76823.0                    * shear modulus
MP,KXX,1,.419E-1                    * thermal conductivity
MP,C,1,487.0                        * specific heat
MP,NUXY,1,0.3                       * poisson's ratio
KNL,1                               * include non-linear properties
```

BASE MODEL NODES

```
n ,1 ,2 ,0
n ,2 ,2.25 ,0
n ,3 ,2.5 ,0
n ,4 ,2.75 ,0
n ,5 ,3 ,0
n ,6 ,3.25 ,0
n ,7 ,3.5 ,0
n ,8 ,3.75 ,0
n ,9 ,4 ,0
n ,10 ,4.25 ,0
n ,11 ,4.5 ,0
n ,12 ,4.75 ,0
n ,13 ,5 ,0
n ,14 ,5.25 ,0
n ,15 ,5.5 ,0
n ,16 ,5.75 ,0
n ,17 ,6 ,0
n ,18 ,6.25 ,0
n ,19 ,6.5 ,0
n ,20 ,6.75 ,0
n ,21 ,2 ,0.25
n ,22 ,2.25 ,0.25
n ,23 ,2.5 ,0.25
n ,24 ,2.75 ,0.25
n ,25 ,3 ,0.25
n ,26 ,3.25 ,0.25
n ,27 ,3.5 ,0.25
n ,28 ,3.75 ,0.25
n ,29 ,4 ,0.25
n ,30 ,4.25 ,0.25
n ,31 ,4.5 ,0.25
n ,32 ,4.75 ,0.25
```

```
n ,33 ,5 ,0.25
n ,34 ,5.25 ,0.25
n ,35 ,5.5 ,0.25
n ,36 ,5.75 ,0.25
n ,37 ,6 ,0.25
n ,38 ,6.25 ,0.25
n ,39 ,6.5 ,0.25
n ,40 ,6.75 ,0.25
n ,41 ,1.75 ,0
n ,42 ,1.75 ,0.25
n ,43 ,1.75 ,0.5
n ,44 ,2 ,0.5
n ,45 ,2.25 ,0.5
n ,46 ,2.5 ,0.5
n ,47 ,2.75 ,0.5
n ,48 ,3 ,0.5
n ,49 ,3.25 ,0.5
n ,50 ,3.5 ,0.5
n ,51 ,3.75 ,0.5
n ,52 ,4 ,0.5
n ,53 ,4.25 ,0.5
n ,54 ,4.5 ,0.5
n ,55 ,4.75 ,0.5
n ,56 ,5 ,0.5
n ,57 ,5.25 ,0.5
n ,58 ,5.5 ,0.5
n ,59 ,5.75 ,0.5
n ,60 ,6 ,0.5
n ,61 ,6.25 ,0.5
n ,62 ,6.5 ,0.5
n ,63 ,6.75 ,0.5
n ,64 ,7 ,0.5
n ,65 ,7 ,0.25
n ,66 ,7 ,0
n ,67 ,1.5 ,0
n ,68 ,1.5 ,0.25
n ,69 ,1.5 ,0.5
n ,70 ,1.5 ,0.75
n ,71 ,1.75 ,0.75
n ,72 ,2 ,0.75
n ,73 ,2.25 ,0.75
n ,74 ,2.5 ,0.75
n ,75 ,2.75 ,0.75
n ,76 ,3 ,0.75
n ,77 ,3.25 ,0.75
n ,78 ,3.5 ,0.75
n ,79 ,3.75 ,0.75
n ,80 ,4 ,0.75
n ,81 ,4.25 ,0.75
n ,82 ,4.5 ,0.75
n ,83 ,4.75 ,0.75
n ,84 ,5 ,0.75
n ,85 ,5.25 ,0.75
n ,86 ,5.5 ,0.75
n ,87 ,5.75 ,0.75
n ,88 ,6 ,0.75
n ,89 ,6.25 ,0.75
n ,90 ,6.5 ,0.75
n ,91 ,6.75 ,0.75
n ,92 ,7 ,0.75
n ,93 ,7.25 ,0.75
n ,94 ,7.25 ,0.5
n ,95 ,7.25 ,0.25
n ,96 ,7.25 ,0
n ,97 ,1.25 ,0
n ,98 ,1.25 ,0.25
n ,99 ,1.25 ,0.5
n ,100 ,1.25 ,0.75
n ,101 ,1.25 ,1
n ,102 ,1.5 ,1
n ,103 ,1.75 ,1
n ,104 ,2 ,1
n ,105 ,2.25 ,1
n ,106 ,2.5 ,1
n ,107 ,2.75 ,1
n ,108 ,3 ,1
n ,109 ,3.25 ,1
n ,110 ,3.5 ,1
n ,111 ,3.75 ,1
n ,112 ,4 ,1
n ,113 ,4.25 ,1
n ,114 ,4.5 ,1
n ,115 ,4.75 ,1
n ,116 ,5 ,1
n ,117 ,5.25 ,1
n ,118 ,5.5 ,1
n ,119 ,5.75 ,1
n ,120 ,6 ,1
n ,121 ,6.25 ,1
n ,122 ,6.5 ,1
n ,123 ,6.75 ,1
n ,124 ,7 ,1
n ,125 ,7.25 ,1
n ,126 ,7.5 ,1
n ,127 ,7.5 ,0.75
n ,128 ,7.5 ,0.5
n ,129 ,7.5 ,0.25
n ,130 ,7.5 ,0
n ,131 ,1 ,0
n ,132 ,1 ,0.5
n ,133 ,1 ,1
n ,134 ,1.25 ,1.25
n ,135 ,1.5 ,1.25
n ,136 ,1.75 ,1.25
n ,137 ,2 ,1.25
n ,138 ,2.25 ,1.25
n ,139 ,2.5 ,1.25
n ,140 ,2.75 ,1.25
n ,141 ,3 ,1.25
n ,142 ,3.25 ,1.25
n ,143 ,3.5 ,1.25
n ,144 ,3.75 ,1.25
n ,145 ,4 ,1.25
n ,146 ,4.25 ,1.25
n ,147 ,4.5 ,1.25
n ,148 ,4.75 ,1.25
n ,149 ,5 ,1.25
n ,150 ,5.25 ,1.25
n ,151 ,5.5 ,1.25
n ,152 ,5.75 ,1.25
n ,153 ,6 ,1.25
n ,154 ,6.25 ,1.25
n ,155 ,6.5 ,1.25
n ,156 ,6.75 ,1.25
n ,157 ,7 ,1.25
n ,158 ,7.25 ,1.25
n ,159 ,7.5 ,1.25
n ,160 ,7.75 ,1.25
n ,161 ,7.75 ,1
n ,162 ,7.75 ,0.75
n ,163 ,7.75 ,0.5
n ,164 ,7.75 ,0.25
n ,165 ,7.75 ,0
n ,166 ,0.5 ,0
n ,167 ,0.5 ,0.5
n ,168 ,0.5 ,1
n ,169 ,0.5 ,1.5
n ,170 ,1 ,1.5
n ,171 ,1.5 ,1.5
n ,172 ,2 ,1.5
n ,173 ,2.5 ,1.5
n ,174 ,3 ,1.5
n ,175 ,3.5 ,1.5
n ,176 ,4 ,1.5
n ,177 ,4.5 ,1.5
n ,178 ,5 ,1.5
n ,179 ,5.5 ,1.5
n ,180 ,6 ,1.5
n ,181 ,6.5 ,1.5
n ,182 ,7 ,1.5
n ,183 ,7.5 ,1.5
n ,184 ,8 ,1.5
n ,185 ,8 ,1
n ,186 ,8 ,0.5
n ,187 ,8 ,0
n ,188 ,0 ,0
n ,189 ,0 ,1
n ,190 ,0 ,2
n ,191 ,0.5 ,2
n ,192 ,1 ,2
n ,193 ,1.5 ,2
n ,194 ,2 ,2
n ,195 ,2.5 ,2
n ,196 ,3 ,2
n ,197 ,3.5 ,2
n ,198 ,4 ,2
n ,199 ,4.5 ,2
n ,200 ,5 ,2
n ,201 ,5.5 ,2
n ,202 ,6 ,2
n ,203 ,6.5 ,2
n ,204 ,7 ,2
n ,205 ,7.5 ,2
n ,206 ,8 ,2
n ,207 ,8.5 ,2
n ,208 ,8.5 ,1.5
n ,209 ,8.5 ,1
n ,210 ,8.5 ,0.5
n ,211 ,8.5 ,0
n ,212 ,0.5 ,2.5
n ,213 ,1 ,2.5
n ,214 ,1.5 ,2.5
n ,215 ,2 ,2.5
n ,216 ,2.5 ,2.5
n ,217 ,3 ,2.5
n ,218 ,3.5 ,2.5
n ,219 ,4 ,2.5
n ,220 ,4.5 ,2.5
n ,221 ,5 ,2.5
n ,222 ,5.5 ,2.5
n ,223 ,6 ,2.5
n ,224 ,6.5 ,2.5
n ,225 ,7 ,2.5
n ,226 ,7.5 ,2.5
n ,227 ,8 ,2.5
n ,228 ,8.5 ,2.5
n ,229 ,9 ,2
n ,230 ,9 ,1
n ,231 ,9 ,0
n ,232 ,0 ,3
n ,233 ,1 ,3
n ,234 ,2 ,3
n ,235 ,3 ,3
n ,236 ,4 ,3
n ,237 ,5 ,3
n ,238 ,6 ,3
n ,239 ,7 ,3
n ,240 ,8 ,3
n ,241 ,9 ,3
n ,242 ,10 ,3
n ,243 ,10 ,2
n ,244 ,10 ,1
n ,245 ,10 ,0
n ,246 ,0 ,4
n ,247 ,1 ,4
n ,248 ,2 ,4
```

```
n ,249 ,3 ,4
n ,250 ,4 ,4
n ,251 ,5 ,4
n ,252 ,6 ,4
n ,253 ,7 ,4
n ,254 ,8 ,4
n ,255 ,9 ,4
n ,256 ,10 ,4
n ,257 ,11 ,4
n ,258 ,11 ,3
n ,259 ,11 ,2
n ,260 ,11 ,1
n ,261 ,11 ,0
n ,262 ,0 ,5
n ,263 ,1 ,5
n ,264 ,2 ,5
n ,265 ,3 ,5
n ,266 ,4 ,5
n ,267 ,5 ,5
n ,268 ,6 ,5
n ,269 ,7 ,5
n ,270 ,8 ,5
n ,271 ,9 ,5
n ,272 ,10 ,5
n ,273 ,11 ,5
n ,274 ,12 ,4
n ,275 ,12 ,2
n ,276 ,12 ,0
n ,277 ,0 ,6
n ,278 ,2 ,6
n ,279 ,4 ,6
n ,280 ,6 ,6
n ,281 ,8 ,6
n ,282 ,10 ,6
n ,283 ,12 ,6
n ,284 ,0 ,8
n ,285 ,2 ,8
n ,286 ,4 ,8
n ,287 ,6 ,8
n ,288 ,8 ,8
n ,289 ,10 ,8
n ,290 ,12 ,8
n ,291 ,14 ,8
n ,292 ,14 ,6
n ,293 ,14 ,4
n ,294 ,14 ,2
n ,295 ,14 ,0
n ,296 ,0 ,10
n ,297 ,2 ,10
n ,298 ,4 ,10
n ,299 ,6 ,10
n ,300 ,8 ,10
n ,301 ,10 ,10
n ,302 ,12 ,10
n ,303 ,14 ,10
n ,304 ,16 ,8
n ,305 ,16 ,4
n ,306 ,16 ,0
n ,307 ,0 ,12
n ,308 ,4 ,12
n ,309 ,8 ,12
n ,310 ,12 ,12
n ,311 ,16 ,12
n ,312 ,20 ,12
n ,313 ,20 ,8
n ,314 ,20 ,4
n ,315 ,20 ,0
n ,316 ,0 ,16
n ,317 ,4 ,16
n ,318 ,8 ,16
n ,319 ,12 ,16
n ,320 ,16 ,16
n ,321 ,20 ,16
n ,322 ,24 ,16
n ,323 ,24 ,12
n ,324 ,24 ,8
n ,325 ,24 ,4
n ,326 ,24 ,0
n ,327 ,0 ,20
n ,328 ,4 ,20
n ,329 ,8 ,20
n ,330 ,12 ,20
n ,331 ,16 ,20
n ,332 ,20 ,20
n ,333 ,24 ,20
n ,334 ,0 ,24
n ,335 ,4 ,24
n ,336 ,8 ,24
n ,337 ,12 ,24
n ,338 ,16 ,24
n ,339 ,20 ,24
n ,340 ,24 ,24
```

BASE MODEL ELEMENTS

```
kan,-1
et,1,55,,,1
e ,1 ,2 ,22 ,21
e ,2 ,3 ,23 ,22
e ,3 ,4 ,24 ,23
e ,4 ,5 ,25 ,24
e ,5 ,6 ,26 ,25
e ,6 ,7 ,27 ,26
e ,7 ,8 ,28 ,27
e ,8 ,9 ,29 ,28
e ,9 ,10 ,30 ,29
e ,10 ,11 ,31 ,30
e ,11 ,12 ,32 ,31
e ,12 ,13 ,33 ,32
e ,13 ,14 ,34 ,33
e ,14 ,15 ,35 ,34
e ,15 ,16 ,36 ,35
e ,16 ,17 ,37 ,36
e ,17 ,18 ,38 ,37
e ,18 ,19 ,39 ,38
e ,19 ,20 ,40 ,39
e ,20 ,66 ,65 ,40
e ,66 ,96 ,95 ,65
e ,96 ,130 ,129 ,95
e ,130 ,165 ,164 ,129
e ,41 ,1 ,21 ,42
e ,42 ,21 ,44 ,43
e ,21 ,22 ,45 ,44
e ,22 ,23 ,46 ,45
e ,23 ,24 ,47 ,46
e ,24 ,25 ,48 ,47
e ,25 ,26 ,49 ,48
e ,26 ,27 ,50 ,49
e ,27 ,28 ,51 ,50
e ,28 ,29 ,52 ,51
e ,29 ,30 ,53 ,52
e ,30 ,31 ,54 ,53
e ,31 ,32 ,55 ,54
e ,32 ,33 ,56 ,55
e ,33 ,34 ,57 ,56
e ,34 ,35 ,58 ,57
e ,35 ,36 ,59 ,58
e ,36 ,37 ,60 ,59
e ,37 ,38 ,61 ,60
e ,38 ,39 ,62 ,61
e ,39 ,40 ,63 ,62
e ,40 ,65 ,64 ,63
e ,65 ,95 ,94 ,64
e ,95 ,129 ,128 ,94
e ,129 ,164 ,163 ,128
e ,67 ,41 ,42 ,68
e ,68 ,42 ,43 ,69
e ,69 ,43 ,71 ,70
e ,43 ,44 ,72 ,71
e ,44 ,45 ,73 ,72
e ,45 ,46 ,74 ,73
e ,46 ,47 ,75 ,74
e ,47 ,48 ,76 ,75
e ,48 ,49 ,77 ,76
e ,49 ,50 ,78 ,77
e ,50 ,51 ,79 ,78
e ,51 ,52 ,80 ,79
e ,52 ,53 ,81 ,80
e ,53 ,54 ,82 ,81
e ,54 ,55 ,83 ,82
e ,55 ,56 ,84 ,83
e ,56 ,57 ,85 ,84
e ,57 ,58 ,86 ,85
e ,58 ,59 ,87 ,86
e ,59 ,60 ,88 ,87
e ,60 ,61 ,89 ,88
e ,61 ,62 ,90 ,89
e ,62 ,63 ,91 ,90
e ,63 ,64 ,92 ,91
e ,64 ,94 ,93 ,92
e ,94 ,128 ,127 ,93
e ,128 ,163 ,162 ,127
e ,97 ,67 ,68 ,98
e ,98 ,68 ,69 ,99
e ,99 ,69 ,70 ,100
e ,100 ,70 ,102 ,101
e ,70 ,71 ,103 ,102
e ,71 ,72 ,104 ,103
e ,72 ,73 ,105 ,104
e ,73 ,74 ,106 ,105
e ,74 ,75 ,107 ,106
e ,75 ,76 ,108 ,107
e ,76 ,77 ,109 ,108
e ,77 ,78 ,110 ,109
e ,78 ,79 ,111 ,110
e ,79 ,80 ,112 ,111
e ,80 ,81 ,113 ,112
e ,81 ,82 ,114 ,113
e ,82 ,83 ,115 ,114
e ,83 ,84 ,116 ,115
e ,84 ,85 ,117 ,116
e ,85 ,86 ,118 ,117
e ,86 ,87 ,119 ,118
e ,87 ,88 ,120 ,119
e ,88 ,89 ,121 ,120
e ,89 ,90 ,122 ,121
e ,90 ,91 ,123 ,122
e ,91 ,92 ,124 ,123
e ,92 ,93 ,125 ,124
e ,93 ,127 ,126 ,125
e ,127 ,162 ,161 ,126
e ,101 ,102 ,135 ,134
e ,102 ,103 ,136 ,135
e ,103 ,104 ,137 ,136
e ,104 ,105 ,138 ,137
e ,105 ,106 ,139 ,138
e ,106 ,107 ,140 ,139
e ,107 ,108 ,141 ,140
e ,108 ,109 ,142 ,141
e ,109 ,110 ,143 ,142
e ,110 ,111 ,144 ,143
e ,111 ,112 ,145 ,144
e ,112 ,113 ,146 ,145
e ,113 ,114 ,147 ,146
e ,114 ,115 ,148 ,147
```

```
e ,115 ,116 ,149 ,148
e ,116 ,117 ,150 ,149
e ,117 ,118 ,151 ,150
e ,118 ,119 ,152 ,151
e ,119 ,120 ,153 ,152
e ,120 ,121 ,154 ,153
e ,121 ,122 ,155 ,154
e ,122 ,123 ,156 ,155
e ,123 ,124 ,157 ,156
e ,124 ,125 ,158 ,157
e ,125 ,126 ,159 ,158
e ,126 ,161 ,160 ,159
e ,131 ,97 ,98 ,98
e ,131 ,98 ,132 ,132
e ,132 ,98 ,99 ,99
e ,132 ,99 ,100 ,100
e ,132 ,100 ,133 ,133
e ,133 ,100 ,101 ,101
e ,133 ,101 ,134 ,134
e ,133 ,134 ,170 ,170
e ,170 ,134 ,171 ,171
e ,134 ,135 ,171 ,171
e ,171 ,135 ,136 ,136
e ,171 ,136 ,172 ,172
e ,172 ,136 ,137 ,137
e ,172 ,137 ,138 ,138
e ,172 ,138 ,173 ,173
e ,173 ,138 ,139 ,139
e ,173 ,139 ,140 ,140
e ,173 ,140 ,174 ,174
e ,174 ,140 ,141 ,141
e ,174 ,141 ,142 ,142
e ,174 ,142 ,175 ,175
e ,175 ,142 ,143 ,143
e ,175 ,143 ,144 ,144
e ,175 ,144 ,176 ,176
e ,176 ,144 ,145 ,145
e ,176 ,145 ,146 ,146
e ,176 ,146 ,177 ,177
e ,177 ,146 ,147 ,147
e ,177 ,147 ,148 ,148
e ,177 ,148 ,178 ,178
e ,178 ,148 ,149 ,149
e ,178 ,149 ,150 ,150
e ,178 ,150 ,179 ,179
e ,179 ,150 ,151 ,151
e ,179 ,151 ,152 ,152
e ,179 ,152 ,180 ,180
e ,180 ,152 ,153 ,153
e ,180 ,153 ,154 ,154
e ,180 ,154 ,181 ,181
e ,181 ,154 ,155 ,155
e ,181 ,155 ,156 ,156
e ,181 ,156 ,182 ,182
e ,182 ,156 ,157 ,157
e ,182 ,157 ,158 ,158
e ,182 ,158 ,183 ,183
e ,183 ,158 ,159 ,159
e ,183 ,159 ,160 ,160
e ,183 ,160 ,184 ,184
e ,184 ,160 ,185 ,185
e ,160 ,161 ,185 ,185
e ,161 ,162 ,185 ,185
e ,185 ,162 ,186 ,186
e ,162 ,163 ,186 ,186
e ,163 ,164 ,186 ,186
e ,186 ,164 ,187 ,187
e ,164 ,165 ,187 ,187
e ,166 ,131 ,132 ,167
e ,167 ,132 ,133 ,168
e ,168 ,133 ,170 ,169
e ,169 ,170 ,192 ,191
e ,170 ,171 ,193 ,192
e ,171 ,172 ,194 ,193
e ,172 ,173 ,195 ,194
e ,173 ,174 ,196 ,195
e ,174 ,175 ,197 ,196
e ,175 ,176 ,198 ,197
e ,176 ,177 ,199 ,198
e ,177 ,178 ,200 ,199
e ,178 ,179 ,201 ,200
e ,179 ,180 ,202 ,201
e ,180 ,181 ,203 ,202
e ,181 ,182 ,204 ,203
e ,182 ,183 ,205 ,204
e ,183 ,184 ,206 ,205
e ,184 ,208 ,207 ,206
e ,185 ,209 ,208 ,184
e ,186 ,210 ,209 ,185
e ,187 ,211 ,210 ,186
e ,191 ,192 ,213 ,212
e ,192 ,193 ,214 ,213
e ,193 ,194 ,215 ,214
e ,194 ,195 ,216 ,215
e ,195 ,196 ,217 ,216
e ,196 ,197 ,218 ,217
e ,197 ,198 ,219 ,218
e ,198 ,199 ,220 ,219
e ,199 ,200 ,221 ,220
e ,200 ,201 ,222 ,221
e ,201 ,202 ,223 ,222
e ,202 ,203 ,224 ,223
e ,203 ,204 ,225 ,224
e ,204 ,205 ,226 ,225
e ,205 ,206 ,227 ,226
e ,206 ,207 ,228 ,227
e ,188 ,166 ,167 ,167
e ,188 ,167 ,189 ,189
e ,189 ,167 ,168 ,168
e ,189 ,168 ,169 ,169
e ,189 ,169 ,190 ,190
e ,190 ,169 ,191 ,191
e ,190 ,191 ,212 ,212
e ,190 ,212 ,232 ,232
e ,232 ,212 ,233 ,233
e ,233 ,212 ,213 ,213
e ,233 ,213 ,214 ,214
e ,233 ,214 ,234 ,234
e ,234 ,214 ,215 ,215
e ,234 ,215 ,216 ,216
e ,234 ,216 ,235 ,235
e ,235 ,216 ,217 ,217
e ,235 ,217 ,218 ,218
e ,235 ,218 ,236 ,236
e ,236 ,218 ,219 ,219
e ,236 ,219 ,220 ,220
e ,236 ,220 ,237 ,237
e ,237 ,220 ,221 ,221
e ,237 ,221 ,222 ,222
e ,237 ,222 ,238 ,238
e ,238 ,222 ,223 ,223
e ,238 ,223 ,224 ,224
e ,238 ,224 ,239 ,239
e ,239 ,224 ,225 ,225
e ,239 ,225 ,226 ,226
e ,239 ,226 ,240 ,240
e ,240 ,226 ,227 ,227
e ,240 ,227 ,228 ,228
e ,240 ,228 ,241 ,241
e ,241 ,228 ,229 ,229
e ,228 ,207 ,229 ,229
e ,207 ,208 ,229 ,229
e ,229 ,208 ,230 ,230
e ,208 ,209 ,230 ,230
e ,209 ,210 ,230 ,230
e ,230 ,210 ,231 ,231
e ,210 ,211 ,231 ,231
e ,232 ,233 ,247 ,246
e ,233 ,234 ,248 ,247
e ,234 ,235 ,249 ,248
e ,235 ,236 ,250 ,249
e ,236 ,237 ,251 ,250
e ,237 ,238 ,252 ,251
e ,238 ,239 ,253 ,252
e ,239 ,240 ,254 ,253
e ,240 ,241 ,255 ,254
e ,241 ,242 ,256 ,255
e ,229 ,243 ,242 ,241
e ,230 ,244 ,243 ,229
e ,231 ,245 ,244 ,230
e ,246 ,247 ,263 ,262
e ,247 ,248 ,264 ,263
e ,248 ,249 ,265 ,264
e ,249 ,250 ,266 ,265
e ,250 ,251 ,267 ,266
e ,251 ,252 ,268 ,267
e ,252 ,253 ,269 ,268
e ,253 ,254 ,270 ,269
e ,254 ,255 ,271 ,270
e ,255 ,256 ,272 ,271
e ,256 ,257 ,273 ,272
e ,242 ,258 ,257 ,256
e ,243 ,259 ,258 ,242
e ,244 ,260 ,259 ,243
e ,245 ,261 ,260 ,244
e ,262 ,263 ,277 ,277
e ,277 ,263 ,278 ,278
e ,278 ,263 ,264 ,264
e ,278 ,264 ,265 ,265
e ,278 ,265 ,279 ,279
e ,279 ,265 ,266 ,266
e ,279 ,266 ,267 ,267
e ,279 ,267 ,280 ,280
e ,280 ,267 ,268 ,268
e ,280 ,268 ,269 ,269
e ,280 ,269 ,281 ,281
e ,281 ,269 ,270 ,270
e ,281 ,270 ,271 ,271
e ,281 ,271 ,282 ,282
e ,282 ,271 ,272 ,272
e ,282 ,272 ,273 ,273
e ,282 ,273 ,283 ,283
e ,283 ,273 ,274 ,274
e ,273 ,257 ,274 ,274
e ,257 ,258 ,274 ,274
e ,274 ,258 ,275 ,275
e ,258 ,259 ,275 ,275
e ,259 ,260 ,275 ,275
e ,275 ,260 ,276 ,276
e ,260 ,261 ,276 ,276
e ,277 ,278 ,285 ,284
e ,278 ,279 ,286 ,285
e ,279 ,280 ,287 ,286
e ,280 ,281 ,288 ,287
e ,281 ,282 ,289 ,288
e ,282 ,283 ,290 ,289
e ,283 ,292 ,291 ,290
e ,274 ,293 ,292 ,283
e ,275 ,294 ,293 ,274
e ,276 ,295 ,294 ,275
e ,284 ,285 ,297 ,296
e ,285 ,286 ,298 ,297
e ,286 ,287 ,299 ,298
e ,287 ,288 ,300 ,299
e ,288 ,289 ,301 ,300
e ,289 ,290 ,302 ,301
```

```
e ,290 ,291 ,303 ,302
e ,296 ,297 ,307 ,307
e ,307 ,297 ,308 ,308
e ,308 ,297 ,298 ,298
e ,308 ,298 ,299 ,299
e ,308 ,299 ,309 ,309
e ,309 ,299 ,300 ,300
e ,309 ,300 ,301 ,301
e ,309 ,301 ,310 ,310
e ,310 ,301 ,302 ,302
e ,310 ,302 ,303 ,303
e ,310 ,303 ,311 ,311
e ,311 ,303 ,304 ,304
e ,303 ,291 ,304 ,304
e ,291 ,292 ,304 ,304
e ,304 ,292 ,305 ,305
e ,292 ,293 ,305 ,305
e ,293 ,294 ,305 ,305
e ,305 ,294 ,306 ,306
e ,294 ,295 ,306 ,306
e ,307 ,308 ,317 ,316
e ,308 ,309 ,318 ,317
e ,309 ,310 ,319 ,318
e ,310 ,311 ,320 ,319
e ,311 ,312 ,321 ,320
e ,304 ,313 ,312 ,311
e ,305 ,314 ,313 ,304
e ,306 ,315 ,314 ,305
e ,316 ,317 ,328 ,327
e ,317 ,318 ,329 ,328
e ,318 ,319 ,330 ,329
e ,319 ,320 ,331 ,330
e ,320 ,321 ,332 ,331
e ,321 ,322 ,333 ,332
e ,312 ,323 ,322 ,321
e ,313 ,324 ,323 ,312
e ,314 ,325 ,324 ,313
e ,315 ,326 ,325 ,314
e ,327 ,328 ,335 ,334
e ,328 ,329 ,336 ,335
e ,329 ,330 ,337 ,336
e ,330 ,331 ,338 ,337
e ,331 ,332 ,339 ,338
e ,332 ,333 ,340 ,339
```

BASE MODEL DISPLACEMENT RESTRAINTS

```
hcrl=6.0      * half crack length in mm
nsel,x,0
d,all,ux
nsel,y,0
nrsel,x,hcrl,30
d,all,uy
nall
```

ANSYS INPUT FILE FOR TRANSIENT THERMAL ANALYSIS

```
$set def [demo.jeff.pipet]
$ansys44
/prep7
resu
hcrl=4.5                          * half crack length in mm
tt0=190.0       $ts0=0.0          * temperature and time of load step 1 'C/s
tt1=151.0       $ts1=0.25         * temperature and time of load step 2 'C/s
tt2=135.0       $ts2=0.5          * temperature and time of load step 3 'C/s
tt3=123.0       $ts3=0.75         * temperature and time of load step 4 'C/s
tt4=115.5       $ts4=1.0          * temperature and time of load step 5 'C/s
tt5=108.0       $ts5=1.5          * temperature and time of load step 6 'C/s
tt6=105.0       $ts6=2.0          * temperature and time of load step 7 'C/s
tt7=102.5       $ts7=3.0          * temperature and time of load step 8 'C/s
```

```
tt8=101.0       $ts8=4.0        * temperature and time of load step 9 'C/s
tt9=100.5       $ts9=5.0        * temperature and time of load step 10 'C/s
tt10=100.25     $ts10=6.0       * temperature and time of load step 11 'C/s
tt11=100.0      $ts11=7.0       * temperature and time of load step 12 'C/s
tt12=100.0      $ts12=8.0       * temperature and time of load step 13 'C/s
tt13=100.0      $ts13=9.0       * temperature and time of load step 14 'C/s
tt14=100.0      $ts14=14.0      * temperature and time of load step 15 'C/s
nall
eall
kan,-1
ktemp,0
tref,tt0
tunif,tt0
iter,5
ntdel,all
nt,all,temp,tt0
time,ts0
lwrite
ntdel,all
nsel,y,9,25
nasel,x,11.5,25
nt,all,temp,tt0
nsel,y,0
nrsel,x,0,hcrl
nt,all,temp,tt1
nall
eall
time,ts1
lwrite
ntdel,all
nsel,y,9,25
nasel,x,11.5,25
nt,all,temp,tt0
nsel,y,0
nrsel,x,0,hcrl
nt,all,temp,tt2
nall
eall
time,ts2
lwrite
ntdel,all
nsel,y,9,25
nasel,x,11.5,25
nt,all,temp,tt0
nsel,y,0
nrsel,x,0,hcrl
nt,all,temp,tt3
nall
eall
time,ts3
lwrite
ntdel,all
nsel,y,9,25
nasel,x,11.5,25
nt,all,temp,tt0
nsel,y,0
nrsel,x,0,hcrl
nt,all,temp,tt4
nall
eall
time,ts4
lwrite
ntdel,all
nsel,y,9,25
nasel,x,11.5,25
nt,all,temp,tt0
nsel,y,0
nrsel,x,0,hcrl
nt,all,temp,tt5
nall
eall
time,ts5
```

```
lwrite
ntdel,all
nsel,y,9,25
nasel,x,11.5,25
nt,all,temp,tt0
nsel,y,0
nrsel,x,0,hcrl
nt,all,temp,tt6
nall
eall
time,ts6
lwrite
ntdel,all
nsel,y,9,25
nasel,x,11.5,25
nt,all,temp,tt0
nsel,y,0
nrsel,x,0,hcrl
nt,all,temp,tt7
nall
eall
time,ts7
lwrite
ntdel,all
nsel,y,9,25
nasel,x,11.5,25
nt,all,temp,tt0
nsel,y,0
nrsel,x,0,hcrl
nt,all,temp,tt8
nall
eall
time,ts8
lwrite
ntdel,all
nsel,y,9,25
nasel,x,11.5,25
nt,all,temp,tt0
nsel,y,0
nrsel,x,0,hcrl
nt,all,temp,tt9
nall
eall
time,ts9
lwrite
ntdel,all
nsel,y,9,25
nasel,x,11.5,25
nt,all,temp,tt0
nsel,y,0
nrsel,x,0,hcrl
nt,all,temp,tt10
nall
eall
time,ts10
lwrite
ntdel,all
nsel,y,9,25
nasel,x,11.5,25
nt,all,temp,tt0
nsel,y,0
nrsel,x,0,hcrl
nt,all,temp,tt11
nall
eall
time,ts11
lwrite
ntdel,all
nsel,y,9,25
nasel,x,11.5,25
nt,all,temp,tt0
nsel,y,0
nrsel,x,0,hcrl
nt,all,temp,tt12
nall
eall
time,ts12
lwrite
ntdel,all
nsel,y,9,25
nasel,x,11.5,25
nt,all,temp,tt0
nsel,y,0
nrsel,x,0,hcrl
nt,all,temp,tt13
nall
eall
time,ts13
lwrite
ntdel,all
nsel,y,9,25
nasel,x,11.5,25
nt,all,temp,tt0
nsel,y,0
nrsel,x,0,hcrl
nt,all,temp,tt14
nall
eall
time,ts14
lwrite
afwrite
finish
/input,27
finish
/eof
```

APPENDIX VIII : ANSYS Input File for Stress Analysis

```
$set def [demo.jeff.pipes]
$ansys44
/prep7
resu
p1=-12.125       *pressure on x=24 face pr/2t
p2=(p1*2)        *pressure on y=24 face
c*** 145=6.6025, 217.5=9.09375, 290=12.125
kan,0
ktemp,1
psf,0,1,24,p1
psf,0,2,24,p2
lwrite
ktemp,2
psf,0,1,24,p1
psf,0,2,24,p2
lwrite
ktemp,3
psf,0,1,24,p1
psf,0,2,24,p2
lwrite
ktemp,4
psf,0,1,24,p1
psf,0,2,24,p2
lwrite
ktemp,5
psf,0,1,24,p1
psf,0,2,24,p2
lwrite
ktemp,6
psf,0,1,24,p1
psf,0,2,24,p2
lwrite
ktemp,7
psf,0,1,24,p1
psf,0,2,24,p2
lwrite
ktemp,8
psf,0,1,24,p1
psf,0,2,24,p2
lwrite
ktemp,9
psf,0,1,24,p1
psf,0,2,24,p2
lwrite
ktemp,10
psf,0,1,24,p1
psf,0,2,24,p2
lwrite
ktemp,11
psf,0,1,24,p1
psf,0,2,24,p2
lwrite
ktemp,12
psf,0,1,24,p1
psf,0,2,24,p2
lwrite
ktemp,13
psf,0,1,24,p1
psf,0,2,24,p2
lwrite
ktemp,14
psf,0,1,24,p1
psf,0,2,24,p2
lwrite
ktemp,15
psf,0,1,24,p1
psf,0,2,24,p2
lwrite
afwrite
finish
/input,27
finish
/eof
```

APPENDIX IX : ANSYS Input File for J-Integral Calculation

```
$SET DEF [DEMO.JEFF.PIPEJ]
$ANSYS44
/POST1
STRESS,SENE
STRESS,VOLU
*CREATE,JIN1                    *create subprogram to do
SEXP,W,SENE,VOLU,1,-1           *calculation from transferred
LPATH,ARG1,ARG2,ARG3,ARG4       *path.
PDEF,INTR,W,W
PCALC,INTG,J,W,YG
*GET,JA,PLAST,J
PDEF,CLEAR
PDEF,NORM,NX,NY,NZ
PDEF,INTR,SX,SX
PDEF,INTR,SY,SY
PDEF,INTR,SXY,SXY
PCALC,MULT,TX,SX,NX
PCALC,MULT,C1,SXY,NY
PCALC,ADD,TX,TX,C1
PCALC,MULT,TY,SXY,NX
PCALC,MULT,C1,SY,NY
PCALC,ADD,TY,TY,C1
*GET,DX,PLAST,S
DX=DX/100
PCALC,ADD,XG,XG,,,,-DX/2
PDEF,INTR,UX1,UX
PDEF,INTR,UY1,UY
PCALC,ADD,XG,XG,,,,DX
PDEF,INTR,UX2,UX
PDEF,INTR,UY2,UY
PCALC,ADD,XG,XG,,,,-DX/2
C=(1/DX)
PCALC,ADD,C1,UX2,UX1,C,-C
PCALC,ADD,C2,UY2,UY1,C,-C
PCALC,MULT,C1,TX,C1
PCALC,MULT,C2,TY,C2
PCALC,ADD,C1,C1,C2
PCALC,INTG,J,C1,S
*GET,JB,PLAST,J
JINT=(2*(JA-JB))
PDEF,CLEAR
*END                            *end of subprogram JIN1
SET,1
NALL
EALL
*USE,JIN1,7,27,23,3             *execute JIN1 with a path
/OUTPUT,JEFF1,DAT               *following nodes 7 to 27
*STAT                           *to 23 to 3.
/OUTPUT
SET,2                           *three different paths were
NALL                            *used to check for convergence.
EALL                            *all results correlated to
*USE,JIN1,7,27,23,3             *within 2%.
/OUTPUT,JEFF2,DAT
*STAT
/OUTPUT
SET,3
NALL
EALL
*USE,JIN1,7,27,23,3
/OUTPUT,JEFF3,DAT
*STAT
/OUTPUT
SET,4
NALL
EALL
*USE,JIN1,7,27,23,3
```

```
/OUTPUT,JEFF4,DAT
*STAT
/OUTPUT
SET,5
NALL
EALL
*USE,JIN1,7,27,23,3
/OUTPUT,JEFF5,DAT
*STAT
/OUTPUT
SET,6
NALL
EALL
*USE,JIN1,7,27,23,3
/OUTPUT,JEFF6,DAT
*STAT
/OUTPUT
SET,7
NALL
EALL
*USE,JIN1,7,27,23,3
/OUTPUT,JEFF7,DAT
*STAT
/OUTPUT
SET,8
NALL
EALL
*USE,JIN1,7,27,23,3
/OUTPUT,JEFF8,DAT
*STAT
/OUTPUT
SET,9
NALL
EALL
*USE,JIN1,7,27,23,3
/OUTPUT,JEFF9,DAT
*STAT
/OUTPUT
SET,10
NALL
EALL
*USE,JIN1,7,27,23,3
/OUTPUT,JEFF10,DAT
*STAT
/OUTPUT
SET,11
NALL
EALL
*USE,JIN1,7,27,23,3
/OUTPUT,JEFF11,DAT
*STAT
/OUTPUT
SET,12
NALL
EALL
*USE,JIN1,7,27,23,3
/OUTPUT,JEFF12,DAT
*STAT
/OUTPUT
SET,13
NALL
EALL
*USE,JIN1,7,27,23,3
/OUTPUT,JEFF13,DAT
*STAT
/OUTPUT
SET,14
NALL
EALL
*USE,JIN1,7,27,23,3
/OUTPUT,JEFF14,DAT
*STAT
/OUTPUT
SET,15
NALL
EALL
*USE,JIN1,7,27,23,3
/OUTPUT,JEFF15,DAT
*STAT
/OUTPUT
/SYS,RENAME JEFF1.DAT J.DAT
/SYS,APPEND JEFF2.DAT J.DAT
/SYS,DEL JEFF2.DAT;1
/SYS,APPEND JEFF3.DAT J.DAT
/SYS,DEL JEFF3.DAT;1
/SYS,APPEND JEFF4.DAT J.DAT
/SYS,DEL JEFF4.DAT;1
/SYS,APPEND JEFF5.DAT J.DAT
/SYS,DEL JEFF5.DAT;1
/SYS,APPEND JEFF6.DAT J.DAT
/SYS,DEL JEFF6.DAT;1
/SYS,APPEND JEFF7.DAT J.DAT
/SYS,DEL JEFF7.DAT;1
/SYS,APPEND JEFF8.DAT J.DAT
/SYS,DEL JEFF8.DAT;1
/SYS,APPEND JEFF9.DAT J.DAT
/SYS,DEL JEFF9.DAT;1
/SYS,APPEND JEFF10.DAT J.DAT
/SYS,DEL JEFF10.DAT;1
/SYS,APPEND JEFF11.DAT J.DAT
/SYS,DEL JEFF11.DAT;1
/SYS,APPEND JEFF12.DAT J.DAT
/SYS,DEL JEFF12.DAT;1
/SYS,APPEND JEFF13.DAT J.DAT
/SYS,DEL JEFF13.DAT;1
/SYS,APPEND JEFF14.DAT J.DAT
/SYS,DEL JEFF14.DAT;1
/SYS,APPEND JEFF15.DAT J.DAT
/SYS,DEL JEFF15.DAT;1
FINISH
/EOF
```